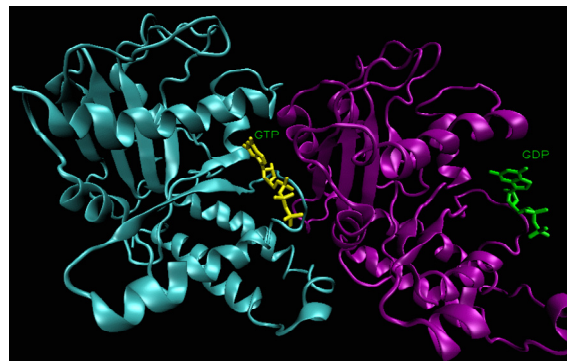




Sapienza Università di Roma

“Arylthioindoles as Tubulin Polymerization and Cell Growth Inhibitors:
New Bioisosteres at the Sulfur Bridging and Ester Groups”



Tutore

Prof. Romano Silvestri

Docente guida

Prof. Romano Silvestri

Coordinatore

Prof. Marco Tripodi

Dottorando

Valerio Gatti

Dottorato di Ricerca in Scienze Pasteuriane

XXIV CICLO

Contents

1.	Introduction	1
2.	Microtubules and tubulin	2
3.	Microtubule interfering agents in cancer chemotherapy	11
3.1	<i>Paclitaxel site binding agents</i>	13
3.2	<i>Colchicine site binding agents</i>	20
3.3	<i>Vinca alkaloid site binding agents</i>	26
4.	Arylthioindoles, potent inhibitors of tubulin polymerization	31
5.	Chemistry	39
6.	Biological activity	47
7.	Molecular modeling studies	75
8.	Conclusions	80
9.	Experimental section	82
9.1	<i>Chemistry</i>	82
9.2	<i>Synthesis</i>	83
9.3	<i>Molecular modeling</i>	111
9.4	<i>Biology</i>	112
10.	References	120
11.	Acknowledgments	138

1. Introduction

During eukaryotic cell division, in order for each daughter cell to inherit one and only one copy of each chromosome, the mother cell must replicate its chromosomes exactly once in the synthetic phase, and then must separate the replicated chromosomes evenly at the end of the mitotic phase to the two daughter cells.

Defects in the coordination of chromosome replication and chromosome segregation can have severe consequences leading to genetic instability and aneuploidy, and eventually fostering tumour malignancy.¹⁻³

To ensure faithful transmission of chromosomes during cell division, eukaryotic cells have evolved cellular regulatory mechanisms termed cell cycle checkpoints.⁴ The checkpoints prevent or delay cell cycle progression if certain cellular processes or proteins are disrupted, to gain time to repair the damage before cell division occurs. When the damage is irreparable, the cell undergoes apoptosis through the triggering of specific biochemical pathways.⁵ However, cancer cells often harbor defective cell cycle checkpoints allowing for uncontrolled cell proliferation, even when cell division does not occur properly.

Therefore, effective cancer treatment can be achieved by drugs that target certain processes or proteins impinging on the cell cycle machinery.⁶ In particular, chemical compounds that target microtubules and inhibit the normal function of the mitotic spindle, have proven to be one of the best classes of cancer chemotherapeutic drugs available to date.⁷ Among these, paclitaxel and vinblastine are clinically used to treat different human tumours, e.g. ovarian, mammary, lung, and haematological cancers.

However, restrictions due to toxicity, drug resistance, complex formulations and limited bioavailability highlight the need for novel tubulin inhibitors.

2. Microtubules and tubulin

Microtubules (MTs), the dynamic pipe-like protein composed of α , β -heterodimers, are essential cytoskeletal polymers and are present in all eukaryotes, affecting cell shape, cell transport, cell motility, and cell division. MTs are long, hollow structures with 5 nm walls surrounding a cavity, usually with internal and external diameters of ~15 and ~25 nm, respectively. They are made up of two globular protein subunits, α - and β -tubulin (TB). The α - and β -subunits form heterodimers which aggregate in a head to tail arrangement to form long tubes made up of stacked rings with each ring usually containing 13 subunits, which is known as protofilament. After an induction period, the protofilaments group together to form a C-shaped protein sheet, which then curl around to give a pipe-like structure known as microtubule (Figure 1).⁷

α - and β -TB, each with a molecular weight of about 50 kDa, are regarded as the main components of MTs. There are six isoforms of each α - and β -TB in human cells, showing tissue-, cell- and tumor-specific patterns of expression as well as differences in protein binding.⁸ Both α - and β -TB bind a guanine nucleotide, which is non-exchangeable when bound in the α -subunit (*N*-site) and exchangeable when bound to the β -subunit (*E*-site).⁷

The structures of α - and β -TB are basically identical: each monomer is formed by a core of two β -sheets surrounded by α -helices. The monomer structure is very compact, but can be divided into three functional domains: the *N*-terminal nucleotide binding domain (residues 1 to 205), an intermediate domain (residues 206 to 384), and the *C*-terminal domain (residues 385 to the *C*-terminus).

TB dimer structure has been solved at 3.7 Å by electron crystallography of the two-dimensional crystalline sheets of TB that form in the presence of zinc ions (Figure 2).^{9,10}

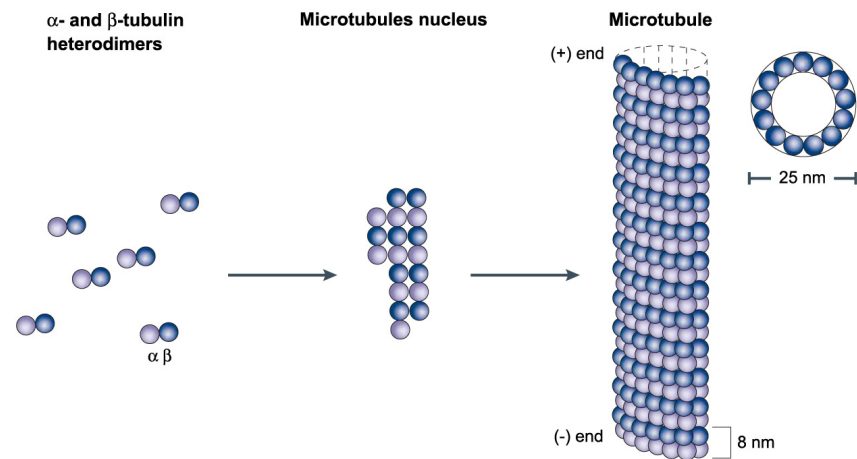


Figure 1. Microtubule components.

TB($\alpha_1\beta_1\alpha_2\beta_2$)/stathmin-like domain complex has been also solved by X-ray crystallography at 3.5 Å resolution (Figure 3).^{11,12} Stathmin is a 17 kDa ubiquitous cytosolic phosphoprotein, recognized as a MT destabilizing factor.

By contrast with the TB in zinc sheets, the TB($\alpha_1\beta_1\alpha_2\beta_2$)/stathmin-like domain complex appears curved. MTs are polar polymers that bind to and hydrolyze GTP, and show distinct (+, plus) and (-, minus) ends. The structural polarity of MTs is created by the regular, parallel orientation of all of their subunits. The plus end is capable of rapid growth and is kinetically more dynamic than the minus end, which tends to lose subunits if not stabilized. Although both ends alternately grow or shorten, net growing occurs at the plus end and net shortening at the minus end.¹³

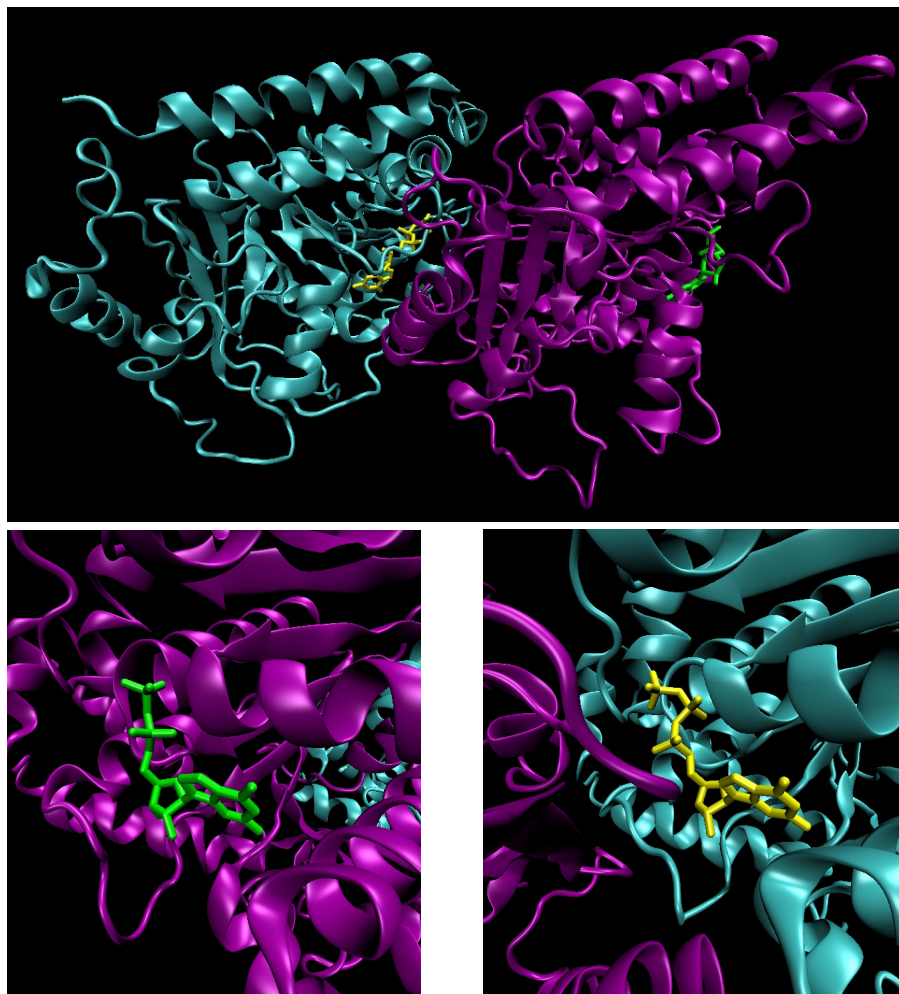


Figure 2. Ribbon diagram of the electron crystallography structure of zinc-induced $\alpha\beta$ -tubulin sheets (α -tubulin in cyan, β -tubulin in purple, GDP in green, GTP in yellow; PDB code: 1JFF¹⁰).



Figure 3. Ribbon diagram of the X-ray structure of tubulin($\alpha_1\beta_1\alpha_2\beta_2$)/ stathmin-like domain complex (α_1 -, α_2 -tubulin in cyan, β_1 -, β_2 -tubulin in purple, GDP in green, GTP in yellow, stathmin-like domain in gray; PDB code: 1SA0¹²).

The plus ends of the MTs are often free in the cytoplasm or located near the plasma membrane, whereas the slow-growing or minus ends of the MTs are frequently associated at a single site in the cell named the microtubule organizing center (MTOC) or centrosome.¹⁴ MTOC represents the specific location from which MTs are nucleated. A major component of the MTOC is γ -TB,¹⁵ which shows a 28–35% homology with α - and β -TB and is expressed in lower amounts than these latter isoforms. A number of γ -TB ring complexes (γ -TuRC) have been isolated and behave as impressive *in vitro* nucleators of MT growth (Figure 4).^{16–18}

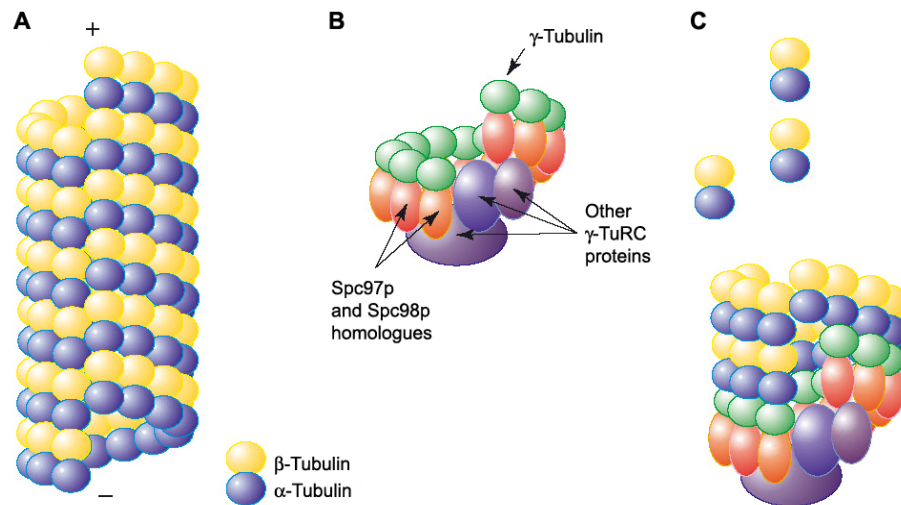


Figure 4. **A:** Schematic diagram of a microtubule. **B:** Model for the structure of the γ -tubulin ring complex (γ -TuRC). **C:** Microtubule nucleation by the γ -TuRC.

In interphase the MTOC or centrosome is normally located to one side of the nucleus, close to the outer surface of the nuclear envelope, and embedded in the

centrosome are the centrioles, a pair of cylindrical structures arranged at right angles to each other in an L-shaped configuration.

Polymerization of MTs occurs by a nucleation-elongation mechanism in which the formation of a short MT nucleus is followed by elongation of the MT at its ends by reversible, non-covalent addition of α/β -TB dimers.

In 1984, Mitchison and Kirschner proposed the dynamic instability model of MT assembly, in which individual MTs exist either in an elongation state or a rapidly shortening state, with abrupt and apparently random transitions between these two states.^{19,20} Several studies performed *in vitro*, using purified TB,^{21,22} or in living cells,²³ have confirmed this mechanism of MT assembly/disassembly.

MTs are thus governed by an intrinsic property involving repetitive spurts of shortening from their plus ends, followed by periods of polymerization. This non-equilibrium behavior is based on the binding and hydrolysis of GTP at *E*-site in β -TB. Only dimers that have GTP in their *E*-site can polymerize. This nucleotide is then hydrolyzed and becomes non-exchangeable. The GTP cap model proposes that the GDP-TB core of MT is stabilized at the plus end by a layer of GTP-TB subunits that may act to maintain association between protofilaments.^{24,25} When this cap is stochastically lost, the protofilaments peel outward and the MT rapidly depolymerizes. Although both MT ends can either grow or shorten, the changes in length at the plus end are much greater than at the minus end (Figure 5). MTs exhibit another important dynamic behavior called treadmilling or flux. It corresponds to a polymer mass steady state resulting from the net growth at one MT end and the net shortening at the opposite end.²⁶ In other words, treadmilling is a process by which TB subunits continuously flux from one end of the polymer to the other, due to net differences in the critical subunit concentrations at the opposite MT ends.

Figure 6 remarks the different movement of the TB dimer involved into the dynamic instability and the treadmilling. Both dynamic instability and treadmilling

can be produced as distinct phenomena *in vitro* using purified TB, and they have also been observed in living cells.^{26,27}

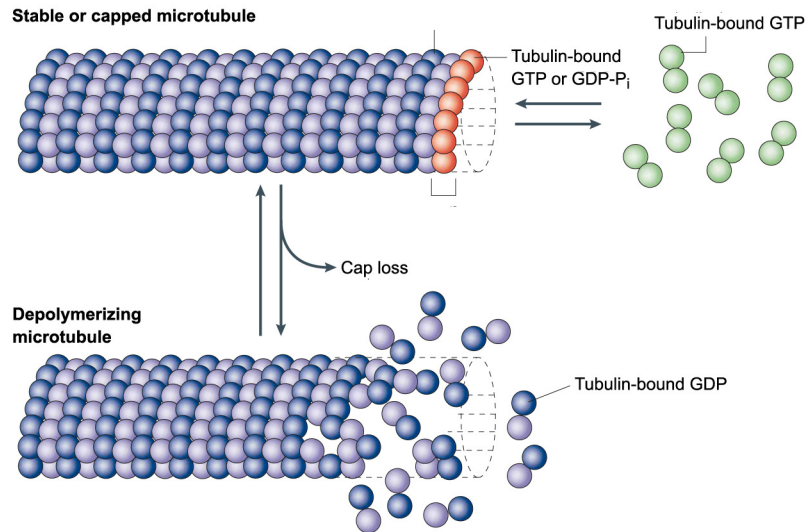


Figure 5. Microtubule polymerization dynamics and GTP cap.

In living cells, MT dynamics are regulated both spatially and temporally. In fact, MTs interact with an impressive number of binding proteins, and cellular MT dynamics are thus the result of the combined effect of stabilizing and destabilizing factors. MT assembly/disassembly is firstly controlled by a balance between MT stabilizing and destabilizing proteins that bind along the MTs.²⁸ Stabilizing proteins include a large group of so-called microtubule associated proteins or MAPs,²⁹ that stabilize MTs against disassembly.

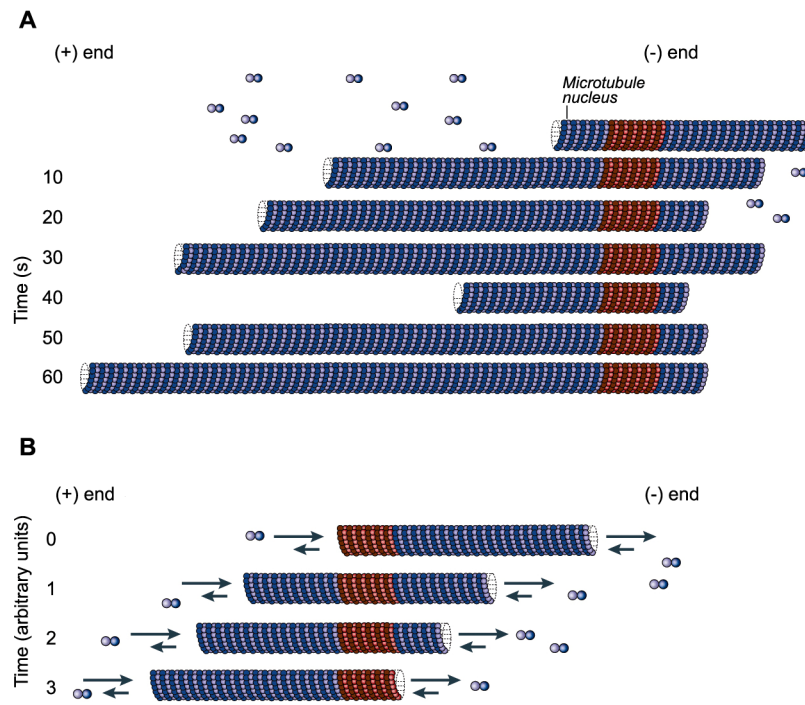


Figure 6. Different movement of the tubulin heterodimer involved into the dynamic instability (**A**) and the treadmilling (**B**).

MAPs are targets for protein kinases, including p34cdc2 kinase (cyclin-dependent kinase 1, CDK1), which control changes in MT dynamic properties at the G2 to M phase transition of the cell cycle. Phosphorylation of MAPs increases during mitosis and reduces their affinity for MTs, thereby reducing their ability to promote MT

polymerization.^{30,31} Major MAPs include MAP1, MAP2, MAP4 and tau. MAP4 is the most abundant and ubiquitous MAP in non neuronal cells that stabilizes MTs.³²

MAP4 phosphorylation by the cyclin B1/p34cdc2 complex decreases its MT stabilizing ability at mitosis.³¹ The destabilizing factors are a growing family of proteins that include Oncoprotein 18 (Op18)/Stathmin, Xenopus kinesin central motor 1 (XKCM1), and katanin.²⁸ Op18/stathmin is a small protein (19 kDa), highly expressed in leukemic cells, that physically interacts with TB dimers and increases the catastrophe rate of MTs.^{33,34} Phosphorylation of Op18/stathmin by p34cdc2 kinase increases the MT catastrophe rate at mitosis.^{35,36} XKCM1 is a kinesin-related protein that promotes MT depolymerization during mitotic spindle assembly, and regulates MT dynamics during mitotic spindle assembly.³⁷

Other MT binding proteins called motor proteins are critical for MT function. Motor proteins bind to MTs and use the energy derived from ATP hydrolysis to move steadily along it. They can carry membrane-enclosed organelles, such as mitochondria, Golgi stacks, or secretory vesicles, to their appropriate locations in the cell, and cause cytoskeletal filaments to slide against each other, a crucial process in cell division. Two major classes of MT dependent motor proteins are collectively grouped as kinesins and dyneins, which in turn comprise a great number of proteins.³⁸ Most of the kinesin superfamily proteins (KIFs) have specific roles in mitotic spindle formation and chromosome separation during cell division as well as in transport, and walk toward the plus end of the MT. However, C-terminal motor domain-type KIFs (KIFCs), including KIFC3, travel towards the minus end of MTs.

Dyneins are a family of minus end-directed MT motor proteins, less diverse than kinesins, and play an important role for vesicle trafficking as well as for the appropriate localization of intracellular organelles. Kinesins and dyneins generally move in opposite directions along MTs, and thereby control bi-directional vesicle transport.³⁸

3. Microtubule interfering agents in cancer chemotherapy

The crucial role of MTs in vital cellular functions for tumour cells, including mitosis, motility and cell-cell contacts, has made of MTs a valuable target for cancer chemotherapy. A large number of chemically diverse compounds, many of which are derived from natural products, are able to bind TB or MTs and inhibit proliferation by acting on the mitotic spindle. Some of these compounds (vinca alkaloids, colchicine) inhibit MT polymerization, whereas others (taxanes) stabilize MTs. But, although these compounds exert opposite effects on MTs, both types of MT interfering agents (MIAs) share the common property of suppressing MT dynamics and thereby MT function, leading to the disruption of the mitotic spindle function and blocking cell cycle progression at the transition from prometaphase/metaphase to anaphase.³⁹ This mitotic arrest is the major action of the distinct MIAs.

MT damaging agents, also named “spindle poisons” due to their inhibitory action on mitotic spindle, represent an important class of anticancer drugs. Agents that target MTs have been used in the treatment of cancer for over 35 years. More recently developed MT active compounds have demonstrated effectiveness against a broad spectrum of tumour. Because MTs are integral and crucial components of the mitotic spindle, interference with MT dynamics results in metaphase arrest in dividing cells. However, because MTs are also involved in a large number of other cellular functions, including chemotaxis, membrane and cellular scaffolding, intracellular transport, secretory processes and transmission of receptor signaling, MT interfering compounds may affect both neoplastic and nonmalignant cells in interphase, in addition to the mitotic phases of the cell cycle. This essential lack of selectivity towards tumour cells leads to a number of toxic side effects and to a rather low therapeutic index, for most of the MT interfering compounds.

All MIAs induce mitotic arrest followed by apoptosis. They block the cell cycle at M phase, mainly due to damage on the mitotic spindle, resulting in activation of

the mitotic spindle assembly checkpoint. Failure to proceed through the cell cycle is responsible for the activation of apoptosis. How disruption of MT dynamics leads to apoptosis is now being explored, but evidence that diffusible factors may be released as the result of changes in MT polymerization is consistent with the hypothesized role of MTs in sequestering signals.⁴⁰ Release or activation of these sequestered elements could allow them to reach their targets and to mount a response, including apoptosis. Although several lines of evidence show important links between cytoskeletal integrity and apoptosis regulation, the molecular mechanisms for these links are likely to be numerous. Because MIAs promote apoptosis mainly through their inhibitory actions on the mitotic spindle, the molecular mechanisms underlying the link between MT interference and the onset of apoptosis is suggested to be essentially similar among these agents. Thus, although there are some differences among the distinct MT active compounds concerning specific alterations in certain signaling pathways,⁴¹ the major signaling route underlying their cytotoxic action seems to be similar to all of them through a mitotic spindle damage-dependent process. In addition, MIAs can promote a number of effects on the spindle poles or centrosomes, including abnormal centriole structure,⁴² centrosome fragmentation,⁴³ and inappropriate centrosome duplication.⁴⁴

Most of the current antitumor drugs target a molecule or cell process present in both tumour and normal cells, leading to a predicted and marked non selective action. However, certain properties acquired by the tumour cells make them sometimes more susceptible to be targeted. In this regard, although the MIA target is present in both tumour and normal cells, and thereby a non selective behaviour could be foreseen for these antitumor drugs, certain properties of tumour cells make them more susceptible for the attack of these agents, such as: (a) a higher capacity to cell proliferation in some tumours giving more opportunities to the MT active drugs to attack on mitotic spindles; and (b) a high percentage of p53 mutations in tumour cells that favors the action of at least some MIAs.^{45,46}

MIA_s act by binding to various sites on the TB dimer and at different positions within the MT and can be classified into three major categories based on their respective TB binding domains which include paclitaxel site binding agents, colchicine site binding agents, and vinca alkaloid site binding agents.

3.1 Paclitaxel site binding agents

Taxoids, a promising group of antimitotic anticancer agents, have a unique mechanism of action, binding mainly to a domain distinct from those of colchicine and vinca alkaloids and inhibiting the depolymerization of polymerized TB.⁴⁷ The first marketed taxoid drug was paclitaxel (**1**), which was isolated from the bark of the Pacific yew tree *Taxus brevifolia*.⁴⁸ This endangered tree produces low yields of paclitaxel that cannot satisfy the increasing demand. Later paclitaxel was also isolated from hazelnut trees (leaves, twigs, and nuts) and the fungi living on these trees but the concentration is only about 10% of the concentration in yew trees. This drug has now been semisynthesized from baccatin III (**2**), an analogue of paclitaxel without the C13 side chain, which is isolated from *Taxus baccata*,⁴⁹ or fully synthesized⁵⁰ and at present is used extensively in the treatment of breast and ovarian cancers. It is also used for skin, lung, and head and neck carcinomas.⁵¹

Chemistry of this diterpinoid is very complex comprising of an unusual oxetane ring at C4-C5 and an isoserine side chain at C13 position. Although some therapeutically active paclitaxel analogues modified at C10 and C2 have been developed as advanced second generation taxoids,⁵² structural variations along the upper part at C6-C12 appear to have less impact on the bioactivity. The lower part, on the other hand, comprising of C14 and C1-C5 appears to be a region which is crucial to the activity. Most changes to the C and D rings, including opening of the oxetane ring, lead to loss of activity,⁵³ although some examples of C ring opened compounds that retain significant activity have been developed.⁵⁴

Extensive structure activity relationship (SAR) studies have provided insight into the structural determinants that are important for the activity of paclitaxel. It is now established that the A ring side chain at C13 with a C2'-OH, the C2 benzoyl group and an intact oxetane ring at C4-C5 are essential for both cytotoxicity and stabilization of MTs.^{55,56} The oxetane ring is a unique feature of paclitaxel and analogues prepared with an opened oxetane ring have a greatly reduced activity.⁵³

The C4 acetyl group does not appear to play a significant role in the biological activity but may contribute to the defined conformation of the molecule. The C1-OH group makes a significant contribution to the overall bioactivity.⁵³ The OH group at C7 is not essential for biological activity.⁵⁶

The structure of the TB/paclitaxel complex has been solved at 3.5 Å by electron crystallography,¹⁰ showing that paclitaxel binds β-TB within the lumen of MT (Figure 7). A considerable number of residues, mostly in the second domain of β-TB, are involved in direct contact with paclitaxel.

To date, more than 350 taxoids have been isolated from *Taxus* species, developed and characterized,^{57,58} but very few are found to be potent cytotoxins. Poor water solubility and a very low yield of paclitaxel motivated researchers to design and develop new analogues of paclitaxel that are more cytotoxic.

Docetaxol (**3**),⁵⁹ with minimal structural modifications at C13 side chain and C10 substitution showed more water solubility and more potency than paclitaxel, whereas baccatin, without C13 side chain, has no significant cytotoxicity. The C13 side chain could be a target for developing new analogues.

2-Debenzoyl-2-(*m*-azidobenzoyl)-paclitaxel (**4**), a C2 modified analogue, was found to be more potent ($IC_{50} = 0.31 \pm 0.01 \mu M$) than paclitaxel ($IC_{50} = 0.42 \pm 0.03 \mu M$).⁶⁰ 14β-Hydroxy-10-deacetylbaccatin III (14β-OHDAB, **5**), first isolated from the needles of Himalayan yew tree, has a higher water solubility.⁶¹

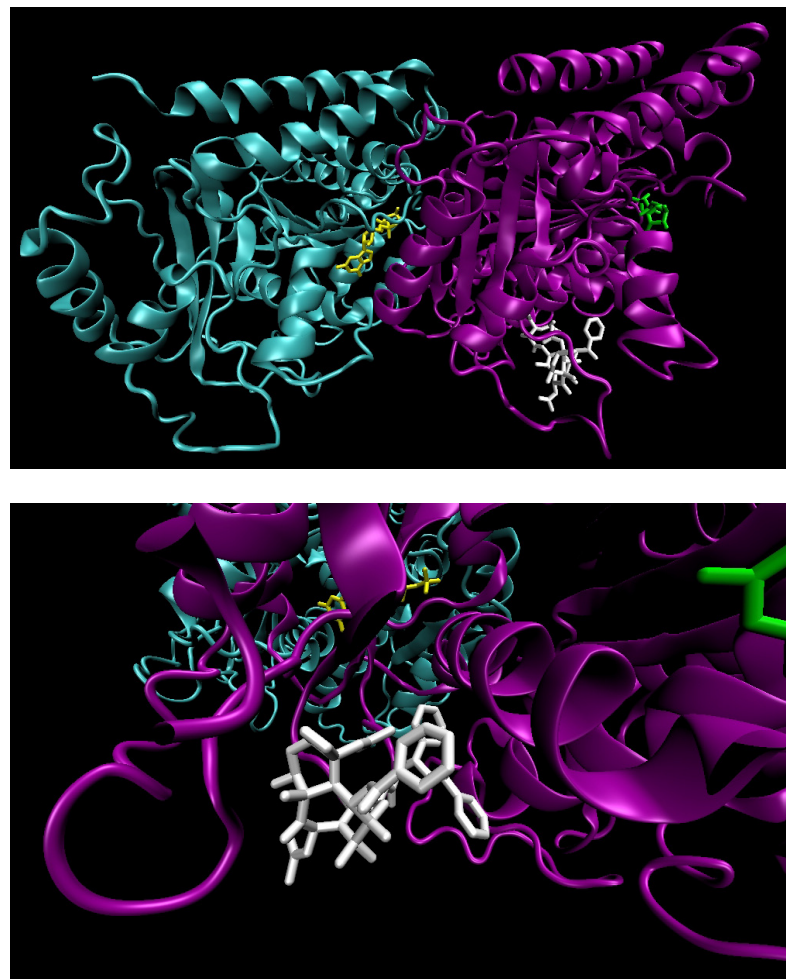


Figure 7. Ribbon diagram of the crystallography structure of $\alpha\beta$ -tubulin/paclitaxel complex (α -tubulin in cyan, β -tubulin in purple, GDP in green, GTP in yellow, paclitaxel in white; PDB code: 1JFF¹⁰).

New taxoids derived from it may show improved water solubility, bioavailability, and reduced hypersensitivity.⁵² Synthesis of second generation taxoids by appropriate modification at C3', C2 and acylation at C10, produces taxoids⁶²⁻⁶⁴ with extremely high potency against drug resistant cancer cells and compound **6** showed two orders of magnitude better activity than those of paclitaxel and docetaxel.⁵²

To evaluate the importance of the taxane core of taxoids, simplified compounds typified by compound **7** with the key pharmacophore properties of paclitaxel, phenylisoserine and an oxetane ring, were synthesised but none showed promising TB inhibitory activity.

This finding justifies the necessity of the diterpene ring.⁶⁵ Novel 7-deoxy-9-dihydropaclitaxel analogues, typified by compound **8**, have been synthesised and found to have potent selectivity against human liver cancer cells.⁶⁶

Synthesis of a new class of borneol esters **9** that might be considered as analogues of paclitaxel has been reported, but these compounds showed reduced cytotoxic activity.⁶⁷ Design of new taxanes has been directed towards solving the limitations of both solubility and resistance.

The paclitaxel ester of malic acid **10** has demonstrated improved solubility and enhanced *in vivo* antitumor activity against P388 murine leukemia indicating a higher therapeutic index than paclitaxel.⁶⁸

Chemical structures of compounds discussed in this section are presented in Figure 8.

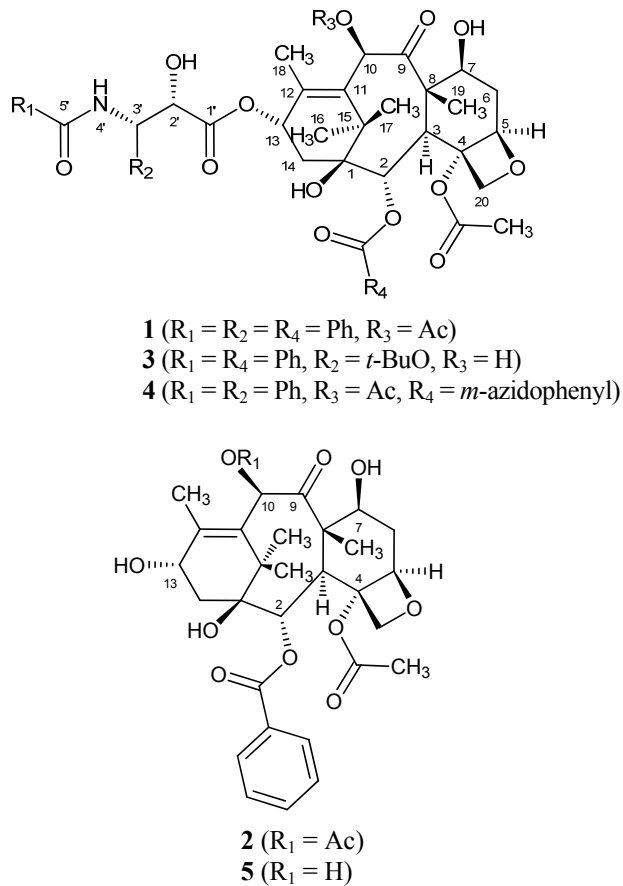


Figure 8. Paclitaxel site binding agents. (*Continued*)

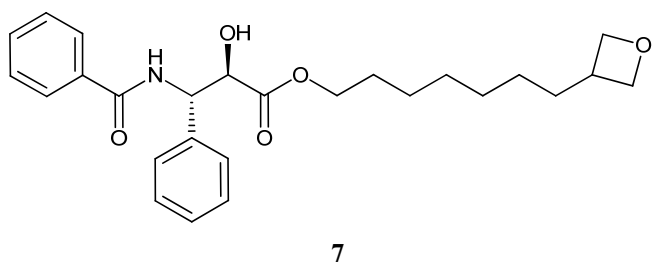
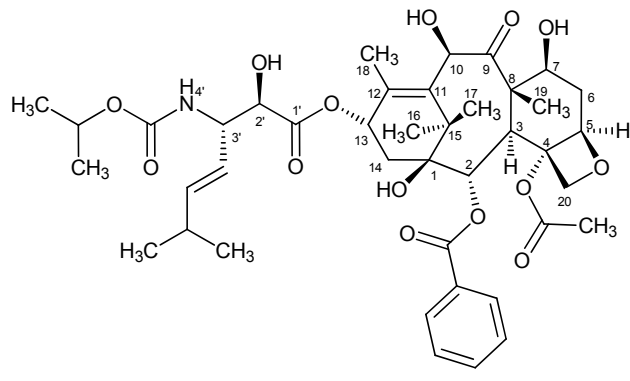


Figure 8. Paclitaxel site binding agents. (*Continued*)

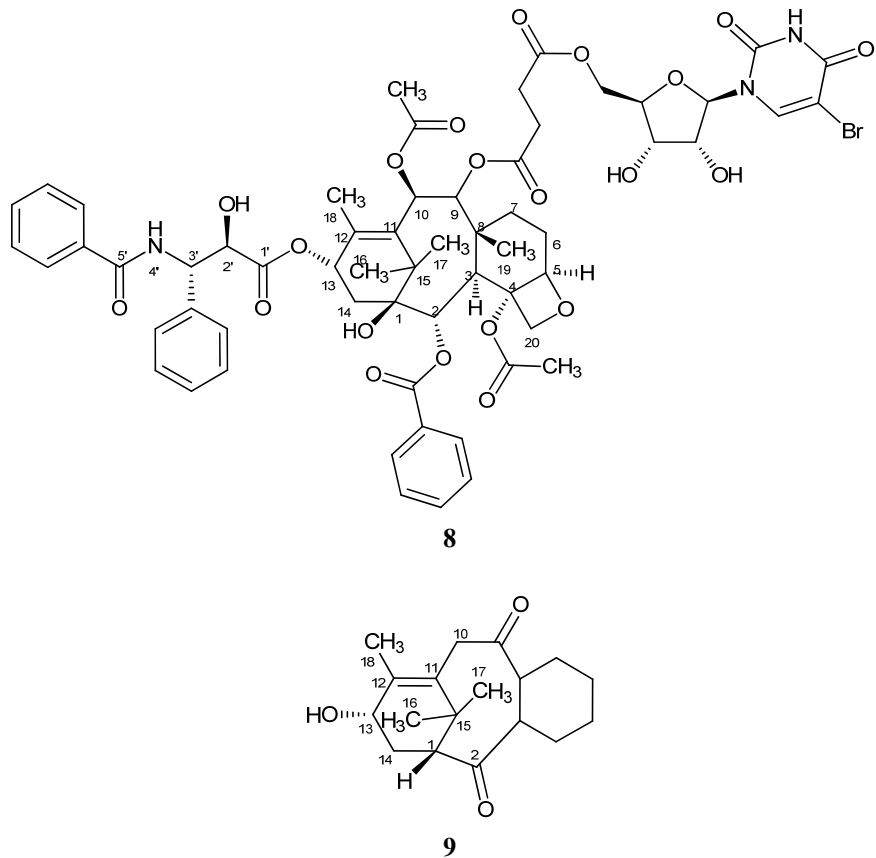
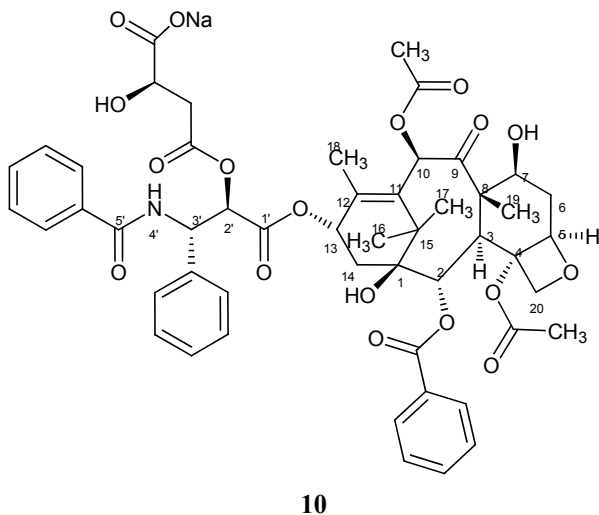


Figure 8. Paclitaxel site binding agents. (*Continued*)



10

Figure 8. Paclitaxel site binding agents.

3.2 Colchicine site binding agents

Colchicine (11), a well known alkaloid, obtained from *Colchicum autumnale* and other plants, a classic TB binding agent,⁶⁹ is used in the treatment of gout, familial Mediterranean fever and liver cirrhosis.⁷⁰ Colchicine binds to soluble TB and forms a TB/colchicine complex, followed by ligand-induced conformational changes in both TB and colchicine itself and thereby causes the MT spindle to disassemble in the metaphase of mitosis. Experimental data showed that colchicine binds to β -TB at its interface with α -TB,⁷¹ resulting in inhibition of TB polymerization. This binding mode was recently confirmed by the determination of a 3.58 Å X-ray structure of TB complexed with *N*-deacetyl-*N*-(2-mercaptopropionyl)colchicine (DAMA-colchicine), which is a close structural analogue of colchicine (Figure 9).¹² The binding site(s) of colchicine on TB have been extensively studied.^{72,73} It has been reported that the β -

subunit of TB is involved in colchicine binding, with the A ring of colchicine lying between Cys-354 and Cys-239 and C ring lying between the peptide region containing Cys-239 and the amino terminal β -TB sequence and region β :1-36.^{74,75}

The seven membered B ring and the C7 side chain are not believed to be crucial for TB binding but may affect the conformation of colchinooids and their TB binding properties.^{76,77} The trimethoxyphenyl group of the A ring of colchicine serves as a complex stabilizing anchor on TB in the inhibition of MTs assembly and is essential for its activity. An important structural feature of colchicine is the α -methoxytropolone, which constitutes the C ring portion of the colchicine molecule.

The tropolone ring and the C9 or C10 substitutes have been implicated in several aspects of the ligand-TB binding mechanism.⁷⁸ This drug has also been reported to bind to a second, lower affinity site on TB in a reversible manner.⁷⁹ Although colchicine is one of the oldest antimitotic drug, its toxicity is similar to its activity. Hundreds of colchicine analogues have been prepared in past decades, including compounds isolated from natural sources, partially synthesized from colchicine, and de novo synthesized. Some have been used clinically as antitumor agents, having less toxicity than colchicine. Most modified colchicine analogues share a common binding site on tubulin, common mechanisms for TB binding and similar pharmacological actions.

Colchicone (**12**), a non-nitrogen containing natural product isolated from *Colchicum richierii* and synthesised by Banwell *et al.* has been reported to show an inhibitory effect on TB polymerization.^{80,81} Compound **13**, a bicyclic analogue of colchicine binds rapidly and reversibly to colchicine binding site of TB, inhibits MTs assemble and promotes apoptosis in human leukemic cells. This drug produces reversible effects on MT disassembly, G2/M phase arrest, more water solubility and has lower toxicity than colchicine.⁸²

Among colchicine analogues, thiocolchicine (**14**) has shown more activity than the parent colchicines.

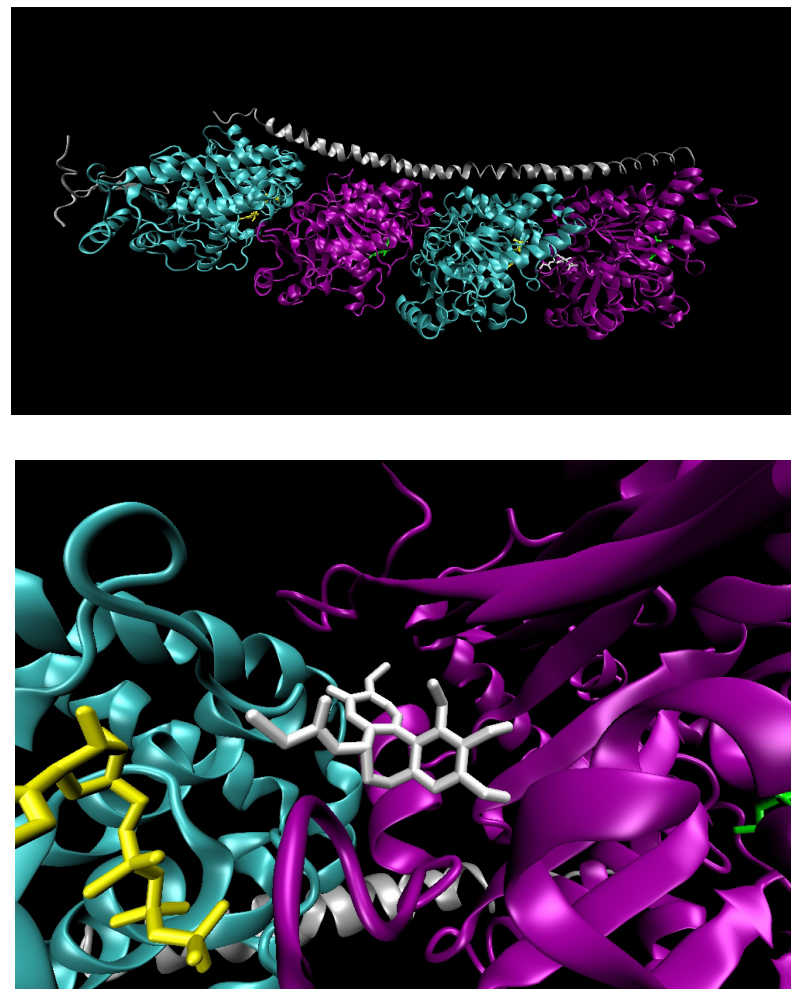


Figure 9. Ribbon diagram of the X-ray structure of tubulin($\alpha_1\beta_1\alpha_2\beta_2$)/stathmin-like domain/DAMA-colchicine complex (α_1 -, α_2 -tubulin in cyan, β_1 -, β_2 -tubulin in purple, GDP in green, GTP in yellow, stathmin-like domain in gray, DAMA-colchicine in white; PDB code: 1SA0¹²).

Most natural analogues are modified in the C7 side chain substituents except allocolchicine (**15**), with an aromatic 6-member ring and a COOCH₃ substituent at C10, and cornigerine (**16**) with an OCH₃ substituent at C10, which have both been obtained from *Colchicum cornigerum*.⁸³ Allocolcichicine which has also been isolated from *Colchicum autumnale* and *N*-acetylcolchinol *O*-methylether, a semisynthetic analogue obtained by reaction of colchicine with hydrogen peroxide, are both more potent inhibitors than colchicine.^{84,85}

Podophyllotoxin (**17**) and its related analogues were isolated from *Podophyllum peltatum* and related species. Podophyllotoxin and its related analogues (**18**, **19**) bind to TB protein at the colchicine site and competitively inhibit colchicine binding to TB although a recent computer modelling study suggested incomplete overlap of the colchicine and podophyllotoxin binding site(s).⁸⁶

Etoposide (**20**) is a potent topoisomerase II (an enzyme involved in the folding and unfolding of DNA during cell replication) inhibitor but a weak TB inhibitor.⁸⁷

It has also been reported that their predominant function is inhibiting topoisomerase II rather than a microtubular interaction.⁸⁸ Etoposide is currently used in the treatment of small cell lung, testicular and malignant lymphoid cancers, among others.⁸⁹ It is also used in combination chemotherapy. Teniposide (**21**) appears to be a less useful clinical agent though it is undergoing trials in combination therapy for the treatment of metastatic brain tumors.⁹⁰ Combretastatin A-4 (**22**), an antineoplastic agent isolated from *Combretum caffrum*,⁹¹ is a simple compound that show antimitotic effects by interacting with the colchicine binding site of TB. Combretastatin A-4 is one of the most potent inhibitors of colchicine binding presently known.⁹² Naturally occurring and synthetic combretastatin and its analogues (**23**, **24**) were identified as antimitotic agents binding to colchicine binding sites.⁹¹ Combretastatin A-4, the most potent cancer cell growth inhibitor of the series,⁹³ is not recognised by the multi-drug resistance (MDR) pump, a cellular pump which rapidly ejects foreign molecules including many anticancer drugs.⁹⁴

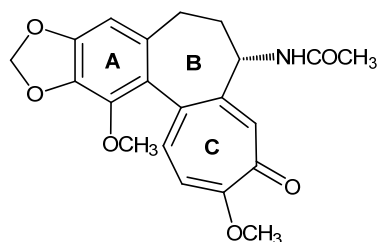
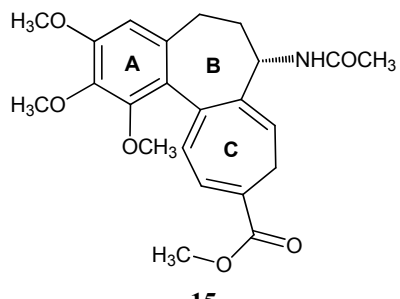
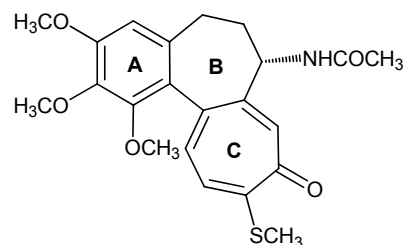
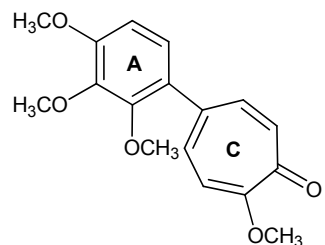
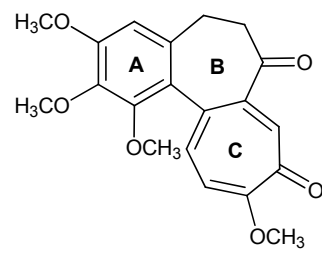
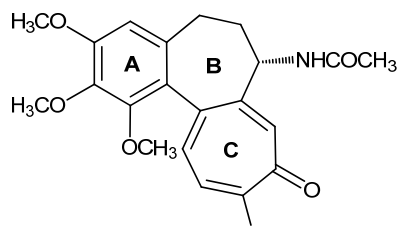


Figure 10. Colchicine binding site agents. (*Continued*)

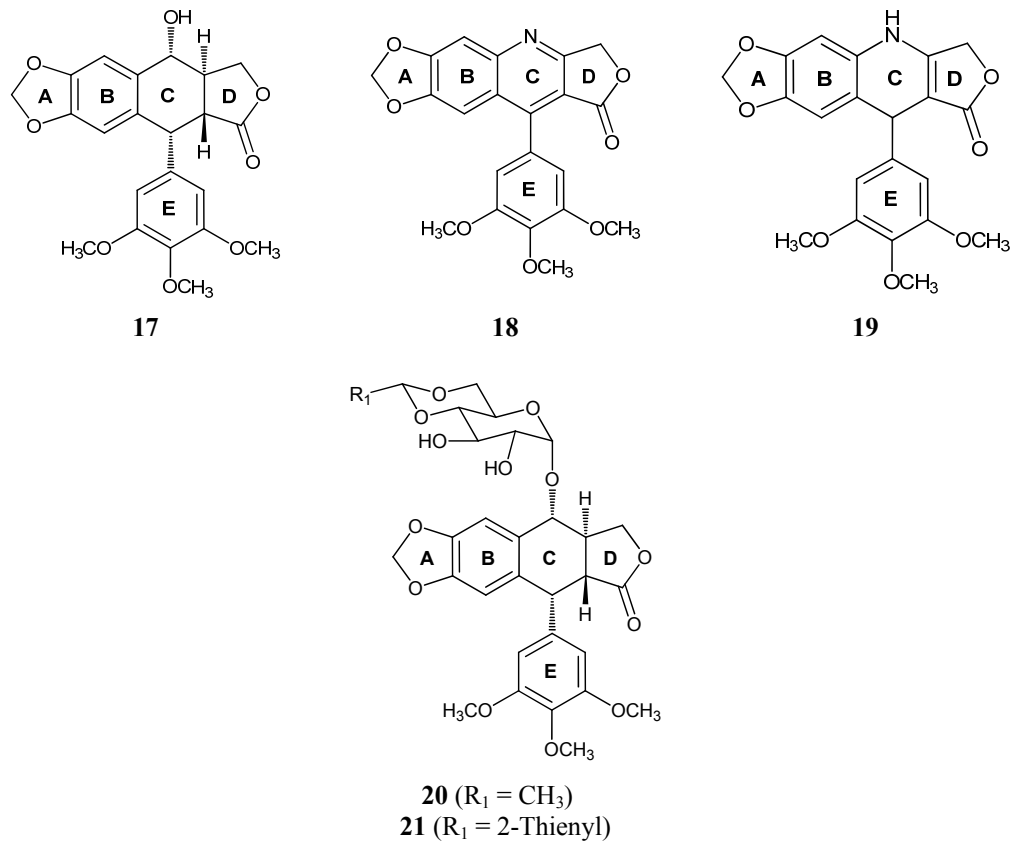


Figure 10. Colchicine binding site agents. (*Continued*)

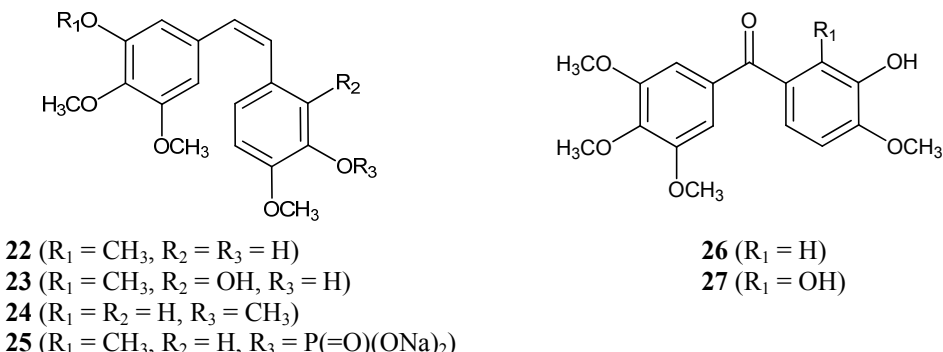


Figure 10. Colchicine binding site agents.

It has also been reported that this compound can inhibit angiogenesis, a process essential for tumour growth.⁹⁵ Combretastatin A-4 itself is insoluble and several attempts have been made to produce an active water soluble derivative.^{96,97} The most effective is the disodium phosphate salt **25** (>20 mg/ml) and is the form of combretastatin A-4 presently in phase II clinical trials.^{98,99} SAR of combretastatin A-4 led to the discovery of the potent cancer cell growth inhibitor phenstatin (**26**) and hydroxyphenstatin (**27**), which showed remarkable antineoplastic activity by inhibiting TB polymerization.

Chemical structures of compounds discussed in this section are presented in Figure 10.

3.3 Vinca alkaloid site binding agents

Vinca alkaloids, vincristine (**28**) and vinblastine (**29**), are the most useful class of antimitotic anticancer agents for the treatment of leukemias, lymphomas and some solid tumours.¹⁰⁰ These agents, isolated from *Catharanthus roseus*, are widely used as anticancer drugs.^{101,102} Vinca alkaloids prevent MT assembly by binding to TB at

a site distinct from colchicine and by blocking the region involved in heterodimer attachment.¹⁰⁰ Vinca alkaloids bind to TB very close to GTP site that is located at both the α and β -subunits with primary sequences around α -339 and β -390 residues.¹⁰³ The structure of vinblastine bound to the TB/stathmin-like domain/vinblastine complex was determined at 4.1 Å resolution by X-ray diffraction (Figure 11).¹⁰⁴ Unlike colchicine, vinca alkaloids bind to TB rapidly, reversibly and temperature independently.^{73,83} The SAR, pharmacology and clinical uses of vinca alkaloids have been reviewed.¹⁰⁵ After the establishment of vinca alkaloids as promising anticancer agents, efforts have been made to develop new congeners that are more effective, have less side effects and have a broad spectrum of antitumor activity. The basic structure of vinca alkaloids is composed of a catharenthine moiety and vindoline nucleus and these alone cannot inhibit MT assembly.¹⁰⁰ Most of the semisynthetic or totally synthetic vinca alkaloids drugs have been developed by the modification of C4, C23, C3' and C4' position of parent vinca alkaloids.¹⁰⁵

Vindesine (**30**), the first semisynthetic vinca alkaloid, was developed by changing the C23 acetyl group in vinblastine to an amide.¹⁰⁶ Modifying the vindoline moiety with L-tryptophane at C23 led to the development of vintripolone (**31**).¹⁰⁷

Vinxaltin (**32**) is in phase II clinical trial for advanced breast cancer showing an excellent antitumour profile.¹⁰⁷ Another semisynthetic compound vinorelbine (**33**) showed promising activity against breast cancer¹⁰⁸ and is in clinical trial for the treatment of other types of tumours.¹⁰⁹ This drug exhibited superior antimitotic activity over others with lower reversible neurotoxicity.

Further modifications in vinorelbine led to the discovery of vinflunine (**34**) which showed significantly superior anticancer activity *in vivo* as compared to vinorelbine.¹¹⁰

Chemical structures of compounds discussed in this section are presented in Figure 12.

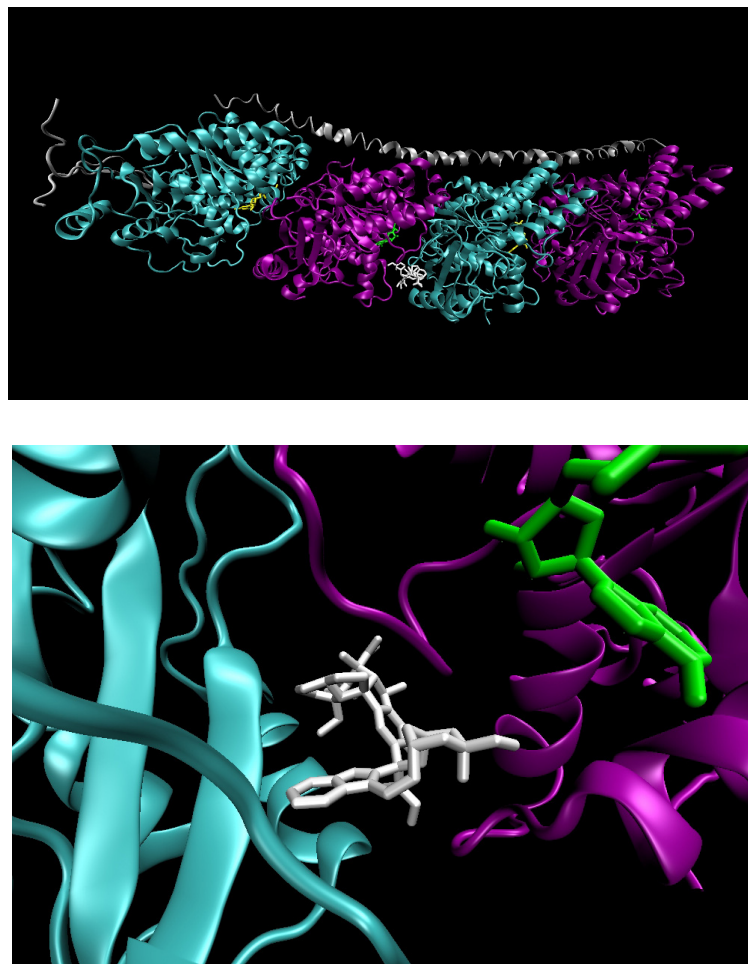


Figure 11 Ribbon diagram of the X-ray structure of tubulin($\alpha_1\beta_1\alpha_2\beta_2$)/stathmin-like domain/vinblastine complex (α_1 -, α_2 -tubulin in cyan, β_1 -, β_2 -tubulin in purple, GDP in green, GTP in yellow, stathmin-like in gray, vinblastine in white; PDB code: 1Z2B¹⁰⁴).

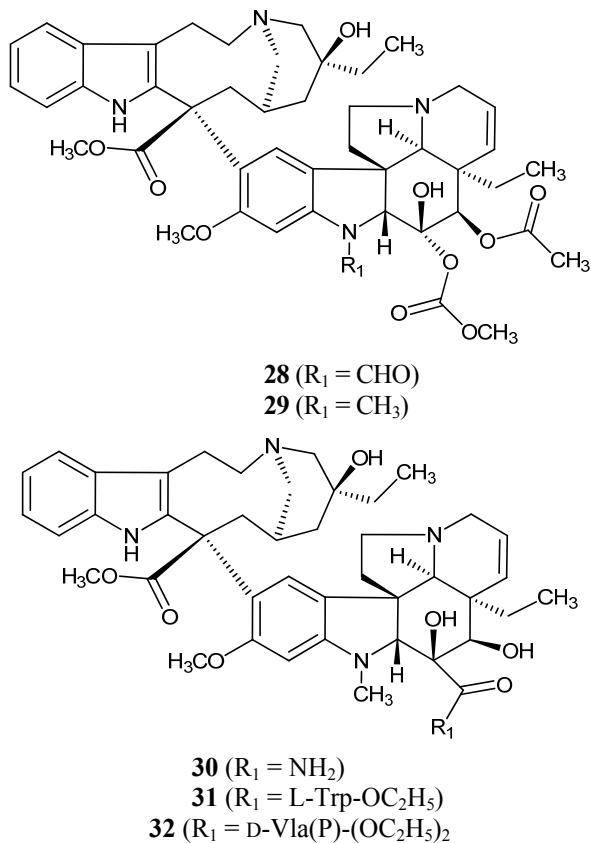


Figure 12. Vinca alkaloid site binding agents. (*Continued*)

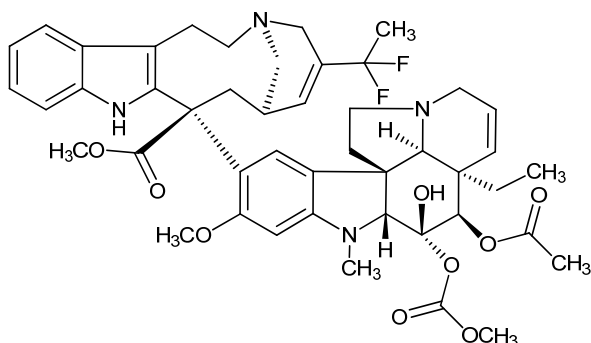
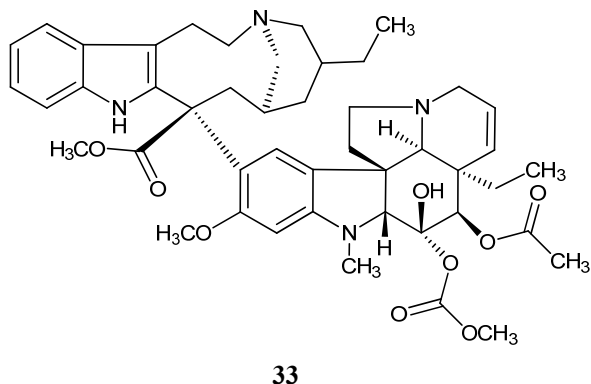


Figure 12. Vinca alkaloid site binding agents.

4. Arylthioindoles, potent inhibitors of tubulin polymerization

Paclitaxel and vinca alkaloids are clinically important chemotherapeutic drugs, and are widely used for the treatment of a variety of tumors. However, side effects and drug resistance reduce their efficacy. Neurological and haematological side effects are the principal and often dose-limiting toxicities.¹¹¹ Drug resistance is another factor hampering the clinical applicability of microtubule targeting agents, involving the overexpression of drug efflux pumps, and alterations in TB/MTs.¹¹²

These findings highlight the need for novel TB dynamic inhibitors. Furthermore, while drugs that act on the vinca and taxane sites have well-established roles in the treatment of human cancers, the therapeutic potential of the colchicine site in cancer treatment has yet to be realized. Recently, we reported a novel class of TB assembly inhibitors, arylthioindoles (ATIs, general structure **35**), that bind to the colchicine site on β -TB close to interface with α -TB.¹¹³⁻¹¹⁵ ATIs efficiently inhibit tubulin polymerization and cancer cell growth, with activities comparable with those of colchicine (**11**) and CSA4 (**22**). To rationalize the structure-activity relationship (SAR) studies we dissected the ATI structure into four regions: (A) the substituent at position 2 of the indole, (B) the sulfur atom bridge, (C) the 3-arylthio group, and (D) the substituent at position 5 of the indole (Figure 13). In our previous papers we reported SAR and molecular modeling studies on ATI derivatives differing in substituent groups and/or position at the A, C and D regions.^{114,115}

However, chemical modification of the sulphur bridge (B region) was not exhaustively explored, although five ATIs were transformed into the corresponding sulphur dioxides.¹¹⁴ Furthermore the sulphur atom could be converted *in vivo* to corresponding inactive sulfone by human oxidase. In contrast to the weak potency displayed by dioxides,¹¹⁴ several CSA4 analogues, characterized by a carbonyl functionality as a bridging group between the indole nucleus and the trimethoxyphenyl ring, show potent inhibition of tubulin polymerization.¹¹⁶

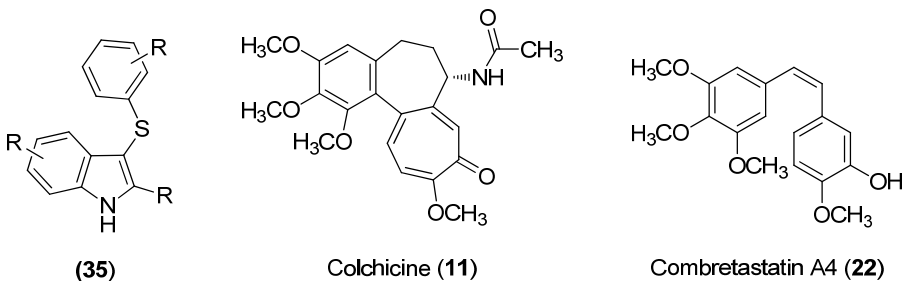


Figure 13. General structure of ATI's (**35**) and reference compounds **11** and **22**.

However, in comparing ATIs with the 3-aryloylindoles reported by Hsieh and coworkers,¹¹⁷ we should note that these two groups of compounds are significantly different, since there are major differences in our SAR findings and those of Hsieh's group. Moreover, our molecular modeling studies indicate that in the colchicine site of tubulin, ATI derivatives preferentially assume a colchicine-like rather than a CSA4-like binding conformation.¹¹³⁻¹¹⁵ These observations prompted the SAR investigations at the B bridge. To this end, we synthesized new indole derivatives by bioisosteric replacement of the sulphur bridge of the ATI's with either carbonyl or methylene moieties, and other related groups (compounds **36-78**, Figure 14, Table 1 and Table 2). The more active compounds, bearing a sulphur or carbonyl bridge and a methoxycarbonyl group at position 2 of indole nucleus, showed an antitumor activity comparable to colchicine (**11**) and CSA4 (**22**).

Modeling studies^{113-115,128} showed that the ester group access to an hydrophobic pocket, this could increase the stability of the ligand/receptor complex. It was confirmed by biological tests.

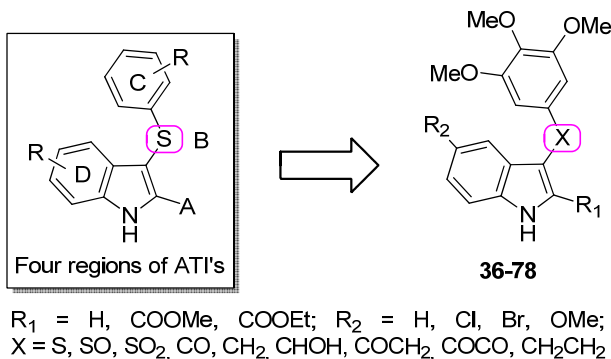
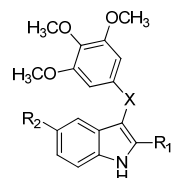


Figure 14. Structure of compounds **36-78**.

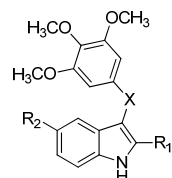
However, ester derivative **42** was extensively transformed to inactive acid in metabolic stability experiments assessed in mouse and human liver microsomes (Table 16). From previous SAR studies at the (A) region, the elongation of the 2-methoxy- or 2-ethoxycarbonyl group by means of C3-C5 alkoxy chains or its replacement with carboxyamide function lead to a decrease or complete loss of both antitubulin and antiproliferative activities, respectively.^{113,114} Therefore, we planned to replace the ethoxycarbonyl group of **42** (A region) with potentially more stable 5-membered heterocyclic nucleus (pyrrole, furan and thiophene) and aromatic group (phenyl, pyridine and naphthyle) as bioisosteres¹¹⁸ (Figure 15 A). Modeling studies showed that, with respect to the small/medium linear chain,¹¹⁴ the 5-membered heterocycle at the position 2 of the indole nucleus could form new hydrophobic interactions with Lys254 and Leu248 into the colchicine site of tubulin (Figure 15 B). Here, we report the discovery of new potent ATI derivatives designed by replacing the ester group of **42** in turn with pyrrole, furane, thiophene, phenyle, pyridine and naphthyle (Table 3 and Table 4).



36-57

Cpd	R ₁	R ₂	X
36	H	H	S
37	H	H	C=O
38	H	H	CH ₂
39	COOMe	H	S
40	COOMe	H	C=O
41	COOMe	H	CH ₂
42	COOEt	H	S
43	COOEt	H	C=O
44	COOEt	H	CH ₂
45	H	5-Cl	S
46	H	5-Cl	C=O
47	H	5-Cl	CH ₂
48	COOMe	5-Cl	S
49	COOMe	5-Cl	C=O
50	COOMe	5-Cl	CH ₂
51	COOEt	5-Cl	S
52	COOEt	5-Cl	C=O
53	COOEt	5-Cl	CH ₂
54	COOEt	5-Cl	COCH ₂
55	COOEt	5-Cl	COCO
56	COOEt	5-Cl	CH ₂ CH ₂
57	H	5-Br	S

Table 1. Structure of compounds **36-57**.

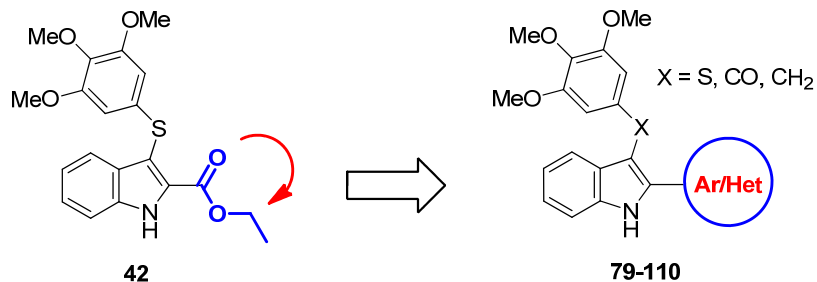


58-78

Cpd	R ₁	R ₂	X
58	H	5-Br	C=O
59	H	5-Br	CH ₂
60	COOMe	5-Br	S
61	COOMe	5-Br	C=O
62	COOMe	5-Br	CH ₂
63	COOEt	5-Br	S
64	COOEt	5-Br	C=O
65	COOEt	5-Br	CH ₂
66	H	5-OMe	S
67	H	5-OMe	C=O
68	H	5-OMe	CH ₂
69	COOMe	5-OMe	S
70	COOMe	5-OMe	S=O
71	COOMe	5-OMe	S(=O) ₂
72	COOMe	5-OMe	C=O
73	COOMe	5-OMe	CHOH
74	COOMe	5-OMe	CH ₂
75	COOEt	5-OMe	S
76	COOEt	5-OMe	C=O
77	COOEt	5-OMe	CHOH
78	COOEt	5-OMe	CH ₂

Table 2. Structure of compounds **58-78**.

A



B

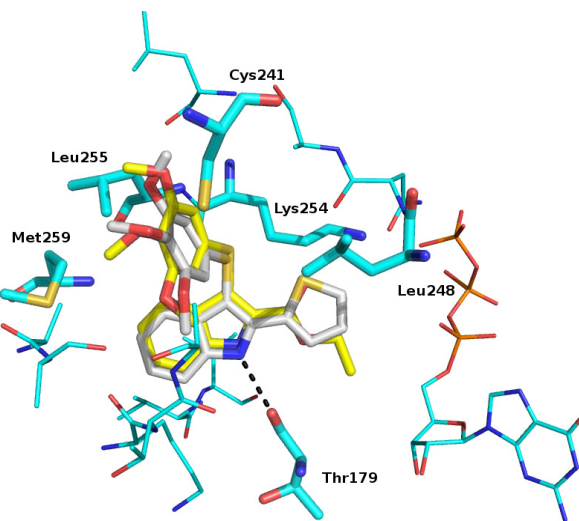
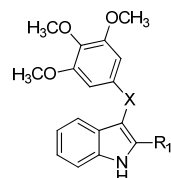


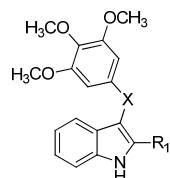
Figure 15. A: new ATIs **79-110**. B: Binding mode proposed by PLANTS for **42** (yellow stick) and **90** (white stick) into the colchicine site. H-bond is shown as a light gray dotted line. Residues of the binding site and GTP are also reported as lines.



79-95

Cpd	R ₁	X
79	Pyrrol-2-yl	S
80	Pyrrol-2-yl	C=O
81	Pyrrol-3-yl	S
82	Pyrrol-3-yl	C=O
83	Pyrrol-3-yl	CH ₂
84	Furan-2-yl	S
85	Furan-2-yl	C=O
86	Furan-2-yl	CH ₂
87	Furan-3-yl	S
88	Furan-3-yl	C=O
89	Furan-3-yl	CH ₂
90	Thiophen-2-yl	S
91	Thiophen-2-yl	C=O
92	Thiophen-2-yl	CH ₂
93	Thiophen-3-yl	S
94	Thiophen-3-yl	C=O
95	Thiophen-3-yl	CH ₂

Table 3. Structure of compounds **79-95**.



96-110

Cpd	R ₁	X
96	Phenyl	S
97	Phenyl	C=O
98	Phenyl	CH ₂
99	Pyridin-2-yl	S
100	Pyridin-2-yl	C=O
101	Pyridin-3-yl	S
102	Pyridin-3-yl	C=O
103	Pyridin-4-yl	S
104	Pyridin-4-yl	C=O
105	α-naphthyl	S
106	α-naphthyl	C=O
107	α-naphthyl	CH ₂
108	β-naphthyl	S
109	β-naphthyl	C=O
110	β-naphthyl	CH ₂

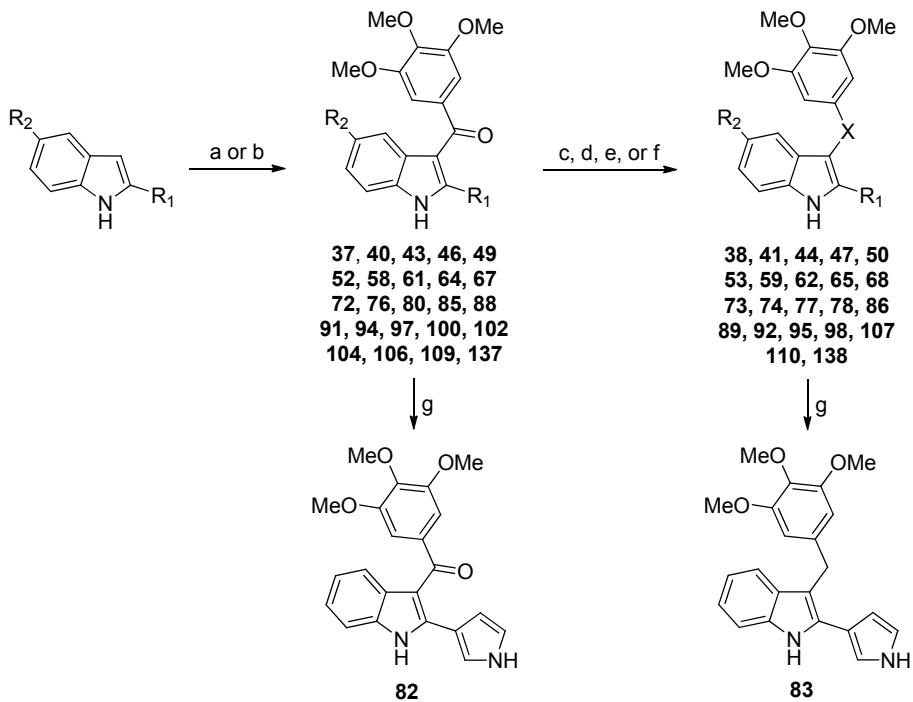
Table 4. Structure of compounds **96-110**.

5. Chemistry

Compounds **37**, **40**, **43**, **46**, **49**, **52**, **58**, **61**, **64**, **67**, **72**, **76**, **85**, **88**, **91**, **94**, **97**, **106**, **109** and **137** were synthesized in a microwave (MW) reactor by treating the appropriate indole with 3,4,5-trimethoxybenzoyl chloride in the presence of aluminium chloride in 1,2-dichloroethane at 110 °C (150 W) for 2 min. The subsequent basic hydrolysis of **137** furnished compound **82** (Scheme 1). Similarly, ethyl 5-chloro-3-[2-(3,4,5-trimethoxyphenyl)acetyl]-1*H*-indole-2-carboxylate **54** was prepared by MW synthesis using ethyl 5-chloro-1*H*-indole-2-carboxylate and 2-(3,4,5-trimethoxyphenyl)acetyl chloride. The latter reagent was obtained by treating the appropriate carboxylic acid with oxalyl chloride in the presence of a catalytic amount of DMF in anhydrous THF at 0 °C for 10 min (Scheme 2). Reaction of the appropriate indole with 3,4,5-trimethoxybenzoyl chloride and methyl magnesium bromide in the presence of SnCl₄ and ZnCl₂ furnished the derivates **80**, **100**, **102** and **104** (Scheme 1). Sodium borohydride (10 eq) reduction of **37**, **46**, **58**, **67** and **91** in boiling ethanol for 3 h furnished the corresponding benzyl derivatives **38**, **47**, **59**, **68**, and **92**, respectively (Scheme 1). Alternatively, benzyl (**41**, **44**, **50**, **53**, **62**, **65**, **74** and **78**) and phenylethyl (**56**) derivatives were obtained in good yield by treating benzoyl (**40**, **43**, **49**, **52**, **61**, **64**, **72** and **76**) (Scheme 1) or oxalyl (**55**) (Scheme 2) compounds with triethylsilane in trifluoroacetic acid at 25 °C for 12 h. Reduction of ketones **72** and **76** with sodium borohydride (1 eq) in refluxing aqueous THF for 2 h gave the corresponding alcohols **73** and **77** (Scheme 1).

MW oxidation of ethyl 3-[2-(3,4,5-trimethoxyphenyl)acetyl]-1*H*-indole-2-carboxylate (**54**) with selenium(IV) oxide in dimethylsulfoxide (DMSO) at 150 °C (150 W) for 2 min furnished the corresponding 2-oxo derivative **55** (Scheme 2).

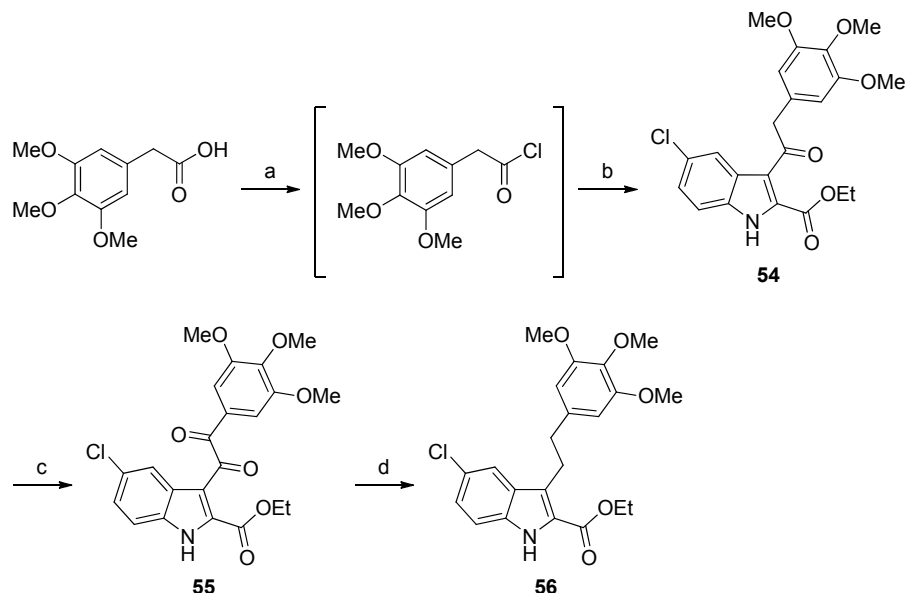
Compounds **86**, **89**, **95**, **98**, **107**, **110** and **138** was prepared by treatment of respective ketones (**85**, **88**, **94**, **97**, **106**, **109** and **137**) with BH₃-THF complex in acetonitrile and methanol at 70 °C for 1 h. The following basic hydrolysis of **138** gave compound **83** (Scheme 1).



137,138 $\text{R}_1 = (1\text{-phenylsulfonyl})\text{pyrrol-3-yl}; \text{R}_2 = \text{H}$

^aReagents and reaction conditions: (a) ($\text{R}_1 = \text{H, COOMe, COOEt, (1-phenylsulfonyl)pyrrol-3-yl, furan-2(3)-yl, thiophen-2(3)-yl, phenyl, } \alpha\text{-}(\beta)\text{-naphthyl; R}_2 = \text{H, Cl, Br, OMe}$) 3,4,5-trimethoxybenzoyl chloride, AlCl_3 , 1,2-dichloroethane, closed vessel, 110°C , 150 W, $\text{Pmax} = 250$ PSI, 2 min, 30-95%; (b) ($\text{R}_1 = \text{pyrrol-2-yl, pyridin-3(4)(5)-yl; R}_2 = \text{H}$) 3,4,5-trimethoxybenzoyl chloride, 3 M CH_3MgBr , 1 M SnCl_4 , ZnCl_2 , anhydrous CH_2Cl_2 , Ar stream, 25°C , 12 h, 3-70%; (c) ($\text{R}_1 = \text{H, thiophen-2-yl; R}_2 = \text{H, Cl, Br, OMe}$) NaBH_4 (10 eq), EtOH , reflux, 3 h, 42-68%; (d) ($\text{R}_1 = \text{COOMe, COOEt; R}_2 = \text{H, Cl, Br, OMe}$) Et_3SiH , CF_3COOH , 25°C , overnight, 46-90%; (e) ($\text{R}_1 = \text{COOMe, COOEt; R}_2 = \text{OMe}$) NaBH_4 (1 eq), $\text{THF/H}_2\text{O}$, reflux, 2 h, 29-53%; (f) ($\text{R}_1 = \text{pyrrol-2-yl, (1-phenylsulfonyl)pyrrol-3-yl, furan-2(3)-yl, thiophen-3-yl, phenyl, } \alpha\text{-}(\beta)\text{-naphthyl; R}_2 = \text{H}$) BH_3/THF , $\text{CH}_3\text{CN}/\text{MeOH}$, 50°C , 1 h, 10-99%; (g) ($\text{R}_1 = (1\text{-phenylsulfonyl})\text{pyrrol-3-yl; R}_2 = \text{H}$) 2N NaOH , MeOH , 70°C , 1 h, 20-98%.

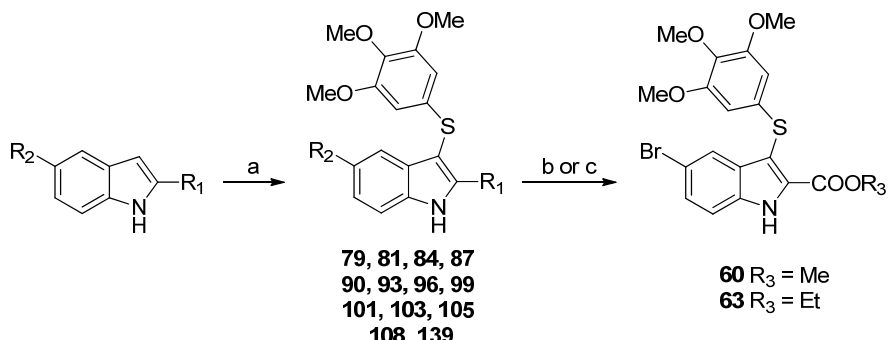
Scheme 1. Synthesis of ketones, alcohols and methylene derivates.



^aReagents and reaction conditions: (a) oxalyl chloride, anhydrous DMF cat., anhydrous THF, 0 °C, 10 min; (b) ethyl 5-chloro-1*H*-indole-2-carboxylate, AlCl₃, 1,2-dichloroethane, closed vessel, 110 °C, 150 W, Pmax = 250 PSI, 2 min, 32%; (c) selenium(IV) oxide, DMSO, closed vessel, 150 °C, 150 W, Pmax = 250 PSI, 2 min, 56%; (d) Et₃SiH, CF₃COOH, 25 °C, overnight, 40%.

Scheme 2. Synthesis of compounds 54-56.

Compounds **79**, **81**, **84**, **87**, **90**, **93**, **96**, **99**, **101**, **103**, **105**, **108** and **139** were obtained by MW reaction of appropriate indole with bis-(3,4,5-trimethoxyphenyl)disulfide¹¹³ in the presence of sodium hydride in anhydrous DMF at 110 °C (150 W) for 2 min (Scheme 3).



139 R₁ = COOH; R₂ = Br

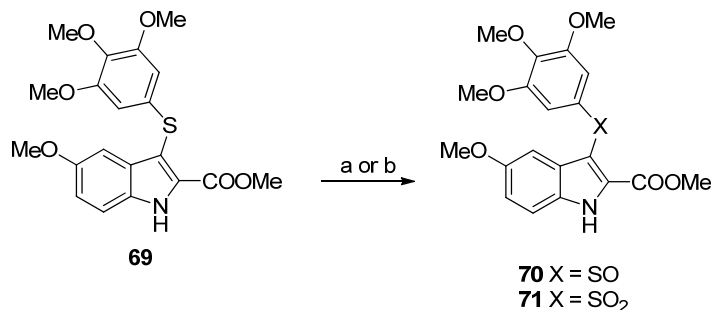
R₁ = COOH, pyrrol-2(3)-yl, furan-2(3)-yl, thiophen-2(3)-yl, phenyl, pyridin-2(3)(4)-yl, α-(β)-naphthyl; R₂ = H, Br

^aReagents and reaction conditions: (a) NaH, bis(3,4,5-trimethoxyphenyl)disulfide, anhydrous DMF, closed vessel, 110 °C, 150 W, Pmax = 250 PSI, PowerMAX, 2 min; (b) (60) TMSDM, CH₂Cl₂/MeOH, 25 °C, 30 min, 79%; (c) (63) SOCl₂, absolute EtOH, 65 °C, 2 h, Ar stream, 70%.

Scheme 3. Synthesis of sulphur derivatives.

The crude carboxylic acid (**139**) was transformed into the corresponding methyl ester **60** with trimethylsilyldiazomethane (TMSDM) in dichloromethane/methanol at 25 °C for 30 min or into the ethyl ester **63** with thionyl chloride in absolute ethanol at 65 °C for 2 h (Scheme 3). Oxidation of methyl 5-methoxy-3-(3,4,5-trimethoxyphenylthio)-1*H*-indole-2-carboxylate (**69**)¹¹³ with 1 or 2 eq of 3-chloroperoxybenzoic acid (MCPBA) in chloroform at 25 °C for 1.5 h gave the corresponding sulfoxide (**70**) or sulfone (**71**) derivatives, respectively (Scheme 4). The required indoles (**117-122**) was prepared by intramolecular cyclization of the

corresponding hydrazone (**111-116**) in polyphosphoric acid (PPA) as a catalyst, according to Fischer's indole synthesis (Scheme 5). The needed hydrazones (**111-116**) was obtained by MW reaction of 4-bromophenylhydrazine and phenylhydrazine hydrochloride with appropriate ketone and sodium acetate in ethanol at 100 °C (250 W) for 5 min (Scheme 5). MW hydrolysis of ester **117** with 3 N sodium hydroxide at 110 °C (150 W) for 1 min furnished 5-bromo-1*H*-indole-2-carboxylic acid (**123**), which was transformed into the corresponding methyl ester **124** by treatment with thionyl chloride in anhydrous methanol at 65 °C for 2 h (Scheme 5). Treatment of 1-*H*-indole with bromine and subsequent reaction of **125** with pyrrole in the presence of trifluoro acetic acid furnished **126** (Scheme 6a).



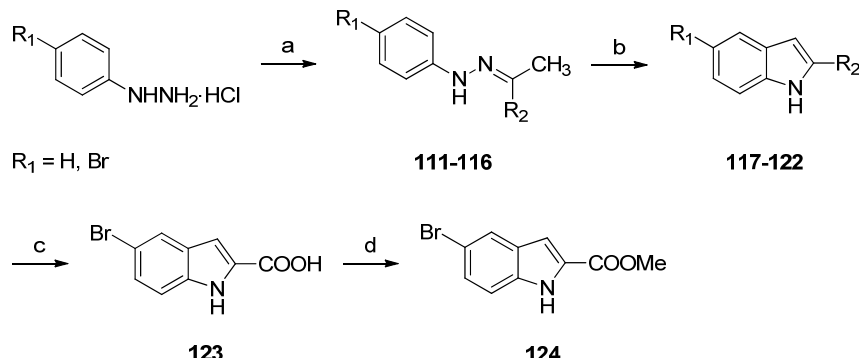
^aReagents and reaction conditions: (a) (**70**) MCPBA (1 eq.), CHCl₃, 25 °C, 1.5 h, 99%;
(b) (**71**) MCPBA (2 eq.), CHCl₃, 25 °C, 1.5 h, 96%.

Schema 4. Synthesis of compound **69-71**.

The chloride of 2-nitrophenyl acetic acid was treated with 1-(phenylsulfonyl)-1*H*-pyrrole in the presence of anhydrous aluminium chloride to give the intermediate **127**, which underwent intramolecular cyclization to **128** with iron powder in glacial

acetic acid at 60 °C (Scheme 6b). Reaction of 2-iodo-1*H*-indole¹¹⁹ (**129**) with the pinacol ester of furan-3-boronic acid in the presence of Pd(II) acetate, potassium carbonate in a closed vessel at 110 °C (200 W) for 15 min gave **130** (Scheme 7a).

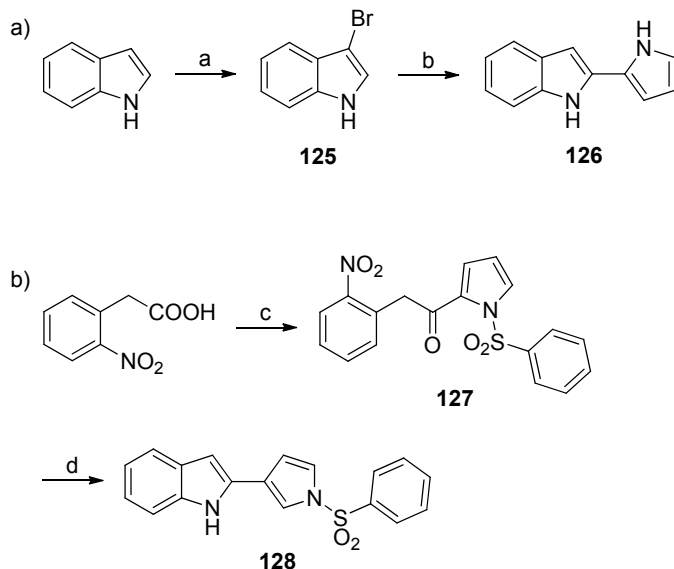
2-Acetyl- and 3-acetylthiophene were brominated to **131** and **132** and transformed into **133** or **134**, respectively, by reaction with aniline in the presence of a catalytic amount of DMF in a closed vessel at 100 °C (150 W) for 1 min (Scheme 7b). Heated at 170 °C of aniline and **135**, prepared by reaction of 2-acethyl naphthalene and bromine, gave **136** (Scheme 7c).



111, 117 R₁ = Br, R₂ = COOEt; **112, 118** R₁ = H, R₂ = furan-2-yl; **113, 119** R₁ = H, R₂ = pyridin-2-yl; **114, 120** R₁ = H, R₂ = pyridin-3-yl; **115, 121** R₁ = H, R₂ = pyridin-4-yl; **116, 122** R₁ = H, R₂ = β -naphthyl

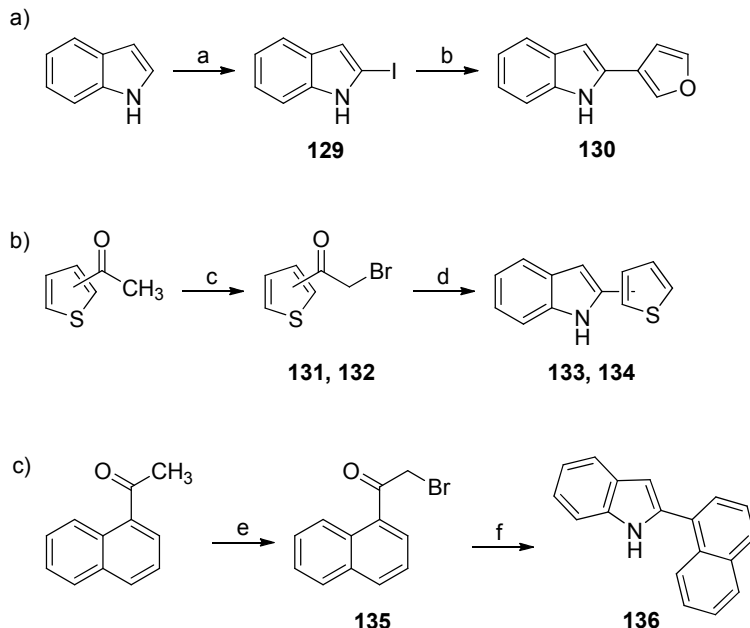
^aReagents and reaction conditions: (a) ethyl pyruvate, 2-acetyl furane, 2-(3)(4)acetylpyridine or 2-acetyl naphthalene, CH₃COONa, EtOH, open vessel, 100 °C, 250 W, PowerMAX, 5 min, 85–96%; (b) PPA, 110 °C, 30 min, 45–75%; (c) 3 N NaOH, closed vessel, 110 °C, 150 W, 1 min, 95%; (d) SOCl₂, absolute MeOH, 65 °C, 2 h, Ar stream, 96%.

Scheme 5. Synthesis of compounds **111-124**.



^aReagents and reaction conditions: (a) bromine, anhydrous DMF, 25 °C, 30 min, light protected; (b) 1-*H*-pyrrole, CF₃COOH, CH₂Cl₂, 25 °C, 20 min, 18%; (c) (i) oxalylchloride, catalytic anhydrous DMF, 1,2-dichloroethane, 0 °C, Ar stream, 30 min (ii) 1-(phenylsulfonyl)-1-*H*-pyrrole, AlCl₃, 0 °C, Ar stream, 15 min, yield 10%; (d) Fe, AcOH, 60 °C, overnight, yield 10%.

Schema 6. Synthesis of compounds **125-128**.



^aReagent and reaction conditions: (a) (i) *n*-butyllithium 2.5 M, CO₂, anhydrous THF, -78 °C, Ar stream, 1 h (ii) *tert*-butyllithium 1.7 M, 1,2-diidoethane, anhydrous THF, 2 h, -78 °C, Ar stream, 90%; (b) 3-furan boronic acid pinacol ester, Pd(II) acetate, K₂CO₃, NMP/H₂O, closed vessel, 200 W, 110 °C, Pmax = 250 PSI, 15 min, 95%; (c) bromine, CH₂Cl₂, 25 °C, 1 h, 57-80%; (d) (i) aniline, 25 °C, 3 h; (ii) catalytic anhydrous DMF, closed vessel, 100 °C, 150 W, Pmax = 250 PSI, 1 min, 16-40%; (e) bromine, CH₂Cl₂, 25 °C, 1 h, 90%; (f) aniline, *N,N*-dimethylaniline, 170 °C, 15 min, 30%.

Scheme 7. Synthesis of compounds **129-136**.

6. Biological Activity

The new bioisosteres at sulphur bridge (**36-78**) was tested for inhibition of tubulin polymerization, growth of MCF-7 human breast carcinoma cells and binding of [³H]colchicine to tubulin (more active compounds only), using CSA4 (**22**) as reference compound. Biological data are summarized in Table 5 and 6.

With few exceptions, tested derivatives showed potent tubulin polymerization inhibitory activity. Replacement of the sulphur atom with a carbonyl functionality led to compounds endowed with comparable ability to inhibit tubulin assembly (compare **36** with **37**, **39** with **40**, **42** with **43**, **45** with **46**, **48** with **49**, **51** with **52**, **57** with **58**, **60** with **61**, **63** with **64**, **66** with **67**, **69** with **70**, and **75** with **76**), while introduction of a methylene group led to inhibitors of tubulin assembly whose potency was dependent on the substituent at position 2 of the indole.

In particular, methylene compounds bearing a methoxy- or ethoxycarbonyl group at this position differed little in activities from the corresponding sulphur/carbonyl compounds (compare **41** with **39** and **40**, **44** with **42** and **43**, **50** with **48** and **49**, **53** with **51** and **52**, **62** with **60** and **61**, **65** with **63** and **64**, **74** with **72** and **69**, and **78** with **75** and **76**). In contrast, when there was a hydrogen atom at position 2, there was a 3-11-fold reduction in inhibitory activity (compare **38** with **36** and **37**, **47** with **45** and **46**, **59** with **57** and **58**, and **68** with **66** and **67**).

Seven compounds (**54-56**, **70**, **71**, **73** and **77**) were completely inactive. These results clearly indicate forbidden chemical modifications at the B region, namely (i) elongation of the bridging group from 1 to 2 atomic units (compounds **54-56**); (ii) oxidation of the sulphur atom to oxide (**70**) or dioxide (**71**), as we also observed in our previous paper;¹¹⁴ and (iii) reduction of the carbonyl bridge to an alcohol (**73** and **77**). As growth inhibitors of MCF-7 human breast carcinoma cells, the sulphur derivatives were superior (compare **36** with **37**, **42** with **43**, **57** with **58**, **66** with **67**, and **75** with **76**) or equivalent (compare **39** with **40**, **45** with **46**, **48** with **49**, **51** with **52**, **60** with **61**, **63** with **64**, **69** with **72**) to the corresponding ketones, while

methylene derivatives were usually less effective (compare **41** with **39** and **40**, **50** with **48** and **49**, **53** with **51** and **52**, **62** with **60** and **61**, **65** with **63** and **64**, **74** with **69** and **72**, and **78** with **75** and **76**). (Generally, only inhibitors of tubulin polymerization with $IC_{50} < 5 \mu M$ were evaluated for inhibition of MCF-7 cell growth). The greatest inhibitory effects on MCF-7 cells were observed with either sulphur or carbonyl derivatives bearing a 2-methoxycarbonyl group at position 2 of the indole. Compounds bearing either a bromine atom or a methoxy group at position 5 and a 2-methoxycarbonyl group at position 2 of the indole were found to be potent inhibitors in both the tubulin polymerization and MCF-7 cell growth assays, with potencies comparable to those of reference compound **22**.

Worthy of note, among these esters, the methylene derivatives **62** and **74** were also highly active in both assays.

Compounds that inhibited tubulin assembly with IC_{50} 's $< 5 \mu M$ were also evaluated for inhibition of the binding of [3H]colchicine to tubulin. Although none was as potent as CSA4, significant inhibition was observed with all active agents.

As usually occurs with a series of antitubulin compounds, there was not a linear correlation between colchicine binding inhibition and inhibition of tubulin assembly.

The most active inhibitor of colchicine binding was compound **69**, which was almost as active as CSA4, although was about half as active as an inhibitor of assembly (IC_{50} 's of 2.0 and $1.1 \mu M$, respectively).

Compounds **60** and **72**, both more active than CSA4 as inhibitors of assembly (IC_{50} 's of 0.99 and $0.67 \mu M$, respectively), were less active than **69** as inhibitors of colchicine binding.

Cpd	R ₁	R ₂	X	Tubulin ^a IC ₅₀ ± SD (μM)	MCF-7 ^b IC ₅₀ ± SD (nM)	Inhibition Colch. binding ^c (% ± SD)
36	H	H	S	2.6 ± 0.2	34 ± 9	68 ± 0.8
37	H	H	C=O	3.5 ± 0.07	150 ± 50	26 ± 0.3
38	H	H	CH ₂	28 ± 2	nd	nd
39	COOMe	H	S	2.9 ± 0.1	25 ± 1	74 ± 2
40	COOMe	H	C=O	2.7 ± 0.3	33 ± 10	49 ± 10
41	COOMe	H	CH ₂	4.2 ± 0.02	190 ± 70	33 ± 7
42	COOEt	H	S	2.9 ± 0.2	40 ± 2	19 ± 7
43	COOEt	H	C=O	2.6 ± 0.3	80 ± 20	51 ± 6
44	COOEt	H	CH ₂	5.4 ± 1	nd	nd
45	H	5-Cl	S	2.6 ± 0.2	77 ± 7	51 ± 4
46	H	5-Cl	C=O	2.5 ± 0.5	53 ± 10	44 ± 9
47	H	5-Cl	CH ₂	24 ± 2	nd	nd
48	COOMe	5-Cl	S	2.5 ± 0.3	42 ± 10	73 ± 0.2
49	COOMe	5-Cl	C=O	1.6 ± 0.1	30 ± 6	61 ± 4
50	COOMe	5-Cl	CH ₂	1.7 ± 0.5	87 ± 30	49 ± 4
51	COOEt	5-Cl	S	2.2 ± 0.2	110 ± 2	53 ± 3
52	COOEt	5-Cl	C=O	1.4 ± 0.2	110 ± 10	49 ± 3
53	COOEt	5-Cl	CH ₂	2.5 ± 0.5	230 ± 60	39 ± 4
54	COOEt	5-Cl	COCH ₂	>40	nd	nd
55	COOEt	5-Cl	COCO	>40	nd	nd
56	COOEt	5-Cl	CH ₂ CH ₂	>40	nd	nd
57	H	5-Br	S	1.6 ± 0.3	43 ± 7	65 ± 3
CSA4	-	-	-	1.1 ± 0.1	2.5 ± 0.6	99 ± 0.7

^aInhibition of tubulin polymerization. Tubulin was 10 μM during polymerization. ^bInhibition of growth of MCF-7 human breast carcinoma cells. ^cInhibition of [³H]colchicine binding. Tubulin was at 1 μM, both [³H]colchicine and inhibitor were at 5 μM.

Table 5. Inhibition of Tubulin Polymerization, Growth of MCF-7 Human Breast Carcinoma Cells and Colchicine Binding by Compounds **36-57** and Reference Compound CSA4 (**22**).

Cpd	R ₁	R ₂	X	Tubulin ^a IC ₅₀ ± SD (μM)	MCF-7 ^b IC ₅₀ ± SD (nM)	Inhibition Colch. binding ^c (% ± SD)
58	H	5-Br	C=O	1.9 ± 0.3	60 ^d	45 ± 5
59	H	5-Br	CH ₂	13 ± 0.8	nd	nd
60	COOMe	5-Br	S	0.99 ± 0.1	33 ± 10	75 ± 3
61	COOMe	5-Br	C=O	1.3 ± 0.08	18 ± 4	67 ± 4
62	COOMe	5-Br	CH ₂	1.3 ± 0.08	30 ± 9	59 ± 7
63	COOEt	5-Br	S	1.6 ± 0.2	83 ± 20	62 ± 7
64	COOEt	5-Br	C=O	1.6 ± 0.05	67 ± 10	58 ± 2
65	COOEt	5-Br	CH ₂	1.7 ± 0.2	100 ^d	53 ± 4
66	H	5-OMe	S	4.1 ± 0.6	22 ± 2	61 ± 4
67	H	5-OMe	C=O	3.4 ± 0.4	200 ^d	32 ± 7
68	H	5-OMe	CH ₂	14 ± 0.5	nd	nd
69	COOMe	5-OMe	S	2.0 ± 0.2	13 ± 3	93 ± 0.8
70	COOMe	5-OMe	S=O	>40	nd	nd
71	COOMe	5-OMe	S(=O) ₂	>40	nd	nd
72	COOMe	5-OMe	C=O	0.67 ± 0.02	17 ± 6	78 ± 6
73	COOMe	5-OMe	CHOH	>40	nd	nd
74	COOMe	5-OMe	CH ₂	1.4 ± 0.2	33 ± 10	59 ± 1
75	COOEt	5-OMe	S	2.4 ± 0.2	46 ± 3	71 ± 2
76	COOEt	5-OMe	C=O	2.6 ± 0.04	90 ± 10	49 ± 4
77	COOEt	5-OMe	CHOH	>40	nd	nd
78	COOEt	5-OMe	CH ₂	2.8 ± 0.3	93 ± 10	42 ± 4
CSA4	-	-	-	1.1 ± 0.1	2.5 ± 0.6	99 ± 0.7

^aInhibition of tubulin polymerization. Tubulin was 10 μM during polymerization. ^bInhibition of growth of MCF-7 human breast carcinoma cells. ^cInhibition of [³H]colchicine binding. Tubulin was at 1 μM, both [³H]colchicine and inhibitor were at 5 μM. ^dSame value obtained in all experiments.

Table 6. Inhibition of Tubulin Polymerization, Growth of MCF-7 Human Breast Carcinoma Cells and Colchicine Binding by Compounds **58–78** and Reference Compound CSA4 (**22**).

The potent esters **57**, **60-62**, **69**, **72** and **74** were evaluated at 0.5 and 1.0 μM for cell growth inhibition on human HeLa and HCT116/chr3 cells, derived from a cervix uterine carcinoma and a colon carcinoma, respectively.

All compounds caused about 50% growth inhibition at the lower concentration tested (Table 7). Compounds **57**, **60-62**, **69**, **72** and **74** also reduced the viability of HEK, M14 and U937 cells in a dose- and time-dependent manner with IC₅₀ values ranging from 78 nM (**61**, M14 cells) to 220 nM (**57**, HEK cells) (Table 8).

Cpd	% of Cell Proliferation ^{a,b}			
	HeLa ^c		HCT116/chr3 ^d	
	0.5 μM	1 μM	0.5 μM	1 μM
57	47 \pm 0.5	56 \pm 1.2	60 \pm 0.8	60 \pm 3.9
60	53 \pm 0.1	60 \pm 0.1	57 \pm 0.9	62 \pm 1.9
61	41 \pm 1.1	47 \pm 0.4	59 \pm 0.2	66 \pm 3.5
62	52 \pm 0.4	45 \pm 1.6	51 \pm 4.6	51 \pm 1.6
69	57 \pm 1.4	43 \pm 0.3	63 \pm 1.0	54 \pm 1.0
72	55 \pm 0.7	54 \pm 0.3	57 \pm 3.4	55 \pm 1.2
74	52 \pm 0.7	51 \pm 0.2	69 \pm 6.7	69 \pm 0.3

^aData are expressed as % mean values \pm SD; control cells are considered as 100% (MTT method). ^bTreatments were performed for 24 h at the indicated concentrations. ^cHeLa cervical cancer cells. ^dHCT116/chr3 human colon cancer cells.

Table 7. Effects of **57**, **60-62**, **69**, **72** and **74** on HeLa and HCT116/chr3 Cell Proliferation.

Cpd	$IC_{50} \pm SD$ (nM) ^a		
	HEK ^b	M14 ^c	U937 ^d
57	220 ± 3	194 ± 3	100 ± 3
60	189 ± 5	155 ± 9	177 ± 10
61	131 ± 3	78 ± 3	191 ± 7
62	160 ± 5	120 ± 10	159 ± 10
69	128 ± 7	111 ± 6	122 ± 6
72	140 ± 1	100 ± 5	155 ± 10
74	181 ± 3	137 ± 5	189 ± 5

^aGrowth inhibition of the indicated cell lines (MTT method); incubation time was 48 h. ^bHEK, human embryonic kidney 293 cells; ^cM14, human melanoma cells; ^dU937, human leukemic monocyte lymphoma cells.

Table 8. Inhibition of Growth of HEK, M14 and U937 Cells by Compounds **57**, **60-62**, **69**, **72** and **74**.

In contrast, at 300 nM these compounds caused only 20% reduction in murine macrophage J744.1 cell growth compared with untreated controls (Figure 16). Thus, these compounds were active in six cancer cell lines, but they showed a reduced cytotoxic effect on the nonmalignant murine macrophage J744.1 cells.

This observation with the J744.1 cells raised the possibility that there might be a differential effect of esters **57**, **60-62**, **69**, **72** and **74** in malignant and nontransformed cells, which in turn would suggest the possibility of a potential improvement in the therapeutic index for the ATI's versus other antitubulin agents.

Accordingly, we expanded our study of nontransformed cells to an epithelial line (PtK2, *Potorus tridactylis* kidney epithelial cells), two aortic smooth muscle lines (human and rat), and an endothelial line (human umbilical vein endothelial cells).

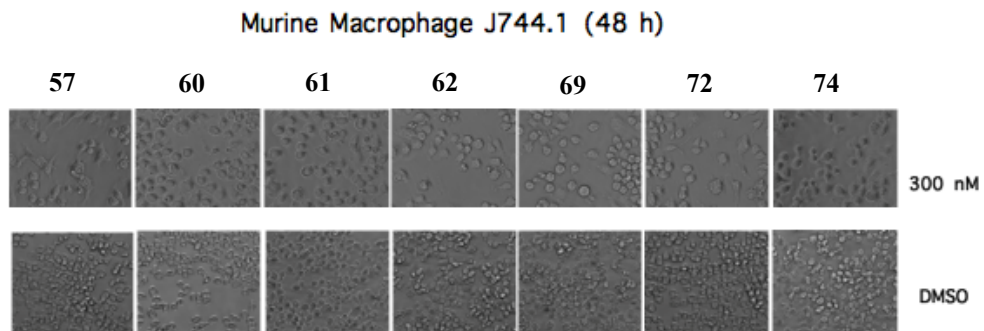


Figure 16. Effects of compounds **57**, **60-62**, **69**, **72** and **74** on murine macrophage J744.1 cell morphology, as visualized by time-lapse microscopy (magnification 20 \times).

We also determined the effects of CSA4 and paclitaxel on the growth of these four lines (Table 9). In all cases, except for compound **57** with the umbilical vein endothelial cells, the ATI's were more inhibitory than they had been with the J744.1 cells (that is, all IC₅₀'s were less than 300 nM). The cytotoxicity pattern with each agent was different, although compound **69** was the most cytotoxic and compound **57** was overall the least cytotoxic with these four nontransformed cell lines.

We devised the MCF-7 SI as a test for the idea that the ATI's would have selective toxicity for a tumor cell line as compared with nonmalignant cells and as compared with previously described antitubulin agents. This hope, raised with the J744.1 macrophage cells, was not confirmed with the additional cell lines. The average SI was 4.8 with CSA4 (**22**) and 6.1 with paclitaxel (**1**), although even with these two agents specific SI's differed from each other (the kidney epithelial cells were highly sensitive to CSA4, while both muscle lines were relatively resistant;

with paclitaxel, the human muscle cells were most sensitive, the rat muscle cells most resistant). The average SI with the esters ranged from 4.3 with compound **74** to 7.3 with compound **61**. We conclude that there is no significant difference between compounds **57**, **60-62**, **69**, **72** and **74** as compared with CSA4 and paclitaxel.

The effect of drug treatment on cell morphology was examined by time-lapse microscopy (TLM) using a Leica CTR6500 microscope. Cells were kept at 37 °C under a 5% carbon dioxide atmosphere for 48 h. The cytotoxic effects of compounds **57**, **60-62**, **69**, **72** and **74** on HEK and M14 cell growth increased in a concentration- and time-dependent manner. Figure 17 shows the effects of **57**, **72** and **74** after a 48 h treatment. Control HEK and M14 cell cultures displayed elongated bipolar or polygonal morphology, while a significant effect on cell morphology and 12-30% growth inhibition was already observed as early as 12 h after compound addition.

The treatment for 48 h with **57**, **72** or **74** induced significant morphologic changes in both cell lines, which became rounded and developed large vacuoles. Moreover, cells of both lines were less elongated than the untreated controls, and some cells that became rounded also had a tendency to detach from the substrate. Similar changes were observed after treatment with **60-62** and **69**.

Saccharomyces cerevisiae budding yeast has been used to enhance understanding of fundamental cellular and molecular processes occurring in mammalian cells, including DNA replication, DNA recombination, cell division, protein turnover, vesicular trafficking and mechanisms involved in longevity of cell life and cell death. Approximately 31% of yeast genes have a mammalian homologue, and an additional 30% of yeast genes show domain similarity.¹²⁰

Potentially, yeast can be a powerful model for the development of cell death-directed drugs. For example, paclitaxel, arsenic, bleomycin and valproate induce apoptotic phenotypes in yeast.¹²¹ Yeast have increased our understanding of the pathogenic role of human proteins in neurodegenerative diseases.¹²²

Cpd	$IC_{50} \pm SD$ (nM) ^a				
	MCF-7	HAOSMC ^b (MCF-7 SI) ^f	PtK2 ^c (MCF-7 SI)	A10 ^d (MCF-7 SI)	HUVEC ^e (MCF-7 SI)
57	43 ± 7	300 ± 200 (7.0)	230 ± 100 (5.3)	210 ± 100 (4.9)	400 ± 100 (9.3)
	-				
60	33 ± 10	100 ± 30 (3.0)	280 ± 30 (8.5)	230 ± 100 (7.0)	140 ± 20 (4.2)
	-				
61	18 ± 4	55 ± 40 (3.1)	110 ± 60 (6.1)	280 ± 40 (16)	150 ± 0 ^g (8.3)
	-				
62	30 ± 9	35 ± 7 (1.2)	270 ± 100 (9.0)	230 ± 100 (7.7)	140 ± 20 (4.7)
	-				
69	13 ± 3	15 ± 7 4 (1.2)	78 ± 50 (6.0)	70 ± 70 (5.4)	38 ± 30 (2.9)
	-				
72	17 ± 6	35 ± 7 (2.1)	190 ± 20 (11)	95 ± 80 (5.6)	110 ± 60 (6.5)
	-				
74	33 ± 10	70 ± 10 (2.1)	190 ± 200 (5.8)	130 ± 100 (3.9)	170 ± 50 (5.2)
	-				
CSA4	2.5 ± 0.6	18 ± 4 (7.2)	1.0 ± 1 (0.4)	23 ± 10 (9.2)	5.0 ± 5 (2.0)
	-				
Ptx^h	3.0 ± 0.5	6.0 ± 6 (2.0)	21 ± 8 (7.0)	38 ± 10 (13)	7.0 ± 4 (2.3)

^aGrowth inhibition of the indicated cell lines. ^bHAOSMC: human aortic smooth muscle cells (ATCC #CLL-1999); ^cPtK2: porcine tridactylis kidney epithelial cells (ATCC #CLL-56); ^dA10, rat embryonic aortic smooth muscle cells (ATCC #CRL-1476); ^eHUVEC: human umbilical vein endothelial cells (ATCC #CRL-2873). ^fMCF-7 SI: selectivity index (SI) for each agent in each cell line versus the MCF-7 cells (IC_{50} in specific cell line divided by IC_{50} in MCF-7 cells; the higher the SI, the more resistant the nontransformed cell line relative to the MCF-7 cells). ^gSame value obtained in both experiments. ^hPtx: paclitaxel.

Table 9. Inhibition of Growth and MCF-7 Selectivity Index of HAOSMC, PtK2, A10 and HUVEC Cells by Compounds **57**, **60-62**, **69**, **72** and **74**, and Reference Compounds **CSA4** (**22**) and Ptx (**1**).

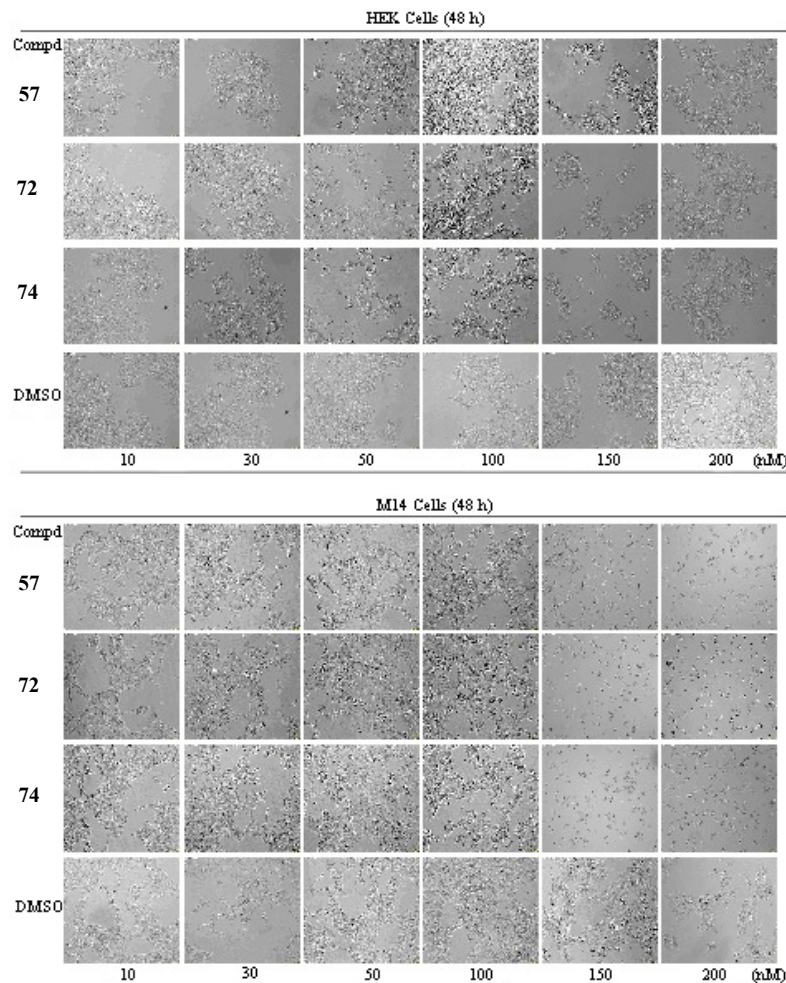


Figure 17. Effects of compounds **57**, **72** and **74** on HEK (top) and M14 (bottom) cell morphology and growth as seen by TLM (magnification 10x).

Finally, Cassidy-Stone and coworkers¹²³ identified MDIVI-1 (mitochondrial division inhibitor-1) by yeast screens of chemical libraries. A protocol was set up to evaluate the toxicity of compounds **57** and **60-62** on BY4741, a standard laboratory wild type strain of *S. cerevisiae*.

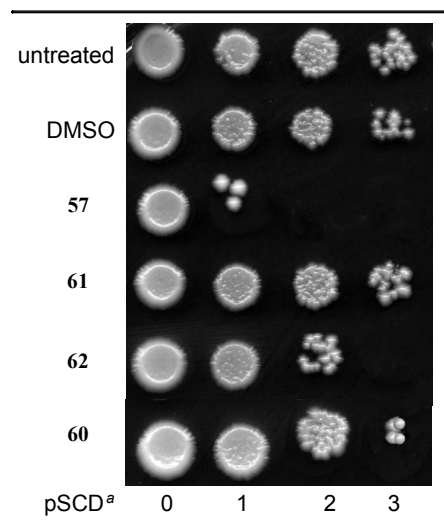


Figure 18. Effect of compounds **57**, and **60-62** on BY4741 wild type strain. Growth was recorded after 3 days at 28 °C; final compound concentration was 20 μ M. ^aSCD, Serial Cell Dilution.

As shown in Figure 18, **57** strongly reduced the viability of the BY4741 strain cells, which were cell growth limited at the first dilution (the second showed limited cell growth). Compound **62** also showed significant BY4741 inhibition (cell growth was limited to the third dilution). Despite the small test set used in this experiment, the ester functionality of **60-62** clearly caused a drop in activity, as compared with the most potent compound **57** lacking the ester group.

The new bioisosteres **79-110** were valued as inhibitors of both tubulin polymerization and growth of MCF-7 human breast carcinoma cells, and for the most active compounds were determined the displacement of the [³H]colchicines from the TB-binding site. Combretastatine A4 (**22**), colchicine (**11**) and **39** were used as reference compounds (Table 10 and Table 11). The new ATIs (**79-95**), bearing a 5-membered heterocyclic nucleus at position 2 of indole, inhibited tubulin polymerization with IC₅₀'s ranging from 0.74 to 6.8 μM, and in particular compounds **90** and **93**, characterized by the presence of a thiophene ring and sulphur bridge at positions 2 and 3 of the indole ring respectively, were more potent than reference compounds (**90**: IC₅₀ = 0.74 μM, **93**: IC₅₀ = 0.91 μM, **22**: IC₅₀ = 1.1 μM, **11**: IC₅₀ = 3.2 μM, **39**: IC₅₀ = 2.9 μM, Table 10). Replacement of the sulphur atom with a carbonyl functionality led to compounds with comparable ability to inhibit tubulin assembly (compare **80** with **79**, **82** with **81**, **84** with **83**, **86** with **85**, **89** with **88**, **91** with **90** and **94** with **93**), while the introduction of a methylene group led to a 2-6 fold reduction in inhibitory activity (compounds **83**, **86**, **89**, **92**, and **95**).

In the inhibition of the growth of human MCF-7 non-metastatic breast cancer epithelial cells assay, the sulphur and carbonyl derivates showed IC₅₀'s ranging from 10 to 60 nM, and the most active compounds were **79** (IC₅₀ = 18 nM), **80** (IC₅₀ = 10 nM) and **81** (IC₅₀ = 20 nM). Compounds with a methylene bridge were usually less effective.

All sulphur and ketones derivatives were strong inhibitors of the binding of [³H]colchicine (61-93% inhibition, although not quite as potent as CSA4). In this assay, the strongest inhibition was observed with compounds **79** (92%) and **87** (93%). In contrast, the methylene derivatives showed an inhibition less of 56%.

Compounds **96-104** bearing a 6-membered aromatic groups at position 2 of the indole ring were less potent as inhibitors of MCF-7 cell grown than the corresponding 5-member heterocyclic; only derivates **101** and **103** were potent as

the reference compounds (Table 11), and showed 88 and 91% inhibition of the binding of [³H]colchicine to tubulin, respectively.

Finally, the introduction of the steric hindered α - or β -naphthalene moiety led to inactive compounds.

The antiproliferative activity of compounds **81** and **90-92** was evaluated in four additional cancer cell lines in comparison with doxorubicin (DOX), a common DNA-targeting drug often employed in association with anti-mitotic agents (Table 12). Compounds **90** and **91** were generally one order of magnitude more potent as growth inhibitors of HeLa (cervix), PC3 (prostate), HT-29 (colon), A549 (non small cell lung) and 231-MDA (metastatic breast) carcinoma-derived cell lines as compared with DOX. Compound **81** was highly effective in the HT-29 and A549 cell lines, and less active in the HeLa and PC3 cell lines. Compound **92** was generally comparable with DOX. These data underscore the effectiveness of ATIs **81** and **90-92** in transformed cell types. Such results also highlighted a differential sensitivity to MT-targeting drugs displayed by cell lines with different genetic background, consistent with results obtained with other drugs that target the mitotic apparatus.^{124,125}

For compound **81** and **91** was analyzed growth inhibition in an ovarian cancer model with high drug sensitivity (A2780wt), its cisplatin-resistant counterpart (A2780-CIS) and a cell line derived from a cisplatin-resistant patient (OVCAR-3) (Table 13). For the acquired cisplatin-resistance (RI-1) model, compounds **81** and **91** yielded even lower IC₅₀ than in the parental line, in contrast to the almost 20-fold resistance to cisplatin. On the other hand, such an increase was not detectable in the endogenous resistance model as the resistance values (RI-2) for the two ATIs were essentially identical to that obtained with cisplatin in OVCAR-3. Taken together, these results indicate the ATIs can target a broad range of cancer tissues, with a selective activity against acquired cisplatin resistance.

Cpd	R ₁	X	Tubulin ^a IC ₅₀ SD (μM)	MCF-7 ^b IC ₅₀ SD (nM)	Inhibition Colch. Binding ^c (% ± SD)
79	Pyrrol-2-yl	S	1.1 ± 0.05	18 ± 6	92 ± 0.6
80	Pyrrol-2-yl	C=O	1.4 ± 0.2	10 ± 0	79 ± 3
81	Pyrrol-3-yl	S	1.2 ± 0.2	20 ± 0	85 ± 1
82	Pyrrol-3-yl	C=O	1.8 ± 0.2	35 ± 7	71 ± 0.7
83	Pyrrol-3-yl	CH ₂	3.0 ± 0.2	600 ± 0	56 ± 7
84	Furan-2-yl	S	1.0 ± 0.1	45 ± 4	-
85	Furan-2-yl	C=O	1.9 ± 0.2	55 ± 7	78 ± 0.3
86	Furan-2-yl	CH ₂	6.8 ± 1	nd	nd
87	Furan-3-yl	S	1.0 ± 0.1	33 ± 5	93 ± 4
88	Furan-3-yl	C=O	1.1 ± 0.007	40 ± 20	77 ± 0.8
89	Furan-3-yl	CH ₂	6.5 ± 0.08	nd	nd
90	Thiophen-2-yl	S	0.74 ± 0.05	39 ± 10	-
91	Thiophen-2-yl	C=O	1.0 ± 0.1	36 ± 6	75 ± 3
92	Thiophen-2-yl	CH ₂	1.9 ± 0.2	200	48 ± 5
93	Thiophen-3-yl	S	0.91 ± 0.2	60 ± 20	-
94	Thiophen-3-yl	C=O	2.1 ± 0.08	40 ± 0	61 ± 3
95	Thiophen-3-yl	CH ₂	2.7 ± 0.08	340 ± 200	52 ± 4
39	COOMe	S	2.9 ± 0.1	25 ± 1	74 ± 2
Colch			3.2 ± 0.4	13 ± 3	-
CSA4			1.1 ± 0.1	2.5 ± 0.6	99 ± 0.7

^aInhibition of tubulin polymerization. Tubulin was 10 μM during polymerization.^bInhibition of growth of MCF-7 human breast carcinoma cells.^cInhibition of [³H]colchicine binding. Tubulin was at 1 μM, both [³H]colchicine and inhibitor were at 5 μM.**Table 10.** Inhibition of Tubulin Polymerization, Growth of MCF-7 Human Breast Carcinoma Cells and Colchicine Binding by Compounds **79–95** and Reference Compounds **39**, **11**, and **22**.

Cpd	R ₁	X	Tubulin ^a IC ₅₀ SD (μM)	MCF-7 ^b IC ₅₀ SD (nM)	Inhibition Colch. Binding ^c (% ± SD)
96	Phenyl	S	3.3 ± 0.1	52 ± 7	nd
97	Phenyl	C=O	5.7 ± 0.06	87 ± 20	nd
98	Phenyl	CH ₂	3.7 ± 0.3	170 ± 60	50 ± 3
99	Pyridin-2-yl	S	1.5 ± 0.2	180 ± 80	48 ± 6
100	Pyridin-2-yl	C=O	> 20	330 ± 100	nd
101	Pyridin-3-yl	S	1.3 ± 0.07	12 ± 7	88 ± 0.1
102	Pyridin-3-yl	C=O	6.3 ± 0.7	200 ± 100	nd
103	Pyridin-4-yl	S	0.95 ± 0.1	16 ± 10	91 ± 2
104	Pyridin-4-yl	C=O	6.0 ± 0.6	170 ± 60	nd
105	α-naphthyl	S	>40	nd	nd
106	α-naphthyl	C=O	>40	nd	nd
107	α-naphthyl	CH ₂	>40	nd	nd
108	β-naphthyl	S	1.0 ± 0.06	530 ± 50	51 ± 6
109	β-naphthyl	C=O	>40	nd	nd
110	β-naphthyl	CH ₂	>40	nd	nd
39	COOMe	S	2.9 ± 0.1	25 ± 1	74 ± 2
Colch			3.2 ± 0.4	13 ± 3	-
CSA4			1.1 ± 0.1	2.5 ± 0.6	99 ± 0.7

^aInhibition of tubulin polymerization. Tubulin was 10 μM during polymerization.^bInhibition of growth of MCF-7 human breast carcinoma cells.^cInhibition of [³H]colchicine binding. Tubulin was at 1 μM, both [³H]colchicine and inhibitor were at 5 μM.**Table 11.** Inhibition of Tubulin Polymerization, Growth of MCF-7 Human Breast Carcinoma Cells and Colchicine Binding by Compounds **96-110** and Reference Compounds **39**, **11** and **22**.

Cpd	$IC_{50} \pm SD (\mu M)^a$			
	HeLa	PC3	HT-29	A549
81	0.4 ± 0.02	0.5 ± 0.1	0.1 ± 0.03	0.08 ± 0.02
90	0.09 ± 0.002	0.2 ± 0.05	0.15 ± 0.03	0.09 ± 0.02
91	0.07 ± 0.004	0.1 ± 0.08	0.08 ± 0.01	0.08 ± 0.01
92	1 ± 0.03	2 ± 0.1	1 ± 0.05	2 ± 0.08
DOX^b	1.5 ± 0.03	1.7 ± 0.02	1.0 ± 0.04	1.0 ± 0.08

^aGrowth inhibition of the indicated cell lines (MTT method); incubation time was 48 h.

^bDoxorubicin as reference compound.

Table 12. Inhibition of Growth of HeLa, PC3, HT29, and A549 Cell Lines by Compounds **81** and **90-92**.

Compounds **81**, **90** and **91** were compared with vinorelbine (**33**), vinblastine (**29**), PTX (**1**) and CSA4 (**22**) in the OVCAR-8 and NCI/ADR-RES cell lines (Table 14).

Derived from OVCAR-8, NCI/ADR-RES is an adriamycin-resistant cell line that overexpresses P-glycoprotein (Pgp), resulting in the type 1 multidrug-resistance phenotype. Compounds **81**, **90** and **91** were uniformly more active in the NCI/ADR-RES line than in the parental OVCAR-8 line. Both compounds showed a less differential activity, however, than did PTX (**1**), and CSA4 (**22**) was the least selective of the compounds evaluated. In contrast, VRB and VBL showed the typical multidrug resistance differential, as did PTX. CSA4 yielded the same IC_{50} in both cell lines and clearly was not a Pgp substrate. Most importantly, as NCI/ADR-RES cell growth inhibitors, ATIs **81**, **90** and **91** were all superior to VRB, VBL and PTX.

Cpd	IC ₅₀ ± SD (nM)				
	A2780wt	A2780-CIS	OVCAR-3	RI-1 ^a	RI-2 ^b
81	21.5 ± 1.2	6.3 ± 1.8	81 ± 21	0.29	3.8
91	30.5 ± 0.7	29.3 ± 3.2	117 ± 18	0.96	3.8
Cisplatin	485 ± 60	8980 ± 565	1816 ± 254	18.5	3.7

^aRI-1 (Resistant Index-1) was calculated by dividing the IC₅₀ obtained in A2780-CIS by the IC₅₀ obtained in A2780wt. ^bRI-2 (Resistant Index-2) was calculated by dividing the IC₅₀ obtained in OVCAR-3 by the IC₅₀ obtained in A2780wt. A value >1 or <1 means either increased cisplatin-resistance or sensitivity, respectively.

Table 13. Growth Inhibition in A2780wt Cells, its Cisplatin Resistant Counterpart A2780-CIS and OVCAR-3 by Compounds **81** and **91**.

These compounds were from 200- (**81** and **90**) to 333-fold (**91**) more potent than VRB, from 13- (**81** and **90**) to 8-fold (**91**) more potent than VBL, and from 100- (**81** and **90**) to 60-fold (**91**) more potent than PTX.

A recurrent problem with MT-targeting drugs is their widespread toxicity on normal cells when used in human patients.^{7,126,127} We therefore used non-transformed cells to evaluate potential differences between compounds **81** and **92**, as representatives of one of the more potent ATIs and the least potent in the current series as MCF-7 grown inhibitor (Table 15). Both compounds **81** and **92** had somewhat greater antiproliferative effects in MCF-7 breast cancer cells as compared with several non-transformed cell lines, with the difference being greater for **81** than **92**.

Cpd	$IC_{50} \pm SD^a$	(nM)
	OVCAR-8 ^b	NCI/ADR-RES ^c
81	70 ± 30	25 ± 7
90	45 ± 20	25 ± 7
91	20 ± 10	15 ± 7
VRB^d	300 ± 0	5000 ± 1000
VBL^e	15 ± 7	200 ± 0
PTX	2 ± 0.7	1500 ± 700
CSA4	1.3 ± 0.6	1.3 ± 0.6

^aCells were grown in RPMI 1640 medium with 5% FBS, 5% CO₂ atmosphere at 37 °C, for 96 h. ^bOVCAR-8: ovarian tumor cell line 8. ^cNCI/ADR-RES: drijamycin resistant cell line derived from OVCAR-8. ^dVinorelbine, tubulin inhibition = 3.1 ± 0.2 μM.

^eVinblastine, tubulin inhibition = 1.1 ± 0.2 μM.

Table 14. Growth Inhibition of OVCAR-8 and NCI/ADR-RES Cells Lines by Compounds **81**, **90**, **91** and Reference Compounds VRB (**33**), VBL (**29**), PTX (**1**) and Colch (**22**).

To further characterize the cell growth inhibitory properties of the new ATIs, compounds **81** and **90-92** were analyzed for their effects on the cell cycle in parallel with VBL (**29**) and CSA4 (**22**) (Figure 19). 24 h after plating, HeLa cells were exposed to each compound for 24 h, and the cell cycle profile was subsequently analyzed by flow cytometry. We found that **81**, **90** and **91** at 100 nM consistently blocked cell cycle progression and induced 70-90% of the cells to accumulate in the G₂/M phases (Figure 19), similar to VBL (**29**) and CSA4 (**22**) (80-90% G₂/M arrest).

The cell cycle effects of ATIs **90** and **91** were further examined in the A549 and HT29 cell lines.

Cpd	$IC_{50} \pm SD$ (nM)				
	MCF-7	HAOSMC ^a	A10 ^b	PtK2 ^c	HUVEC ^d
81	20 ± 0	33 ± 10	40 ± 30	60 ± 0	30 ± 0
92	200 ± 0	250 ± 90	150 ± 90	300 ± 0	180 ± 40
CSA4	13 ± 3	5 ± 3	1 ± 1	3 ± 1	1 ± 1
PTX^e	3 ± 0.5	6 ± 6	38 ± 10	21 ± 8	7 ± 4

^aHAOSMC: human aortic smooth muscle cells (ATCC #CLR-1999); ^bA10, rat embryonic aortic smooth muscle cells (ATCC #CRL-1476); ^cPtK2: porcine tridactylis kidney epithelial cells (ATCC #CLL-56); ^dHUVEC: human umbilical vein endothelial cells (ATCC #CRL-2873). ^eData from Lit.¹²⁸

Table 15. Growth Inhibition of MCF-7, HOSMAC, A10, PtK2 and HUVEC Cells Lines by Compounds **81**, **92**, CSA4 (**22**) and PTX (**1**).

Both **90** and **91** induced a gradual accumulation of cells in the G₂/M phase of the cell cycle in a dose-dependent manner, could be detected as early as 7 h after treatment (Figure 20 and Figure 21 A). In these cells we evaluated both the cell cycle profile and the accumulation of cyclin B1 (Figure 21 B) following treatment with the compounds. Both flow cytometry and the Western blot assay for cyclin B1 provide information about the entire cell population. Yet, these experiments do not provide definitive proof that the cells are actually arrested in mitosis, as would be expected following treatment with a microtubule inhibitor.

Cells arrested in mitosis can either induce cell death or re-enter interphase and further replicate their DNA, becoming polyploid and increasing the degree of genetic instability of the cell population. To distinguish between these cell fates after ATI treatment, we processed cell cultures for immunofluorescence to α-tubulin and stained chromosomes with the DNA dye 4',6-diamidino-2-phenylindole (DAPI).

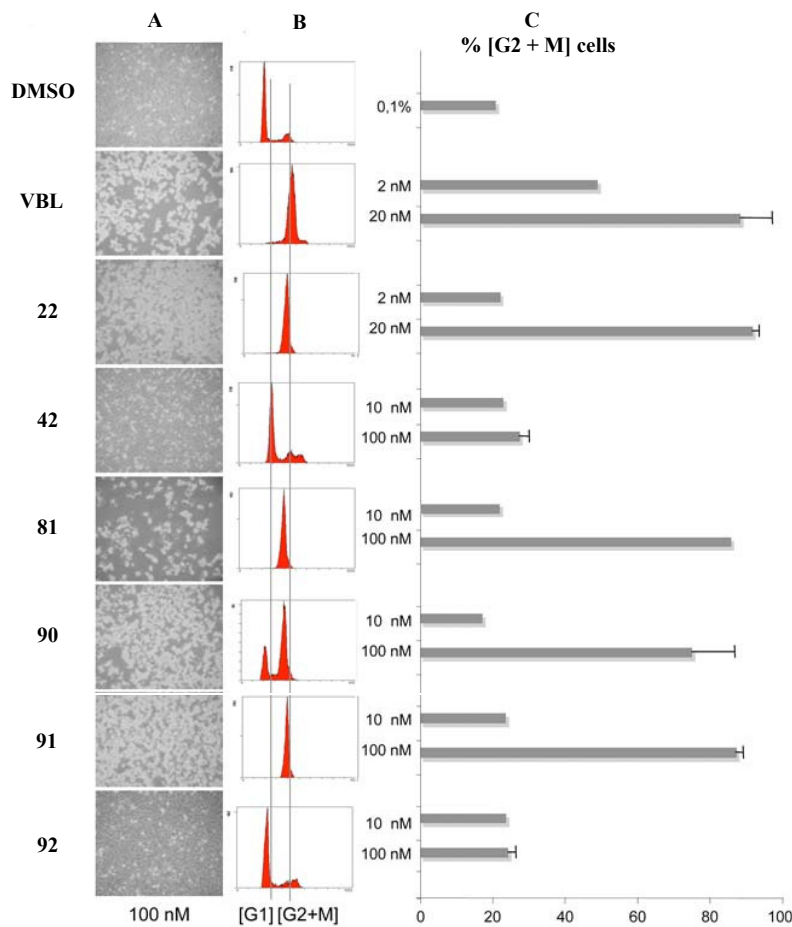


Figure 19. The effect of ATIs on cell cycle progression in HeLa cell cultures. **A.** Bright-field panels from HeLa cell cultures exposed to the DMSO solvent only or exposed to the indicated compounds (VBL and **22** at 20 nM and the other compounds at 100 nM). Cells arrested in mitosis show a typical rounded, highly refractive morphology resulting in a highly refractive phenotype (10x objective). **B.** Typical flow cytometry profiles of cell cultures exposed to the indicated compounds at the same concentrations as in A. **C.** Bars represent the % of cells with G2/M genomic content after treatment with each compound at the indicated concentration (mean values ± SD were calculated from 2 to 6 independent experiments).

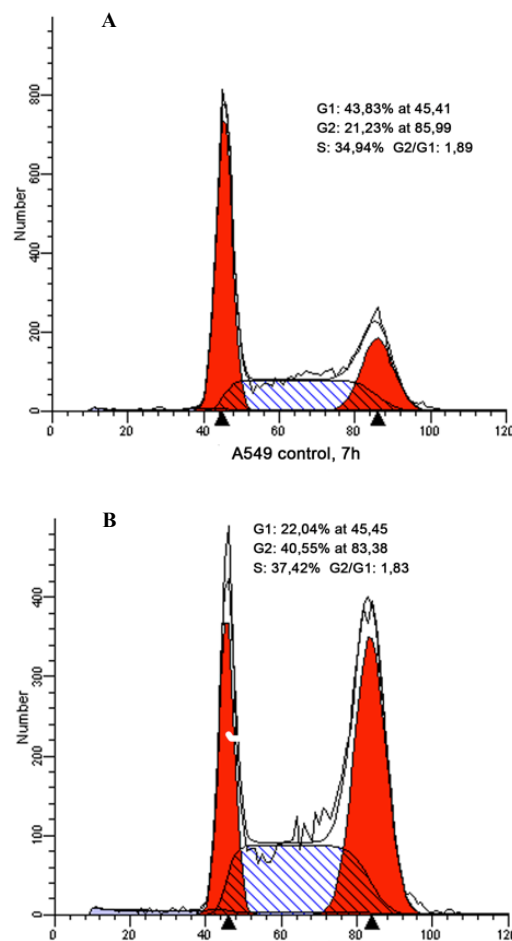


Figure 20. Dose-dependent cell cycle effects of **91** in A549 cell cultures. Typical cell cycle profiles after flow cytometric analysis of A549 cell populations treated with DMSO only (A) or with **91** (B) (100 nM, 7 h).

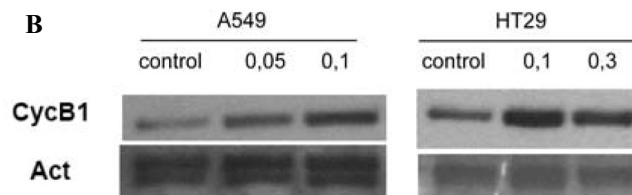
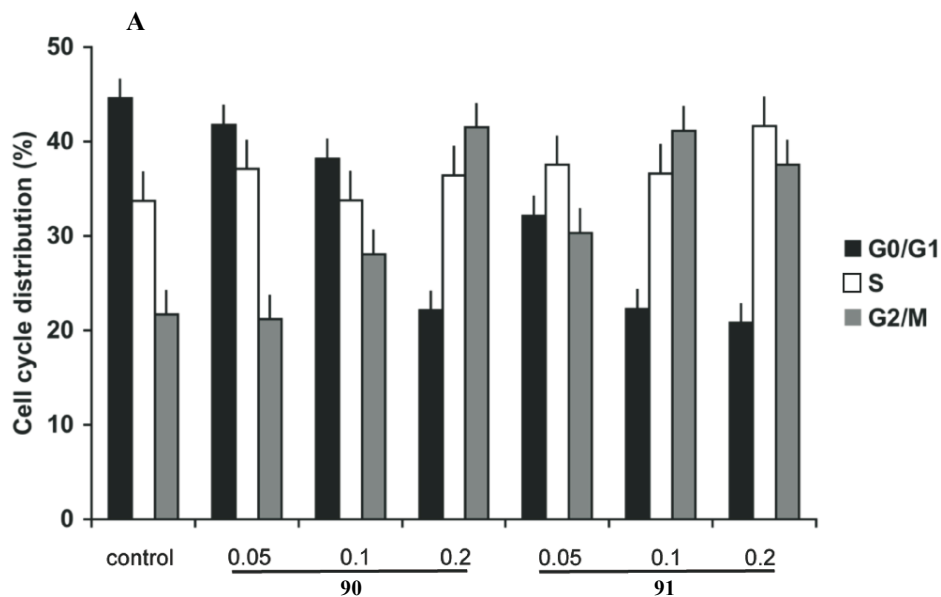


Figure 21. **A.** The histograms represent the % of cells with G1, S and G2/M DNA content, based on flow cytometric analyses in A549 cells exposed to increasing μM concentrations of ATIs **90** and **91** (7 h). **B.** Cyclin B1 accumulation in A549 and HT29 cell lines exposed to the indicated μM concentrations of **91** (7 h).

Treated and control cells were then scored for their mitotic index (MI) calculated as mitotic cells/(mitotic + interphase cells) ratio. In control cultures, about 10% of cells were in the various stages of mitosis with well-formed spindles interacting with condensed chromosomes (Figure 22 A). In cultures exposed to ATI **81**, **90** or **91**, over 60% of the cells were arrested in prometaphase with condensed chromosomes but no spindle (Figure 22 B). Thus, the accumulation of G₂/M cells detected by flow cytometry does indeed reflect a true mitotic arrest. The MI in cell populations treated with **81**, **90** and **91** was significantly higher compared to treatment with the weak tubulin inhibitor **92**. The MIs observed with **81** and **91** were in the same range as CSA4 (**22**) and VBL (**29**), although a higher concentration of the ATIs was required (Figure 22 C). The data at this point indicate that most ATIs that effectively inhibited tubulin polymerization *in vitro* did indeed arrest mitotic progression in cultured cells, thereby causing decreased cell proliferation in human transformed cell lines. To investigate more closely the link between mitotic arrest and reduced cell growth, we analyzed HeLa cell populations exposed to **81** and **90-92** for induction of cell death under the same conditions used in the mitotic arrest experiments. Control cultures were compared with cultures treated with ATIs **81**, **90** and **91** for their reactivity to annexin V, which binds to phosphatidylserine residues that are translocated from the inner to the outer cell membrane in early apoptosis.

Annexin V-reactive cells were quantitated by flow cytometry (Figure 23 A). The results showed that **81**, **90** and **91** induced apoptosis as efficiently as CSA4 (**22**) and VBL (**29**) at the concentrations examined (Figure 23 B). To extend these results, we analyzed the induction of caspase-3 expression at the single cell level.

Caspase-3 regulates the induction of apoptosis in mitotic cells, and it is required for the apoptotic response to MT-targeting drugs.¹²⁹

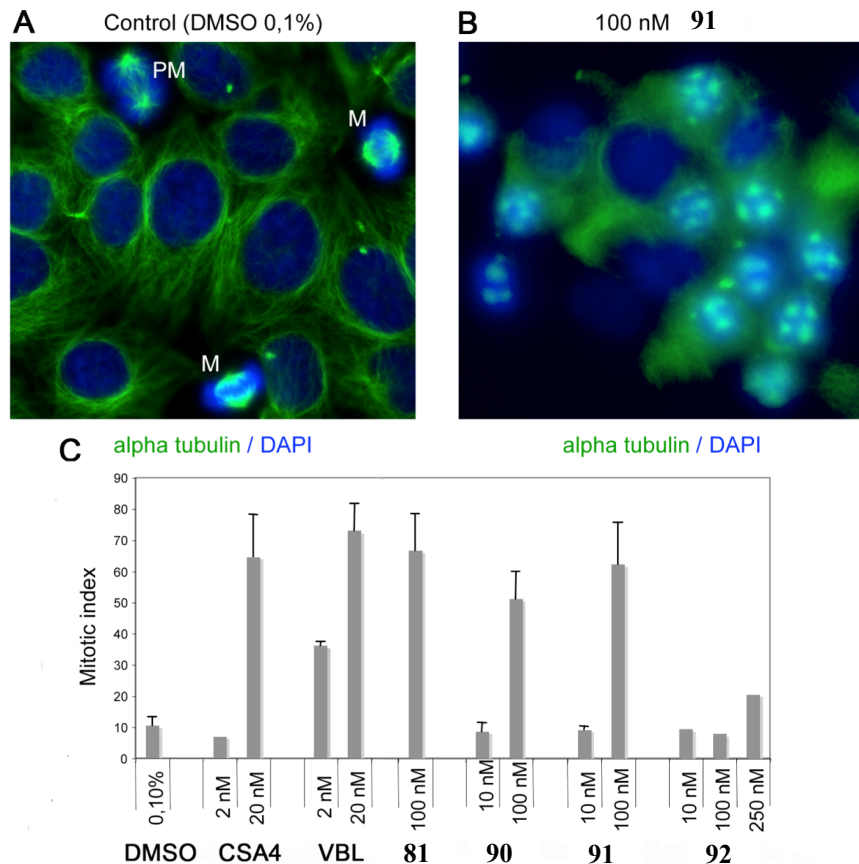


Figure 22. Induction of mitotic arrest by ATIs. **A.** HeLa control cultures exposed to DMSO solvent (0.1%, 24 h); MTs are visualized by α -tubulin staining (green) and chromosomes by DNA staining (blue); most cells are in interphase; cells in various stages of mitotic progression (PM, prometaphase; M; metaphase) are indicated. **B.** A typical field from a HeLa culture exposed to ATI **91** (100 nM, 24 h); note that most cells are arrested in early mitotic stages with condensed chromosomes and a failure to assemble proper MTs; disorganized tubulin foci are seen throughout the mitotic cells. **C.** MIs in HeLa cell cultures that were treated with DMSO solvent, with known anti-MT compounds, or with ATIs **81** and **90-92** (mean values \pm SD were calculated from 2 to 4 independent experiments).

Immunofluorescence showed that **81**, **90** and **91**, but not **92**, induced caspase-3 activity in a significant fraction of cells (an apoptotic cell treated with **91** is shown in Figure 23 C), further demonstrating the strong link between the ability of ATIs to arrest mitotic progression and to induce apoptosis.

The metabolic stability of **42**, **81**, **90** and **91** was evaluated in mouse and human liver microsomes to estimate stability to phase I oxidative metabolism (Table 16).

Compounds **81** and **91**, respectively, showed a medium and low metabolic stability in both human and mouse liver microsomes, while **90** exhibited medium stability in the human microsomes and low stability in the mouse microsomes. In contrast, the metabolic stability of **42** was dramatically low.

The metabolic stability of **81**, **90** and **91** seemed to be dependent on the nature of the 2-heterocyclic nucleus rather than the structure of the bridging group. Such an effect may be explained by steric hindrance exerted by the two aromatic moieties attached to the bridging group.

The aqueous solubility of **81** increased 4 times over that of compound **42**, as a result of the introduction of the pyrrole nucleus for the ester function. The aqueous solubility of **81** at pH 7.4 was 20 μ M, while under the same conditions the solubility of **42** was 5 μ M. Most importantly, such an improvement of the solubility of **81** impacted with 2.4- and 2.0-times increases, respectively, of tubulin polymerization and MCF-7 growth inhibitory potencies.

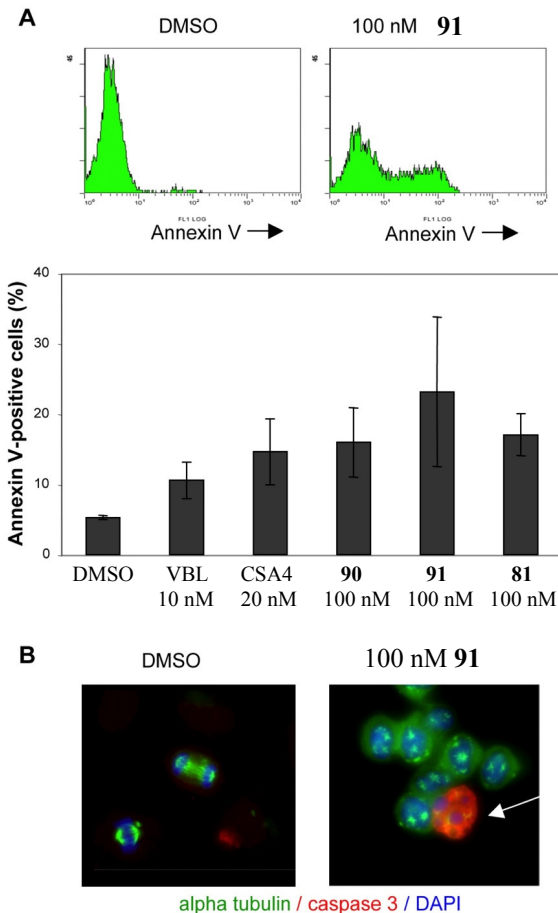


Figure 23. Induction of apoptosis by ATIs. **A.** Typical flow cytometry studies of HeLa cell populations incubated with annexin V after exposure to DMSO only (control) or to **91** (100 nM). **B.** The histograms represent the % apoptotic cells, as determined by annexin V-reactivity, after exposure to the indicated compounds for 24 h (means \pm SD were calculated from 2 to 3 experiments). **C.** Single-cell level immunofluorescence analysis revealed by the induction of active caspase-3 (recognized by a specific antibody): the panels depict typical fields from HeLa cultures exposed to only DMSO (note the two cells progressing through mitosis) or to **91** (a mitotic cell expressing active caspase-3 is indicated by a arrow among a group of cells arrested in mitosis).

Cpd	% remaining at 30 min. ^a	
	Human Liver microsomes	Mouse Liver microsomes
81	34.8 ± 1.4	23.1 ± 0.6
90	22.0 ± 1.0	2.2 ± 0.3
91	4.6 ± 0.2	0.60 ± 0.01
42	0.37 ± 0.01	0.5 ± 0.03
7-Ethoxycoumarin ^b	6.6 ± 0.2	0.07 ± 0.02
Propranolol ^b	54.1 ± 0.4	20.6 ± 0.5

^aMetabolic stability: >95, high; 50-95, good; 10-50, medium; <10, low. ^bResults are expressed as mean ± SD, n=2. ^bThe standard compounds 7-ethoxycoumarin and propranolol showed metabolic stability in agreement with the literature and internal validation data.¹³⁰

Table 16. Metabolic stability results of **42**, **81**, **90** and **91** in human and mouse liver microsomes.^a

Finally, for its interesting *in vitro* properties, the intravenous pharmacokinetic and oral bioavailability of **81** was investigated in the mouse. Pharmacokinetic studies were carried out in male CD-1 mice. The compound was either administered in single intravenous (*iv*) injections of 5 mg/kg or oral (*os*) dose of 15 mg/kg, respectively. The main pharmacokinetic parameters obtained are reported in Table 17. Compound **81** showed a systemic plasma clearance slightly lower than the hepatic blood flow of 86 mL/min/kg in mice, an estimated elimination half life of 40 minutes and a calculated steady state volume of distribution suggestive of good tissue distribution. Moreover, the compound was quickly absorbed after oral administration and showed a very high oral bioavailability.

Parameter	
$C_{\max}^a iv$ (ng/mL)	35.67
$AUC_{0-\infty}^b iv$ (ng.min/mL)	174346
$t_{1/2}^c$ (min)	40
Cl^d (mL/min/kg)	28.6
V_{ss}^e (L/kg)	1.59
$C_{\max}^a os$ (ng/mL)	1340
$t_{\max}^f os$ (min)	120
$AUC_{0-\infty}^b os$ (ng.min/mL)	583315
F ^g (%)	110

^aMaximum concentration; ^barea under the curve calculated up $0-\infty$ timepoint; ^chalf-time; ^dclearance; ^emean distribution volume; ^fmax-time; ^goral bioavailability.

Table 17. Pharmacokinetic Properties of **81** in Mice.

7. Molecular modeling

The binding mode of ATIs was extensively studied by means of docking experiment. Based on our previous modeling results,¹¹³⁻¹¹⁵ we performed a series of docking simulations on a virtual library of structures with different bridges (B) in order to identify the most promising compounds before their actual synthesis. The aim of the simulations was to find a bridge group able to retain or improve the biological activity with an increased metabolic stability in comparison with sulphur atom which could be metabolized *in vivo*. The results obtained for the new series showed that the sulphur atom (B) replacement with a methylene or carbonyl moiety led to virtually identical docking poses previously reported for ATIs (Figure 24).

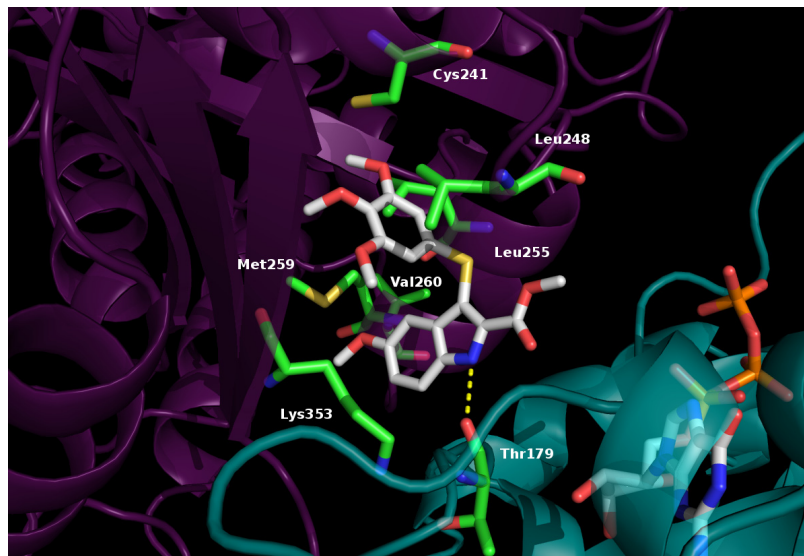


Figure 24. Docking poses for reference compounds **69** (white stick). H-bonds are reported as yellow dotted lines. Residues of the binding site and GTP are also reported as lines.

In particular, the trimethoxyphenyl moiety was situated in close proximity to Cys241, and the indole NH formed a hydrogen bond with Thr179 (Figure 25). These results let to suppose as these bridge modifications would lead to strong biological activity, it was confirmed by the experimental results. Conversely, results for compounds with a two-carbon bridge were different. Such structures adopted a binding conformation in the colchicine site far from the one observed for previously reported ATIs: the trimethoxyphenyl ring was far away from Cys241, that could be related with poor binding and low biological activity. To test the model we synthesized only three 2-carbon bridge analogues (**54-56**) for which the experimental data confirmed the predictions of the docking studies.

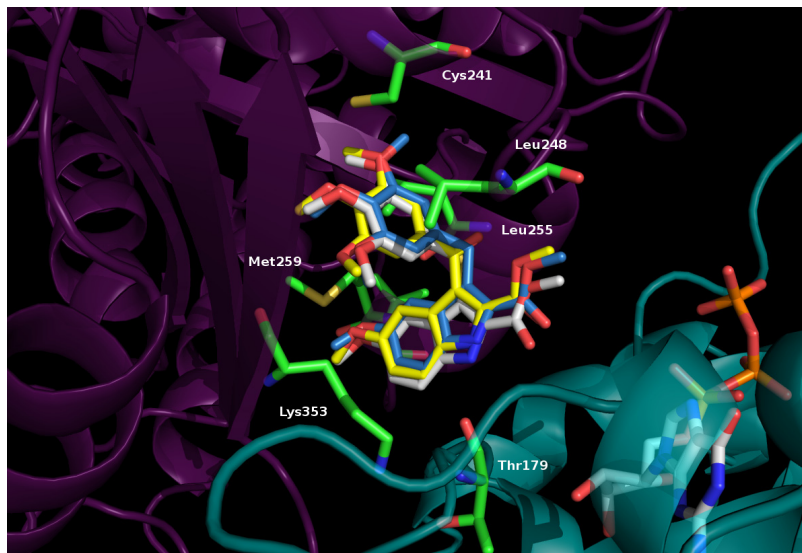


Figure 25. Docking poses for compounds **69** (white stick), **72** (yellow stick) and **74** (light blue stick). Residues of the binding site and GTP are also reported as lines.

The metabolic instability showed by the sulphur bridge atom was overcame by an *in silico* approach. Thanks to the good results obtained we decided to repeat the same approach to solve the metabolic instability also of the ester moieties that might be hydrolyzed to the corresponding acid *in vivo*. With this goal in mind we built a small virtual library of structures in which the ester groups of ATI **69** (Figure 24) was replaced by different 5-membered heterocycles (pyrrole, furan or thiophene).

Docking simulations with FlexX¹³¹ into the colchicine site on tubulin showed a consistent binding pose for the new 5-membered ring analogues (Compound **79** and **90**) (Figure 26).

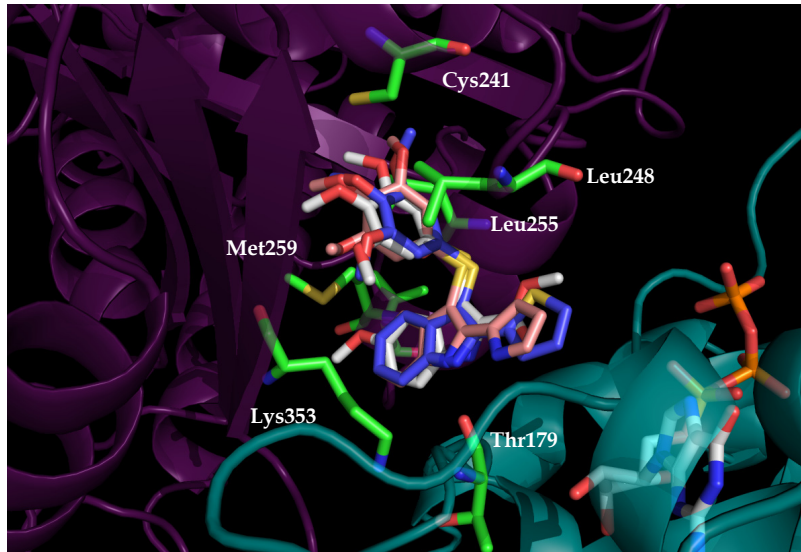


Figure 26. Binding mode proposed by PLANTS for **69** (white stick), **79** (light pink stick) and **90** (light blue stick) into the colchicine site. Residues of the binding site and GTP are also reported as lines.

In particular, the 5-membered heterocycle introduced into the ATIs scaffold formed new hydrophobic interaction with the Lys254 and Leu248 side chains, while occupying the same pocket of the ester function. As a validation of these findings, we repeated the docking simulations with PLANTS¹³² and GLIDE¹³³. The obtained binding pose were consistent with the binding conformations obtained by FlexX. In particular, the trimethoxyphenyl group lay in proximity to the Cys241, Met259 and Leu255 residues, and the indole NH established a key H-bond with Thr179 (conventional residue numbering was used).¹¹⁵

For one of the most active compounds (**90**) we carried out a molecular dynamics simulation of the tubulin/**90** complex. The trajectory analysis showed that, during the 5 ns of simulation, the binding pose of **90** remained relatively stable. The H-bond between the Thr179 and the indole NH had a percentage of stability of 53%, and the interactions with Cys241 and Leu255 were stable throughout the simulation time. The distance between the Cys241 SH and the closest methoxy group of the trimethoxyphenyl moiety was always less than 3.8 Å.

This analysis brought out a hydrophobic interaction between the thiophen-2-yl nucleus and Lys254 side chain that was never observed for ATI derivatives bearing the ester functionality.¹³⁴ In particular the δ and τ carbon atoms of Lys254 side chain lay to a bond distance from thiophen-2-yl centroid ring forming a stable hydrophobic interaction. From dynamic simulations, Leu248 played an important role in the stabilization of the trimethoxyphenyl moiety rather than of the heterocycle (RMSD = 1.70 Å for the tubulin α carbon atoms; 0.67 Å for derivative **90**) (Figure 27).

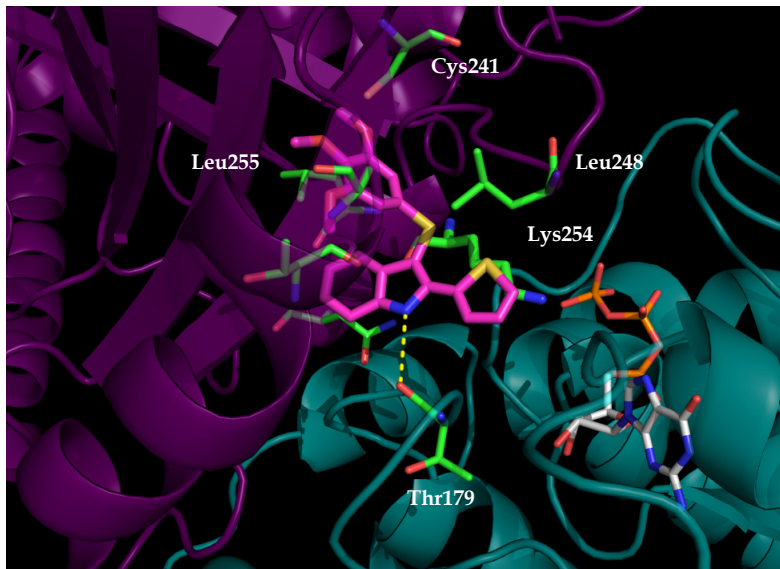


Figure 27. Snapshot of tubulin/compound **90** (pink) trajectories. H-bonds are reported as yellow dotted lines. Residues of the binding site and GTP are also reported as lines.

8. Conclusions

New ATIs were designed and synthesized by bioisosteric replacement of both sulphur bridge and ester function.¹¹⁴⁻¹¹⁵

The replacement of the sulphur atom with a carbonyl group led to compounds endowed with comparable inhibition of tubulin assembly, while the introduction of a methylene moiety led to inhibitors of tubulin assembly whose potency was dependent on the substituent at position 2 of the indole ring. However, as inhibitors of the growth of MCF-7 human breast carcinoma cells, sulphur derivatives were superior or equivalent to the ketones, while methylene derivatives were generally less effective. Compounds bearing either a bromine atom or a methoxy group at position 5 and the 2-methoxycarbonyl group at position 2 of the indole ring were potent inhibitors of both tubulin polymerization and MCF-7 cell growth, with potencies comparable to those of CSA4 (**22**). The most active esters showed ~50% inhibition of human HeLa and HCT116/chr3 cell growth at 0.5 µM, and these compounds also reduced cell viability of HEK, M14 and U937 cells, with IC₅₀'s in the 78-220 nM range. In contrast, murine macrophage J744.1 cell growth was significantly less affected (20% at the highest concentrations).

The ester function of ATIs was replaced with 5-membered heterocycle nucleus and aromatic group to improve the pharmacokinetics properties, because the ester function was rapidly hydrolyzed in the corresponding acid. The new synthesized ATIs were potent inhibitors of the tubulin polymerization and the efficacy was improved compared with the previously synthesized ester **42** and classical MT inhibitors used as reference compounds. In particular, the new ATIs **81**, **90** and **91**, bearing a pyrrole and thiophene moiety, showed a valuable biological profile: (i) they were potent tubulin polymerization inhibitors in the low/submicromolar range of concentration; (ii) such compounds were uniformly more active in the Pgp-overexpressing NCI/ADR-RES cell line than in the parental OVCAR-8 line and

were superior to VRB, VBL and PTX; (iii) compounds **81** and **91** showed selective activity against cells with acquired cisplatin resistance; (iv) they reduced cell growth in a panel of human transformed cell lines *via* arrest of mitotic progression and induction of cell death; (v) the induction of mitotic arrest in cell populations treated with these ATIs was in the same range as was observed with CSA4 and VBL; (vi) they induced apoptosis in the same range or above the level induced by VBL and CSA4, and triggered caspase-3 activation; (vii) the sulphur bridging group of ATIs showed satisfactory metabolic stability. We would like to highlight their effectiveness in HeLa and MDA-231 cell lines, both of which lack functional p53: this indicates that the cell death pathway triggered by ATIs is p53-independent.

This is of relevance from a therapeutic perspective, given that about 50% of all human tumors are defective for p53 function and cannot respond to DNA-targeting drugs, which induce p53-dependent apoptosis. On the whole, the present data, strongly support the therapeutic potential and further development of the new ATIs.

Finally, the metabolic stability data of compound **81**, obtained both in mouse and human microsomes, concurrently to the excellent mouse pharmacokinetic profile, warrant further *in vivo* efficacy experiments.

9. Experimental section

9.1 Chemistry.

MW-assisted reactions were performed on Discover LabMate (CEM), setting temperature, irradiation power, maximum pressure (Pmax), PowerMAX (*in situ* cooling during the MW irradiation), ramp and hold times, and open and closed vessel modes as indicated. Melting points (mp) were determined on a Büchi 510 apparatus and are uncorrected. Infrared spectra (IR) were run on a SpectrumOne FT spectrophotometer. Band position and absorption ranges are given in cm^{-1} . Proton nuclear magnetic resonance (^1H NMR) spectra were recorded on Bruker 400 MHz FT spectrometers in the indicated solvent. Chemical shifts are expressed in δ units (ppm) from tetramethylsilane. Column chromatography was performed on columns packed with alumina from Merck (70-230 mesh) or silica gel from Macherey-Nagel (70-230 mesh). Aluminum oxide TLC cards from Fluka (aluminum oxide precoated aluminum cards with fluorescent indicator visualizable at 254 nm) and silica gel TLC cards from Macherey-Nagel (silica gel precoated aluminum cards with fluorescent indicator visualizable at 254 nm) were used for thin layer chromatography (TLC). Developed plates were visualized by a Spectroline ENF 260C/F UV apparatus. Organic solutions were dried over anhydrous sodium sulfate. Evaporation of the solvents was carried out on a Büchi Rotavapor R-210 equipped with a Büchi V-850 vacuum controller and Büchi V-700 and V-710 vacuum pumps. Elemental analyses of the biologically tested compounds were found within $\pm 0.4\%$ of the theoretical values. Purity of tested compounds was $>95\%$. Compounds **36**¹¹⁵, **39**¹¹³, **42**¹¹³, **45**¹¹⁵, **48**¹¹³, **51**¹¹⁴, **57**¹¹⁵, **66**¹¹⁵, **69**¹¹³ and **75**¹¹⁴ were prepared as previously reported. 2-Phenyl-1*H*-indole was purchased by Sigma Aldrich.

9.2 Synthesis.

General Procedure for the Synthesis of Compounds 37, 40, 43, 46, 49, 52, 58, 61, 64, 67, 72, 76, 85, 88, 91, 94, 97, 106, 109 and 137. Example: (1*H*-Indol-3-yl)-(3,4,5-trimethoxyphenyl)methanone (37). A mixture of AlCl₃ (0.57 g; 0.0043 mol), 1*H*-indole (0.5 g, 0.0043 mol) and 3,4,5-trimethoxybenzoyl chloride (0.99 g, 0.0043 mol) in 1,2-dichloroethane (2 mL) was placed into the MW cavity (closed vessel mode, Pmax = 250 PSI). MW irradiation of 150 W was used, the temperature being ramped from 25 °C to 110 °C, while stirring. Once 110 °C was reached, taking about 1 min, the reaction mixture was held at this temperature for 2 min, then cooled, diluted cautiously with water, and extracted with chloroform; the organic layer was washed with brine, dried and filtered. Removal of the solvent gave a residue that was purified by silica gel column chromatography (ethyl acetate:*n*-hexane = 1:1 as eluent) to furnish 37 as a white solid (0.71 g, 53%), mp 210–213 °C (from ethanol), differing from lit.¹³⁵ 174–176 °C and lit.¹³⁶ 132–133 °C. ¹H NMR (DMSO-*d*₆): δ 3.73 (s, 3H), 3.83 (s, 6H), 7.06 (s, 2H), 7.20–7.24 (m, 2H), 7.48 (d, *J* = 9.1 Hz, 1H), 8.06 (d, *J* = 3.0 Hz, 1H), 8.21 (d, *J* = 8.5 Hz, 1H), 11.99 ppm (broad s, disappeared on treatment with D₂O, 1H). IR: ν 1571, 3179 cm^{−1}. Anal calcd for C₁₈H₁₇NO₄ (311.33) C, 69.44; H, 5.50; N, 4.50; found: C, 69.43; H, 5.48; N, 4.51.

Methyl 3-(3,4,5-trimethoxybenzoyl)-1*H*-indole-2-carboxylate (40). Was synthesized as 37, starting from methyl 1*H*-indole-2-carboxylate, yield 55%, yellow solid, mp 163–168 °C (from ethanol/water). ¹H NMR (DMSO-*d*₆): δ 3.52 (s, 3H), 3.73 (s, 6H), 3.74 (s, 3H), 7.03 (s, 2H), 7.17 (t, *J* = 7.2 Hz, 1H), 7.34 (t, *J* = 7.2 Hz, 1H), 7.54 (d, *J* = 7.5 Hz, 1H), 7.60 (d, *J* = 7.3 Hz, 1H), 12.56 ppm (broad s, disappeared on treatment with D₂O, 1H). IR: ν 1634, 1710, 3279 cm^{−1}. Anal calcd for C₂₀H₁₉NO₆ (369.37) C, 65.02; H, 5.19; N, 3.79; found: C, 65.01; H, 5.18; N, 3.79.

Ethyl 3-(3,4,5-trimethoxybenzoyl)-1*H*-indole-2-carboxylate (43). Was synthesized as **37**, starting from ethyl 5-methoxy-1*H*-indole-2-carboxylate, yield 39%, white solid, mp 105-110 °C (ethanol/*n*-hexane). ^1H NMR (CDCl_3): δ 1.01 (t, J = 7.1 Hz, 3H), 3.82 (s, 6H), 3.93 (s, 3H), 4.14 (q, J = 7.1 Hz, 2H), 7.18 (s, 2H), 7.24 (t, J = 7.1 Hz, 1H), 7.41 (t, J = 7.1 Hz, 1H), 7.5 (d, J = 8.3 Hz, 1H), 7.73 (d, J = 8.1 Hz, 1H), 9.26 ppm (broad s, disappeared on treatment with D_2O , 1H). IR: ν 1648, 1686, 3303 cm^{-1} . Anal calcd for $\text{C}_{21}\text{H}_{21}\text{NO}_6$ (383.39) C, 65.77; H, 5.52; N, 3.65; found: C, 65.77; H, 5.53; N, 3.64.

(5-Chloro-1*H*-indol-3-yl)-(3,4,5-trimethoxyphenyl)methanone (46). Was synthesized as **37**, starting from 5-chloro-1*H*-indole, yield 68%, white solid, mp 240-245 °C (from ethanol). ^1H NMR ($\text{DMSO}-d_6$): δ 3.76 (s, 3H), 3.86 (s, 6H), 7.09 (s, 2H), 7.28 (dd, J = 8.7 Hz, 1H), 7.54 (t, J = 8.1 Hz, 1H), 8.19 (s, 1H), 8.23 (d, J = 2.2 Hz, 1H), 12.21 ppm (broad s, disappeared on treatment with D_2O , 1H). IR: ν 1600, 3261 cm^{-1} . Anal calcd for $\text{C}_{18}\text{H}_{16}\text{ClNO}_4$ (345.78) C, 65.29; H, 4.67; Cl, 10.13; N, 4.06; found: C, 65.30; H, 4.67; Cl, 10.14; N, 4.05.

Methyl 5-chloro-3-(3,4,5-trimethoxybenzoyl)-1*H*-indole-2-carboxylate (49). Was synthesized as **37**, starting from methyl 5-chloro-1*H*-indole-2-carboxylate, yield 68%, yellow solid, mp 188-193 °C (from ethanol/water). ^1H NMR (CDCl_3): δ 3.69 (s, 3H), 3.84 (s, 6H), 3.96 (s, 3H), 7.16 (s, 2H), 7.36 (dd, J = 8.8 Hz, 1H), 7.44 (t, J = 8.8 Hz, 1H), 7.66 (d, J = 1.9 Hz, 1H), 9.50 ppm (broad s, disappeared on treatment with D_2O , 1H). IR: ν 1645, 1711, 3259 cm^{-1} . Anal calcd for $\text{C}_{20}\text{H}_{18}\text{ClNO}_6$ (403.81) C, 59.54; H, 4.50; Cl, 8.67; N, 3.47; found: C, 59.53; H, 4.51; Cl, 8.66; N, 3.47.

Ethyl 5-chloro-3-(3,4,5-trimethoxybenzoyl)-1*H*-indole-2-carboxylate (52). Was synthesized as **37**, starting from ethyl 5-chloro-1*H*-indole-2-carboxylate, yield 38%, yellow solid, mp 160-163 °C (from ethanol). ^1H NMR ($\text{DMSO}-d_6$): δ 0.86 (t, J = 7.1 Hz, 3H), 3.73 (s, 3H), 3.75 (s, 6H), 3.96 (q, J = 7.1 Hz, 2H), 7.04 (s, 2H), 7.38

(dd, $J = 10.1$ Hz, 1H), 7.58 (d, $J = 7.4$ Hz 1H), 7.69 (d, $J = 2.1$ Hz, 1H), 12.78 ppm (broad s, disappeared on treatment with D₂O, 1H). IR: ν 1636, 1684, 3294 cm⁻¹. Anal calcd for C₂₁H₂₀ClNO₆ (417.84) C, 60.42; H, 4.83; Cl, 8.38; N, 3.36; found: C, 60.44; H, 4.83; Cl, 8.37; N, 3.35.

Ethyl 5-chloro-3-(2-(3,4,5-trimethoxyphenyl)acetyl)-1*H*-indole-2-carboxylate (54). Was synthesized as **37**, starting from ethyl 5-chloro-1*H*-indole-2-carboxylate and 2-(3,4,5-trimethoxyphenyl)acetyl chloride, yield 32%, yellow solid, mp 129-134 °C (from ethanol). ¹H NMR (CDCl₃): δ 1.46 (t, $J = 7.1$ Hz, 3H), 3.80 (s, 6H), 3.83 (s, 3H), 4.40 (s, 2H), 4.50 (q, $J = 7.1$ Hz, 2H), 6.46 (s, 2H), 7.32 (dd, $J = 8.8$ Hz, 1H), 7.33 (dd, $J = 9.5$ Hz, 1H), 7.96 (d, $J = 1.8$ Hz, 1H), 9.22 ppm (broad s, disappeared on treatment with D₂O, 1H). IR: ν 1641, 1721, 3169 cm⁻¹. Anal calcd for C₂₂H₂₂ClNO₆ (431.87) C, 61.24; H, 5.14; Cl, 8.11; N, 3.25; found: C, 61.25; H, 5.13; Cl, 8.11; N, 3.26.

(5-Bromo-1*H*-indol-3-yl)(3,4,5-trimethoxyphenyl)methanone (58). Was synthesized as **37**, starting from 5-bromo-1*H*-indole, yield 53%, yellow solid, mp 235-240 °C (from ethanol). ¹H NMR (DMSO-d₆): δ 3.76 (s, 3H), 3.86 (s, 6H), 7.09 (s, 2H), 7.40 (dd, $J = 6.6$ Hz, 1H), 7.50 (d, $J = 8.1$ Hz, 1H), 8.18 (s, 1H), 8.39 (d, $J = 2.5$ Hz, 1H), 12.19 ppm (broad s, disappeared on treatment with D₂O, 1H). IR: ν 1599, 3279 cm⁻¹. Anal calcd for C₁₈H₁₆BrNO₄ (390.23) C, 55.52; H, 4.14; Br, 20.28; N, 3.59; found: C, 55.51; H, 4.13; Br, 20.28; N, 3.59.

Methyl 5-bromo-3-(3,4,5-trimethoxybenzoyl)-1*H*-indole-2-carboxylate (61). Was synthesized as **37**, starting from **124**, yield 40%, white solid, mp 207-210 °C (from ethanol/n-hexane). ¹H NMR (CDCl₃): δ 3.68 (s, 3H), 3.83 (s, 6H), 3.95 (s, 3H), 7.14 (s, 2H), 7.38 (d, $J = 8.2$ Hz, 1H), 7.48 (dd, $J = 6.9$ Hz, 1H), 7.81 (d, $J = 1.8$ Hz, 1H), 9.45 ppm (broad s, disappeared on treatment with D₂O, 1H). IR: ν 1642, 1711, 3248 cm⁻¹. Anal calcd for C₂₀H₁₈BrNO₆ (448.26) C, 53.69; H, 4.06; Br, 17.65; N, 3.13; found: C, 53.69; H, 4.07; Br, 17.64; N, 3.14.

Ethyl 5-bromo-3-(3,4,5-trimethoxybenzoyl)-1*H*-indole-2-carboxylate (64).

Was synthesized as **37**, starting from **117**, yield 46%, yellow solid, mp 135-140 °C (from ethanol/*n*-hexane). ^1H NMR (DMSO- d_6): δ 0.85 (t, J = 7.1 Hz, 3H), 3.73 (s, 3H), 3.75 (s, 6H), 3.98 (q, J = 7.1 Hz, 2H), 7.03 (s, 2H), 7.33 (d, J = 1.2 Hz, 1H), 7.48 (dd, J = 6.9 Hz, 1H), 7.53 (dd, J = 8.8 Hz, 1H), 12.74 ppm (broad s, disappeared on treatment with D₂O, 1H). IR: ν 1638, 1702, 3292 cm⁻¹. Anal calcd for C₂₁H₂₀BrNO₆ (462.29) C, 54.66; H, 4.37; Br, 17.12; N, 3.04; found: C, 54.65; H, 4.36; Br, 17.12; N, 3.04.

(5-Methoxy-1*H*-indol-3-yl)-(3,4,5-trimethoxyphenyl)methanone (67). Was synthesized as **37**, starting from 5-methoxy-1*H*-indole, yield 42%, yellow solid, mp 202-207 °C (from ethanol), lit.¹¹⁷ 194-195 °C.

Methyl 5-methoxy-3-(3,4,5-trimethoxybenzoyl)-1*H*-indole-2-carboxylate (72).

Was synthesized as **37**, starting from methyl 5-methoxy-1*H*-indole-2-carboxylate, yield 20%, yellow solid, mp 168-173 °C (from ethanol/water). ^1H NMR (DMSO- d_6): δ 3.47 (s, 3H), 3.71 (s, 3H), 3.73 (s, 3H), 3.74 (s, 6H), 6.99-7.02 (m, 3H), 7.07 (d, J = 2.3 Hz, 1H), 7.44 (d, J = 8.95 Hz, 1H), 12.49 ppm (broad s, disappeared on treatment with D₂O, 1H). IR: ν 1635, 1710, 3274 cm⁻¹. Anal calcd for C₂₁H₂₁NO₇ (399.39) C, 63.14; H, 5.30; N, 3.51; found: C, 63.13; H, 5.31; N, 3.51.

Ethyl 5-methoxy-3-(3,4,5-trimethoxybenzoyl)-1*H*-indole-2-carboxylate (76).

Was synthesized as **37**, starting from ethyl 5-methoxy-1*H*-indole-2-carboxylate, yield 60%, yellow solid, mp 150-155 °C (from ethanol). ^1H NMR (CDCl₃): δ 0.97 (t, J = 7.1 Hz, 3H), 3.82 (s, 3H), 3.84 (s, 6H), 3.94 (s, 3H), 4.09 (q, J = 7.1 Hz, 2H), 7.07 (dd, J = 6.5 Hz, 1H), 7.18 (s, 2H), 7.26 (d, J = 1.9 Hz, 1H), 7.39 (d, J = 9.0 Hz, 1H), 9.21 ppm (broad s, disappeared on treatment with D₂O, 1H). IR: ν 1647, 1694, 3353 cm⁻¹. Anal calcd for C₂₂H₂₃NO₇ (413.42) C, 63.90; H, 5.61; N, 3.39; found: C, 63.91; H, 5.62; N, 3.40.

(2-(Furan-2-yl)-1*H*-indol-3-yl)(3,4,5-trimethoxyphenyl)methanone (85). Was synthesized as **37**, starting from **118**, yield 6%, yellow solid, mp 115-117 °C (from ethanol). ^1H NMR (CDCl_3): δ 3.80 (s, 6H), 3.95 (s, 3H), 6.50-6.51 (m, 1H), 7.10-7.15 (m, 3H), 7.22-7.26 (m, 2H), 7.41-7.46 (m, 2H), 7.52-7.53 (m, 1H), 9.11 ppm (broad s, disappeared on treatment with D_2O , 1H). IR: ν 3358 cm^{-1} . Anal calcd. for $\text{C}_{22}\text{H}_{19}\text{NO}_5$ (377.39) C, 70.02; H, 5.07; N, 3.71; found: C, 70.02; H, 5.06; N, 3.73.

(2-(Furan-3-yl)-1*H*-indol-3-yl)(3,4,5-trimethoxyphenyl)methanone (88). Was synthesized as **37**, starting from **130**, yield 32%, yellow oil. ^1H NMR (CDCl_3): δ 3.78 (s, 6H), 3.93 (s, 3H), 6.60-6.61 (m, 1H), 7.13 (s, 2H), 7.15-7.19 (m, 1H), 7.25-7.27 (m, 1H), 7.43-7.46 (m, 2H), 7.58-7.60 (m, 1H), 8.05-8.06 (m, 1H), 8.70 ppm (broad s, disappeared on treatment with D_2O , 1H). IR: ν 3349 cm^{-1} . Anal calcd. for $\text{C}_{22}\text{H}_{19}\text{NO}_5$ (377.39) C, 70.02; H, 5.07; N, 3.71; found: C, 70.01; H, 5.05; N, 3.72.

(2-(Thiophen-2-yl)-1*H*-indol-3-yl)-(3',4',5'-trimethoxyphenyl)methanone (91). Was synthesized as **37**, starting from **133**, yield 34%, yellow solid, mp 155-159 °C (from ethanol). ^1H NMR ($\text{DMSO}-d_6$): δ 3.75 (s, 6H), 3.88 (s, 3H), 6.96-6.98 (m, 1H), 7.08 (s, 2H), 7.20-7.24 (m, 2H), 7.30-7.34 (m, 2H), 7.45 (d, $J = 8.0$ Hz, 1H), 7.80 (d, $J = 7.8$ Hz, 1H), 8.73 ppm (broad s, disappeared on treatment with D_2O , 1H). IR: ν 1570, 3214 cm^{-1} . Anal calcd. for $\text{C}_{22}\text{H}_{19}\text{NO}_4\text{S}$ (393.46) C, 67.16; H, 4.87; N, 3.56; found: C, 66.92; H, 4.79; N, 3.41.

(2-(Thiophen-3-yl)-1*H*-indol-3-yl)-(3',4',5'-trimethoxyphenyl)methanone (94). Was synthesized as **37**, starting from **134**, yield 25%, yellow solid, mp 118-120 °C (from ethanol). ^1H NMR (CDCl_3): δ 3.74 (s, 6H), 3.87 (s, 3H), 7.04 (s, 2H), 7.11-7.12 (m, 1H), 7.23-7.28 (m, 2H), 7.29-7.33 (m, 1H), 7.44-7.47 (m, 1H), 7.50-7.51 (m, 1H), 7.91-7.93 (m, 1H), 8.60 ppm (broad s, disappeared on treatment with D_2O , 1H). IR: ν 3337 cm^{-1} . Anal calcd. for $\text{C}_{22}\text{H}_{19}\text{NO}_4\text{S}$ (393.46) C, 67.16; H, 4.87; N, 3.56; found: C, 66.95; H, 4.81; N, 3.43.

(2-Phenyl-1*H*-indol-3-yl)(3,4,5-trimethoxyphenyl)methanone (97). Was synthesized as **37**, starting from 2-phenyl-1*H*-indole, yield 95%, grey solid, mp 207-212 °C (from ethanol). ^1H NMR (DMSO-d_6): δ 3.59 (s, 3H), 3.60 (s, 6H), 6.82 (s, 2H), 7.18-7.28 (m, 5H), 7.36-7.38 (m, 2H), 7.50-7.53 (m, 1H), 7.92-7.94 (m, 1H), 12.20 ppm (broad s, disappeared on treatment with D_2O , 1H). IR: ν 3213 cm^{-1} . Anal calcd. for $\text{C}_{24}\text{H}_{21}\text{NO}_4$ (387,43) C, 74.40; H, 5.46; N, 3.62; found: C, 74.36; H, 5.41; N, 3.59.

(2-(Naphthalen-1-yl)-1*H*-indol-3-yl)(3,4,5-trimethoxyphenyl)methanone (106). Was synthesized as **37**, starting from **136**, yield 50%, white solid, mp 177-179 °C (from ethanol). ^1H NMR (CDCl_3): δ 3.40 (s, 6H), 3.64 (s, 3H), 6.61 (s, 2H), 7.26-7.30 (m, 1H), 7.34-7.36 (m, 1H), 7.37-7.41 (m, 2H), 7.43-7.53 (m, 3H), 7.73 (d, J = 8.2 Hz, 1H), 7.78-7.83 (m, 1H), 7.94-8.00 (m, 1H), 8.31-8.36 (m, 1H), 8.81 ppm (broad s, disappeared on treatment with D_2O , 1H). IR: ν 3158 cm^{-1} . Anal calcd. for $\text{C}_{28}\text{H}_{23}\text{NO}_4$ (437,49) C, 76.87; H, 5.30; N, 3.20; found: C, 76.81; H, 5.24; N, 3.17.

(2-(Naphthalen-2-yl)-1*H*-indol-3-yl)(3,4,5-trimethoxyphenyl)methanone (109). Was synthesized as **37**, starting from **122**, yield 33%, yellow solid, mp 182-186 °C (from ethanol). ^1H NMR (CDCl_3): δ 3.56 (s, 3H), 3.63 (s, 6H), 6.98 (s, 2H), 7.29-7.37 (m, 2H), 7.43 (dd, J = 8.5 and 1.8 Hz, 1H), 7.47-7.52 (m, 3H), 7.68-7.78 (m, 3H), 7.87 (m, 1H), 8.10-8.11 (m, 1H), 8.80 ppm (broad s, disappeared on treatment with D_2O , 1H). IR: ν 3170 cm^{-1} . Anal calcd. for $\text{C}_{28}\text{H}_{23}\text{NO}_4$ (437,49) C, 76.87; H, 5.30; N, 3.20; found: C, 76.78; H, 5.22; N, 3.15.

(2-(1-(Phenylsulfonyl)-1*H*-pyrrol-3-yl)-1*H*-indol-3-yl)(3,4,5-trimethoxyphenyl)methanone (137). Was synthesized as **37**, starting from **128**, yield 64%, green solid, mp 124-126 °C (from ethanol). ^1H NMR (CDCl_3): δ 3.71 (s, 6H), 3.91 (s, 3H), 6.48-6.49 (m, 1H), 7.08-7.17 (m, 4H), 7.22-7.28 (m, 1H), 7.39-7.40 (m, 1H), 7.51-7.66 (m, 5H), 7.83-7.85 (m, 2H), 8.76 ppm (broad s, disappeared on treatment with D_2O , 1H). IR: ν 3284 cm^{-1} .

(2-(1*H*-Pyrrol-3-yl)-1*H*-indol-3-yl)(3,4,5-trimethoxyphenyl)methanone (82). A mixture of **137** (0.1 g, 0.00019 mol) and 2N NaOH (0.59 mL) in MeOH (1.7 mL) was heated at 70 °C for 3 h. After cooling 2 N HCl was added and the mixture was extracted with AcOEt; organic layer was washed with brine, dried and filtered. Removal of the solvent gave a residue that was purified by silica gel column chromatography (ethyl acetate : *n*-exane = 1:1 as eluent) to furnish **82** as a yellow solid (0.07 g, 98%), mp 114-115 °C (from ethanol). ¹H NMR (CDCl₃): δ 3.77 (s, 6H), 3.90 (s, 3H), 6.42-6.44 (m, 1H), 6.77-6.79 (m, 1H), 7.10 (s, 2H), 7.14-7.25 (m, 3H), 7.40-7.42 (m, 1H), 7.67-7.71 (m, 1H), 8.38 (broad s, disappeared on treatment with D₂O, 1H), 8.53 ppm (broad s, disappeared on treatment with D₂O, 1H). IR: ν 3241, 3333 cm⁻¹. Anal calcd. for C₂₂H₂₀N₂O₄ (376.41) C, 70.20; H, 5.36; N, 7.44; found: C, 70.19; H, 5.35; N, 7.45.

General Procedure for the Synthesis of Compounds **80**, **100**, **102** and **104**.

Example: **(2-(1*H*-Pyrrol-2-yl)-1*H*-indol-3-yl)(3,4,5-trimethoxyphenyl)methanone (80).** To a mixture of **126** (0.5 g, 0.003 mol) and anhydrous ZnCl₂ (0.818 g, 0.006 mol) in anhydrous CH₂Cl₂ (20 mL), CH₃MgBr (3M diethylether solution) (1.3 mL, 0.0041 mol) was added dropwise at 25 °C and under Ar stream. The resulting suspension was stirred for 1 h and to it a solution of 3,4,5-trimethoxybenzoylchloride (0.76 g, 0.0033 mol) in anhydrous CH₂Cl₂ (16 mL) was added dropwise over 5 min at 25 °C. The resulting mixture was stirred for 1 h followed by addition of SnCl₄ (1M dichloromethane solution) (3 mL, 0.003 mol). The resulting mixture was stirred overnight at 25 °C, then quenched on bath ice and extracted with dichloromethane; organic layer was washed with brine, dried and filtered. Removal of the solvent gave a residue that was twice purified by silica gel column chromatography (ethyl acetate : *n*-exane = 1:1 and ethyl acetate : *n*-exane = 1.2 as eluents) to furnish **80** as a green solid (0.03 g, 3%), mp 55-60 °C (from ethanol). ¹H NMR (DMSO_d₆): δ 3.70 (s, 6H), 3.75 (s, 3H), 6.24-6.26 (m, 1H), 6.84-

6.85 (m, 1H), 6.96-7.07 (m, 5H), 7.14-7.18 (m, 1H), 7.43-7.45 (m, 1H), 11.94 (broad s, disappeared on treatment with D₂O, 1H), 12.15 ppm (broad s, disappeared on treatment with D₂O, 1H). IR: ν 3235, 3328 cm⁻¹. Anal calcd. for C₂₂H₂₀N₂O₄ (376.41) C, 70.20; H, 5.36; N, 7.44; found: C, 70.18; H, 5.36; N, 7.46.

(2-(Pyridin-2-yl)-1*H*-indol-3-yl)(3,4,5-trimethoxyphenyl)methanone (100).
Was synthesized as **80** starting from **119**, yield 67%, yellow solid, mp 65-70 °C (from ethanol). ¹H NMR (DMSO_d₆): δ 3.61 (s, 6H), 3.64 (s, 3H), 6.89 (s, 2H), 7.19-7.21 (m, 1H), 7.26-7.28 (m, 2H), 7.39-7.41 (m, 1H), 7.56-7.58 (m, 1H), 7.63-7.65 (m, 1H), 7.79-7.81 (m, 1H), 8.55-8.57 (m, 1H), 12.36 ppm (broad s, disappeared on treatment with D₂O, 1H). IR: ν 3241 cm⁻¹. Anal calcd. for C₂₃H₂₀N₂O₄ (388.42) C, 71.12; H, 5.19; N, 7.21; found: C, 71.07; H, 5.15; N, 7.19.

(2-(Pyridin-3-yl)-1*H*-indol-3-yl)(3,4,5-trimethoxyphenyl)methanone (102).
Was synthesized as **80** starting from **120**, yield 45%, yellow solid, mp 130-135 °C (from ethanol). ¹H NMR (DMSO_d₆): δ 3.60 (s, 3H), 3.61 (s, 6H), 6.82 (s, 2H), 7.21-7.31 (m, 3H), 7.53-7.55 (m, 1H), 7.75-7.78 (m, 1H), 7.96 (d, *J* = 7.7 Hz, 1H), 8.44 (dd, *J* = 4.8 and 1.6 Hz, 1H), 8.56-8.57 (m, 1H), 12.38 ppm (broad s, disappeared on treatment with D₂O, 1H). IR: ν 3094 cm⁻¹. Anal calcd. for C₂₃H₂₀N₂O₄ (388.42) C, 71.12; H, 5.19; N, 7.21; found: C, 71.09; H, 5.17; N, 7.20.

(2-(Pyridin-4-yl)-1*H*-indol-3-yl)(3,4,5-trimethoxyphenyl)methanone (104).
Was synthesized as **80** starting from **121**, yield 10%, yellow solid, mp 50-55 °C (from ethanol). ¹H NMR (DMSO_d₆): δ 3.62 (s, 3H), 3.63 (s, 6H), 6.86 (s, 2H), 7.21-7.25 (m, 1H), 7.29-7.33 (m, 1H), 7.35-7.37 (m, 2H), 7.55-7.57 (m, 1H), 7.87-7.90 (m, 1H), 8.46-8.47 (m, 2H), 12.43 ppm (broad s, disappeared on treatment with D₂O, 1H). IR: ν 3179 cm⁻¹. Anal calcd. for C₂₃H₂₀N₂O₄ (388.42) C, 71.12; H, 5.19; N, 7.21; found: C, 71.05; H, 5.13; N, 7.18.

General Procedure for the Synthesis of Compounds 38, 47, 59, 68 and 92.

Example: 3-(3,4,5-trimethoxybenzyl)-1*H*-indole (38). Sodium borohydride (0.80 g, 0.021 mol) was added to a solution of **37** (0.66 g, 0.0021 mol) in ethanol (85 mL). The reaction mixture was refluxed for 3 h, then cooled, cautiously diluted with water and extracted with ethyl acetate; the organic layer was washed with brine, dried and filtered. Evaporation of the solvent gave a residue that was purified by silica gel column chromatography (ethyl acetate:*n*-hexane = 1:1 as eluent) to furnish **38** as a white solid (0.26 g, 42%), mp 133-136 °C (from ethanol), lit.¹³⁵ 125-126 °C and lit.¹³⁷ 128-130 °C.

5-Chloro-3-(3,4,5-trimethoxybenzyl)-1*H*-indole (47). Was synthesized as **38** starting from **46**, yield 47%, orange solid, mp 145-150 °C (from ethanol). ¹H NMR (CDCl_3): δ 3.80 (s, 6H), 3.83 (s, 3H), 4.00 (s, 2H), 6.49 (s, 2H), 6.95 (d, J = 2.3 Hz, 1H), 7.14 (dd, J = 8.6 Hz, 1H), 7.28 (d, J = 8.1 Hz, 1H), 7.51 (d, J = 2.0 Hz, 1H), 8.40 ppm (broad s, disappeared on treatment with D_2O , 1H). IR: ν 3372 cm^{-1} . Anal calcd for $\text{C}_{18}\text{H}_{18}\text{ClNO}_3$ (331.79) C, 65.24; H, 5.48; Cl, 10.56; N, 4.23; found: C, 65.24; H, 5.49; Cl, 10.58; N, 4.21.

5-Bromo-3-(3,4,5-trimethoxybenzyl)-1*H*-indole (59). Was synthesized as **38**, starting from **58**, yield 58%, white solid, mp 145-150 °C (from ethanol). ¹H NMR (CDCl_3): 3.81 (s, 6H), 3.84 (s, 3H), 4.01 (s, 2H), 6.50 (s, 2H), 6.94 (d, J = 2.3 Hz, 1H), 7.24-7.28 (m, 2H), 7.69 (d, J = 1.7 Hz, 1H), 8.05 ppm (broad s, disappeared on treatment with D_2O , 1H). IR: ν 3353 cm^{-1} . Anal calcd for $\text{C}_{18}\text{H}_{18}\text{BrNO}_3$ (376,24) C, 57.59; H, 4.84; Br, 21.04; N, 3.73; found: C, 57.60; H, 4.85; Br, 21.04; N, 3.73.

5-Methoxy-3-(3,4,5-trimethoxybenzyl)-1*H*-indole (68). Was synthesized as **38**, starting from **67**, yield 68%, white solid, mp 110-113 °C (from ethanol). ¹H NMR (CDCl_3): δ 3.78 (s, 6H), 3.80 (s, 3H), 3.81 (s, 3H), 4.01 (s, 2H), 6.51 (s, 2H), 6.84 (d, J = 8.8 Hz, 1H), 6.88 (t, J = 2.4 Hz, 1H), 6.97 (d, J = 2.4 Hz, 1H), 7.24 (t, J = 4.7 Hz, 1H), 7.90 ppm (broad s, disappeared on treatment with D_2O , 1H). IR: ν 3365

cm^{-1} . Anal calcd for $\text{C}_{19}\text{H}_{21}\text{NO}_4$ (327.37) C, 69.69; H, 6.47; N, 4.28; found: C, 69.69; H, 6.48; N, 4.29.

2-(Thiophen-2-yl)-3-(3',4',5'-trimethoxybenzyl)-1*H*-indole (92) Was synthesized as **38**, starting from **91**, yield 21%, brown solid, mp 43-47 °C (from ethanol). ^1H NMR (CDCl_3): δ 3.73 (s, 6H), 3.80 (s, 3H), 4.27 (s, 2H), 6.47 (s, 2H), 7.07-7.13 (m, 2H), 7.19-7.23 (m, 2H), 7.35-7.39 (m, 2H), 7.49 (d, $J = 7.9$ Hz, 1H), 8.17 ppm (broad s, disappeared on treatment with D_2O , 1H). IR: ν 3340 cm^{-1} . Anal calcd. for $\text{C}_{22}\text{H}_{21}\text{NO}_3\text{S}$ (379.47) C, 69.63; H, 5.58; N, 3.69; found: C, 69.41; H, 5.55; N, 3.50.

General Procedure for the Synthesis of Compounds 41, 44, 50, 53, 56, 62, 65, 74, and 78. Example: Methyl 3-(3,4,5-trimethoxybenzyl)-1*H*-indole-2-carboxylate (41). To a cold solution of **40** (0.31 g, 0.00084 mol) in trifluoroacetic acid (0.96 g, 0.65 mL, 0.0084 mol) was added dropwise triethylsilane (0.22 g, 0.30 mL, 0.0019 mol). The reaction mixture was stirred at 25 °C for 24 h, then neutralized with a saturated solution of sodium hydrogen carbonate and extracted with ethyl acetate; the organic layer was washed with brine, dried and filtered. Removal of the solvent gave a residue that was purified by silica gel column chromatography (ethyl acetate:*n*-hexane = 3:2 as eluent) to furnish **41** as a yellow solid (0.15 g, 50%), mp 156-161 °C (from ethanol/*n*-hexane). ^1H NMR (CDCl_3): δ 3.69 (s, 6H), 3.72 (s, 3H), 3.89 (s, 3H), 4.38 (s, 2H), 6.46 (s, 2H), 7.05 (t, $J = 8.1$ Hz, 1H), 7.25 (t, $J = 8.3$ Hz, 1H), 7.33 (d, $J = 7.4$ Hz, 1H), 7.57 (d, $J = 8.2$ Hz, 1H), 8.75 ppm (broad s, disappeared on treatment with D_2O , 1H). IR: ν 1690, 3318 cm^{-1} . Anal calcd for $\text{C}_{20}\text{H}_{21}\text{NO}_5$ (355.38) C, 67.58; H, 5.95; N, 3.94; found: C, 67.57; H, 5.95; N, 3.92.

Ethyl 3-(3,4,5-trimethoxybenzyl)-1*H*-indole-2-carboxylate (44). Was synthesized as **41**, starting from **43**, yield 73%, white solid, mp 115-118 °C (from ethanol/*n*-hexane). ^1H NMR (CDCl_3): δ 1.42 (t, $J = 7.1$ Hz, 3H), 3.77 (s, 6H), 3.80

(s, 3H), 4.44 (q, $J = 7.1$ Hz, 2H), 4.47 (s, 2H), 6.55 (s, 2H), 7.13 (t, $J = 7.0$ Hz, 1H), 7.33 (t, $J = 6.9$ Hz, 1H), 7.39 (d, $J = 7.5$ Hz, 1H), 7.64 (d, $J = 7.4$ Hz, 1H), 8.82 ppm (broad s, disappeared on treatment with D₂O, 1H). IR: ν 1672, 3337 cm⁻¹. Anal calcd for C₂₁H₂₃NO₅ (369.41) C, 68.23; H, 6.28; N, 3.79; found: C, 68.22; H, 6.25; N, 3.79.

Methyl 5-chloro-3-(3,4,5-trimethoxybenzyl)-1*H*-indole-2-carboxylate (50). Was synthesized as **41**, starting from **49**, yield 69%, white solid, mp 172-175 °C (from ethanol/n-hexane). ¹H NMR (CDCl₃): δ 3.70 (s, 6H), 3.73 (s, 3H), 3.89 (s, 3H), 4.33 (s, 2H), 6.42 (s, 2H), 7.21 (d, $J = 1.9$ Hz, 1H), 7.24 (t, $J = 8.7$ Hz, 1H), 7.51 (d, $J = 1.9$ Hz, 1H), 8.74 ppm (broad s, disappeared on treatment with D₂O, 1H). IR: ν 1682, 3322 cm⁻¹. Anal calcd for C₂₀H₂₀ClNO₅ (389.83) C, 61.68; H, 5.18; Cl, 8.99; N, 3.60; found: C, 61.69; H, 5.17; Cl, 8.98; N, 3.60.

Ethyl 5-chloro-3-(3,4,5-trimethoxybenzyl)-1*H*-indole-2-carboxylate (53). Was synthesized as **41**, starting from **52**, yield 95%, yellow solid, mp 147-150 °C (from ethanol/n-hexane). ¹H NMR (CDCl₃): δ 1.41 (t, $J = 7.1$ Hz, 3H), 3.79 (s, 6H), 3.81 (s, 3H), 4.41 (s, 2H), 4.43 (q, $J = 6.4$ Hz, 2H), 6.51 (s, 2H), 7.25-7.28 (m, 1H), 7.33 (dd, $J = 8.1$ Hz, 1H), 7.59-7.60 (m, 1H), 8.91 ppm (broad s, disappeared on treatment with D₂O, 1H). IR: ν 1666, 3315 cm⁻¹. Anal calcd for C₂₁H₂₂ClNO₅ (417.84) C, 62.51; H, 5.50; Cl, 8.67; N, 3.47; found: C, 62.51; H, 5.51; Cl, 8.66; N, 3.46.

Ethyl 5-chloro-3-(3,4,5-trimethoxyphephenethyl)-1*H*-indole-2-carboxylate (56). Was synthesized as **41**, starting from **55**, yield 40%, white solid, mp 163-165 °C (from ethanol). ¹H NMR (CDCl₃): δ 1.44 (t, $J = 7.5$ Hz, 3H), 2.88 (t, $J = 7.4$ Hz, 2H), 3.35 (t, $J = 7.3$ Hz, 2H), 3.79 (s, 6H), 3.83 (s, 3H), 4.42 (t, $J = 7.1$ Hz, 2H), 6.38 (s, 2H), 7.24 (dd, $J = 9.2$ Hz, 1H), 7.31 (d, $J = 8.8$ Hz, 1H), 7.49 (d, $J = 1.9$ Hz, 1H), 9.01 ppm (broad s, disappeared on treatment with D₂O, 1H). IR: ν 1669, 3318 cm⁻¹. Anal calcd for C₂₂H₂₄ClNO₅ (417.88) C, 62.29; H, 5.80; Cl, 8.38; N, 3.36; found: C, 62.30; H, 5.81; Cl, 8.38; N, 3.36.

Methyl 5-bromo-3-(3,4,5-trimethoxybenzyl)-1*H*-indole-2-carboxylate (62).

Was synthesized as **41**, starting from **61**, yield 97%, yellow solid, mp 177-182 °C (from ethanol/n-hexane). ^1H NMR ($\text{DMSO}-d_6$): δ 3.57 (s, 3H), 3.67 (s, 6H), 3.92 (s, 3H), 4.34 (s, 2H), 6.62 (s, 2H), 7.36-7.36 (m, 2H), 7.90 (d, J = 2.3 Hz, 1H), 11.88 ppm (broad s, disappeared on treatment with D_2O , 1H). IR: ν 1675, 3322 cm^{-1} . Anal calcd for $\text{C}_{20}\text{H}_{20}\text{BrNO}_5$ (434.28) C, 55.42; H, 4.65; Br, 18.22; N, 3.23; found: C, 55.43; H, 4.64; Br, 18.22; N, 3.22.

Ethyl 5-bromo-3-(3,4,5-trimethoxybenzyl)-1*H*-indole-2-carboxylate (65). Was synthesized as **41**, starting from **64**, yield 46%, white solid, mp 150-155 °C (from ethanol/n-hexane). ^1H NMR (CDCl_3): δ 1.41 (t, J = 7.1 Hz, 3H), 3.79 (s, 6H), 3.82 (s, 3H), 4.43 (q, J = 7.1 Hz, 2H), 6.51 (s, 2H), 7.28 (d, J = 9.4 Hz, 1H), 7.29 (s, 2H), 7.40 (dd, J = 6.9 Hz, 1H), 7.77 (d, J = 1.8 Hz, 1H), 8.90 ppm (broad s, disappeared on treatment with D_2O , 1H). IR: ν 1665, 3317 cm^{-1} . Anal calcd for $\text{C}_{21}\text{H}_{22}\text{BrNO}_6$ (448.31) C, 54.42; H, 7.79; Br, 17.04; N, 3.02; found: C, 54.43; H, 7.79; Br, 17.05; N, 3.02.

Methyl 5-methoxy-3-(3,4,5-trimethoxybenzyl)-1*H*-indole-2-carboxylate (74).

Was synthesized as **41**, starting from **72**, yield 58%, white solid, mp 125-128 °C (from ethanol/n-hexane). ^1H NMR (CDCl_3): δ 3.77 (s, 6H), 3.79 (s, 3H), 3.80 (s, 3H), 3.94 (s, 3H), 4.42 (s, 2H), 6.53 (s, 1H), 6.96 (d, J = 2.3 Hz, 1H), 7.00 (dd, J = 6.4 Hz, 1H), 7.28 (d, J = 8.9 Hz, 1H), 8.67 (s, 1H), 11.91 ppm (broad s, disappeared on treatment with D_2O , 1H). IR: ν 1687, 3331 cm^{-1} . Anal calcd for $\text{C}_{21}\text{H}_{23}\text{NO}_6$ (385.41) C, 65.43; H, 6.01; N, 3.63; found: C, 65.44; H, 6.02; N, 3.63.

Ethyl 5-methoxy-3-(3,4,5-trimethoxybenzyl)-1*H*-indole-2-carboxylate (78).

Was synthesized as **41**, starting from **76**, yield 90%, white solid, mp 132-135 °C (from ethanol). ^1H NMR (CDCl_3): δ 1.42 (t, J = 7.1 Hz, 3H), 3.78 (s, 9H), 3.81 (s, 3H), 4.44 (q, J = 7.2 Hz, 2H), 4.45 (s, 2H), 6.56 (s, 2H), 6.98-7.03 (m, 2H), 7.28-7.32 (m, 1H), 8.76 ppm (broad s, disappeared on treatment with D_2O , 1H). IR: ν

1672, 3330 cm^{-1} . Anal calcd for $\text{C}_{22}\text{H}_{25}\text{NO}_6$ (399.44) C, 66.14; H, 6.31; N, 3.51; found: C, 66.13; H, 6.32; N, 3.50.

General Procedure for the Synthesis of Compounds 73 and 77. Example: Methyl 3-(hydroxy(3,4,5-trimethoxyphenyl)methyl)-5-methoxy-1*H*-indole-2-carboxylate (73). A mixture of **72** (0.34 g, 0.00085 mol) and sodium borohydride (0.03 g, 0.00085 mol) in THF (2.1 mL) and water (0.12 mL) was refluxed for 2 h. After cooling, water and ethyl acetate were added. The organic layer was removed and washed with brine, dried and filtered. Removal of the solvent gave a residue that was purified by silica gel column chromatography (ethyl acetate:*n*-hexane = 1:1 as eluent) to furnish **73** as a brown solid (0.1 g, 29%), mp 100–103 °C (from ethanol). ^1H NMR (CDCl_3): δ 3.76 (s, 3H), 3.79 (s, 6H), 3.82 (s, 3H), 3.97 (s, 3H), 4.53 (d, J = 1.2 Hz, 1H), 6.50 (d, J = 7.4 Hz, 1H), 6.77 (s, 2H), 6.95 (d, J = 2.4 Hz, 1H), 7.02 (dd, J = 6.5 Hz, 1H), 7.28 (d, J = 8.4 Hz, 1H), 8.78 ppm (broad s, disappeared on treatment with D_2O , 1H). IR: ν 1707, 2937, 3322 cm^{-1} . Anal calcd for $\text{C}_{21}\text{H}_{23}\text{NO}_7$ (401.41) C, 62.82; H, 5.78; N, 3.49; found: C, 62.83; H, 5.79; N, 3.49.

Ethyl 3-(hydroxy(3,4,5-trimethoxyphenyl)methyl)-5-methoxy-1*H*-indole-2-carboxylate (77). Was synthesized as **73**, starting from **76**, yield 53%, white solid, mp 115–120 °C (from ethanol). ^1H NMR (CDCl_3): δ 1.42 (t, J = 7.2 Hz, 3H), 3.76 (s, 3H), 3.79 (s, 3H), 3.81 (s, 3H), 3.83 (s, 3H), 4.43 (q, J = 6.0 Hz, 2H), 4.44 (d, J = 1.2 Hz, 1H), 6.49 (d, J = 7.2 Hz, 1H), 6.77 (s, 2H), 6.95 (d, J = 2.3 Hz, 1H), 7.01 (dd, J = 6.6 Hz, 1H), 7.29 (d, J = 7.3 Hz, 1H), 8.78 ppm (broad s, disappeared on treatment with D_2O , 1H). IR: ν 1676, 3209, 3402 cm^{-1} . Anal calcd for $\text{C}_{22}\text{H}_{25}\text{NO}_7$ (415.44) C, 63.59; H, 6.07; N, 3.37; found: C, 63.60; H, 6.06; N, 3.38.

Ethyl 5-chloro-3-(2-oxo-2-(3,4,5-trimethoxyphenyl)acetyl)-1*H*-indole-2-carboxylate (55). A mixture of **54** (0.05 g, 0.00012 mol) and selenium(IV) oxide (0.05 g; 0.00045 mol) in DMSO (2 mL) was placed into the MW cavity (closed vessel mode, Pmax = 250 PSI). MW irradiation of 150 W was used, the temperature

being ramped from 25 °C to 150 °C. Once 150 °C was reached, taking about 1 min, the reaction mixture was held at this temperature for 2 min, while stirring, then cooled, diluted with water, and extracted with ethyl acetate; organic layer was washed with brine, dried and filtered. Removal of the solvent gave a residue that was purified by silica gel column chromatography (ethyl acetate:*n*-hexane = 1:2 as eluent) to furnish **55** as a yellow solid (0.03 g, 56%), mp 177-181 °C (from ethanol). ¹H NMR (CDCl₃): δ 1.07(t, *J* = 7.2 Hz, 3H), 3.93 (s, 6H), 3.98 (s, 3H), 4.12 (q, *J* = 7.1 Hz, 2H), 7.35 (s, 2H), 7.42-7.43 (m, 2H), 8.40 (s, 1H), 9.50 ppm (broad s, disappeared on treatment with D₂O, 1H). IR: ν 1650, 1672, 1724, 3275 cm⁻¹. Anal calcd for C₂₂H₂₀ClNO₇ (445.85) C, 59.31; H, 4.53; Cl, 7.86; N, 3.15; found: C, 59.31; H, 4.54; Cl, 7.85; N, 3.14.

General Procedure for the Synthesis of Compounds 86, 89, 95, 98, 107, 110 and 138. Example: 2-(furan-2-yl)-3-(3,4,5-trimethoxybenzyl)-1*H*-indole (86). To a cooled solution of **85** (0.07 g, 0.000185 mol) in CH₃CN (1.09 mL) containing MeOH (0.017 mL) was added BH₃-THF (1M, 0.8 mL) and the resulting mixture was stirred at 50 °C for 1 h. After cooling the mixture was diluted of water and extracted with AcOEt; organic layer was washed with brine, dried and filtered. Removal of the solvent gave a residue that was purified by silica gel column chromatography (ethyl acetate : *n*-hexane = 1:1 as eluent) to furnish **86** as brown solid (0.0062 g, 10%), mp 78-80 °C (from ethanol). ¹H NMR (CDCl₃): δ 3.76 (s, 6H), 3.82 (s, 3H), 4.30 (s, 2H), 6.51-6.55 (m, 4H), 7.09-7.13 (m, 1H), 7.21-7.24 (m, 1H), 7.40-7.43 (m, 1H), 7.52-7.54 (m, 2H), 8.49 ppm (broad s, disappeared on treatment with D₂O, 1H). IR: ν 3347 cm⁻¹. Anal calcd. for C₂₂H₂₁NO₄ (363.41) C, 72.71; H, 5.82; N, 3.85; found: C, 72.69; H, 5.78; N, 3.84.

2-(Furan-3-yl)-3-(3,4,5-trimethoxybenzyl)-1*H*-indole (89). Synthesized as **86**, starting from **88**, yield 13% as a brown solid, mp 102-105 °C (from ethanol). ¹H NMR (CDCl₃): δ 3.73 (s, 6H), 3.80 (s, 3H), 4.18 (s, 2H), 6.44 (s, 2H), 6.65-6.66 (m,

1H), 7.07-7.11 (m, 1H), 7.17-7.19 (m, 1H), 7.37-7.39 (m, 1H), 7.47-7.49 (m, 1H), 7.52-7.53 (m, 1H), 7.63-7.64 (m, 1H), 8.07 ppm (broad s, disappeared on treatment with D₂O, 1H). IR: ν 3326 cm⁻¹. Anal calcd. for C₂₂H₂₁NO₄ (363,41) C, 72.71; H, 5.82; N, 3.85; found: C, 72.67; H, 5.79; N, 3.86.

2-(Thiophen-3-yl)-3-(3,4,5-trimethoxybenzyl)-1*H*-indole (95). Synthesized as **86**, starting from **94**, yield 61% as a yellow solid, mp 165-168 °C (from ethanol). ¹H NMR (CDCl₃): δ 3.74 (s, 6H), 3.83 (s, 3H), 4.25 (s, 2H), 6.48 (s, 2H), 7.10-7.14 (m, 1H), 7.21-7.25 (m, 1H), 7.34-7.35 (m, 1H), 7.40-7.46 (m, 3H), 7.51-7.53 (m, 1H), 8.22 ppm (broad s, disappeared on treatment with D₂O, 1H). IR: ν 3353 cm⁻¹. Anal calcd. for C₂₂H₂₁NO₃S (379.47) C, 69.63; H, 5.58; N, 3.69; found: C, 69.45; H, 5.54; N, 3.53.

2-Phenyl-3-(3,4,5-trimethoxybenzyl)-1*H*-indole (98). Synthesized as **86**, starting from **97**, yield 26% as a white solid, mp 187-192 °C (from ethanol). ¹H NMR (DMSO_d₆): δ 3.59 (d, 9H), 4.17 (s, 2H), 6.46 (s, 2H), 6.97-7.01 (m, 1H), 7.09-7.13 (m, 1H), 7.37-7.41 (m, 2H), 7.47-7.53 (m, 3H), 7.64-7.66 (m, 2H), 11.28 ppm (broad s, disappeared on treatment with D₂O, 1H). IR: ν 3351 cm⁻¹. Anal calcd. for C₂₄H₂₃NO₃ (373,44) C, 77.19; H, 6.21; N, 3.75; found: C, 77.15; H, 6.19; N, 3.71.

2-(Naphthalen-1-yl)-3-(3,4,5-trimethoxybenzyl)-1*H*-indole (107). Synthesized as **86**, starting from **106**, yield 99% as a yellow solid, mp 142-147 °C (from ethanol). ¹H NMR (CDCl₃): δ 3.60 (s, 6H), 3.74 (s, 3H), 4.03 (s, 2H), 6.26 (s, 2H), 7.18-7.20 (m, 1H), 7.25-7.29 (m, 1H), 7.43-7.47 (m, 2H), 7.52-7.58 (m, 3H), 7.63-7.65 (m, 1H), 7.84-7.86 (m, 1H), 7.94-7.96 (m, 2H), 8.19 ppm (broad s, disappeared on treatment with D₂O, 1H). IR: ν 3317 cm⁻¹. Anal calcd. for C₂₈H₂₅NO₃ (423,50) C, 79.41; H, 5.95; N, 3.31; found: C, 79.32; H, 5.84; N, 3.26.

2-(Naphthalen-2-yl)-3-(3,4,5-trimethoxybenzyl)-1*H*-indole (110). Synthesized as **86**, starting from **109**, yield 73% as a white solid, mp 138-140 °C (from ethanol). ¹H NMR (CDCl₃): δ 3.73 (s, 6H), 3.83 (s, 3H), 4.29 (s, 2H), 6.52 (s, 2H), 7.13-7.17

(m, 1H), 7.24-7.28 (m, 1H), 7.46 (d, J = 8.1 Hz, 1H), 7.51-7.58 (m, 3H), 7.70 (dd, J = 8.5 and 1.8 Hz, 1H), 7.82-7.94 (m, 3H), 7.99 (m, 1H), 8.30 ppm (broad s, disappeared on treatment with D₂O, 1H). IR: ν 3359 cm⁻¹. Anal calcd. for C₂₈H₂₅NO₃ (423,50) C, 79.41; H, 5.95; N, 3.31; found: C, 79.35; H, 5.86; N, 3.28.

2-(1-(Phenylsulfonyl)-1*H*-pyrrol-3-yl)-3-(3,4,5-trimethoxybenzyl)-1*H*-indole (138). Synthesized as **86**, starting from **137**, yield 84% as a yellow solid, mp 176-180 °C (from ethanol). ¹H NMR (DMSO_d₆): δ 3.55 (s, 6H), 3.59 (s, 3H), 4.15 (s, 2H), 6.46 (s, 2H), 6.81-6.82 (m, 1H), 6.97-6.99 (m, 1H), 7.06-7.08 (m, 1H), 7.32 (d, J = 8.0 Hz, 1H), 7.48-7.50 (m, 2H), 7.62-7.66 (m, 3H), 7.75-7.76 (m, 1H), 7.94-7.96 (m, 2H), 11.16 ppm (broad s, disappeared on treatment with D₂O, 1H). IR: ν 3293 cm⁻¹.

2-(1*H*-Pyrrol-3-yl)-3-(3,4,5-trimethoxybenzyl)-1*H*-indole (83). Synthesized as **82**, starting from **138**, yield 20% as a white solid, mp 195-197 °C (from ethanol). ¹H NMR (DMSO_d₆): δ 3.59 (s, 3H), 3.61 (s, 6H), 4.14 (s, 2H), 6.48-6.49 (m, 1H), 6.53 (s, 2H), 6.86-6.92 (m, 2H), 6.97-7.01 (m, 1H), 7.12-7.13 (m, 1H), 7.29 (d, J = 7.8 Hz, 1H), 7.37 (d, J = 7.7 Hz, 1H), 10.88 (broad s, disappeared on treatment with D₂O, 1H), 11.03 ppm (broad s, disappeared on treatment with D₂O, 1H). IR: ν 3242 cm⁻¹. Anal calcd. for C₂₂H₂₂N₂O₃ (362,42) C, 72.91; H, 6.12; N, 7.73; found: C, 72.85; H, 6.09; N, 7.71.

Methyl 5-bromo-3-(3,4,5-trimethoxyphenylthio)-1*H*-indole-2-carboxylate (60). A mixture of **124** (0.25 g, 0.001 mol), 3,4,5-bis(3,4,5-trimethoxyphenyl)disulfide¹¹³ (0.55 g, 0.0014 mol) and sodium hydride (0.071 g, 0.003 mol, 60% in mineral oil) in anhydrous DMF (2 mL) was placed into the MW cavity (closed vessel mode, Pmax = 250 PSI). MW irradiation of 150 W was used, the temperature being ramped from 25 °C to 110 °C. Once 110 °C was reached, taking about 1 min, the reaction mixture was held at this temperature for 2 min, while stirring, then cooled and quenched on crushed ice and extracted with ethyl

acetate. The organic layer was washed with brine, dried and filtered. Removal of the solvent gave crude 5-bromo-3-(3,4,5-trimethoxyphenylthio)-1*H*-indole-2-carboxylic acid (**139**), which was used without further purification. The crude acid (**139**) was dissolved in methanol (2.5 mL) and dichloromethane (10 mL) and treated with TMSDM (0.78 mL, 0.0015 mol, 2.0 M in hexane), while stirring at 25 °C for 30 min. Removal of the solvent gave a crude product that was purified by silica gel column chromatography (ethyl acetate:*n*-hexane = 1:1) to furnish **60** as a white solid (0.36 g, overall yield 79%), mp 160–162 °C (from ethanol). ¹H NMR (CDCl₃): δ 3.72 (s, 6H), 3.81 (s, 3H), 3.98 (s, 3H), 6.48 (s, 2H), 7.33 (d, *J* = 9.3 Hz, 1H), 7.42 (dd, *J* = 1.9 and 9.3 Hz, 1H), 7.72 (d, *J* = 1.9 Hz, 1H), 9.20 ppm (broad s, disappeared on treatment with D₂O, 1H). IR: ν 1680, 3296 cm⁻¹. Anal calcd for C₁₉H₁₈BrNO₅S (452.32) C, 50.55; H, 4.02; Br, 17.50; N, 3.10; found: C, 50.54; H, 4.01; Br, 17.50; N, 3.11.

Ethyl 5-bromo-3-(3,4,5-trimethoxyphenylthio)-1*H*-indole-2-carboxylate (63). Was synthesized as **60**, starting from **117** and 3,4,5-bis(3,4,5-trimethoxyphenyl)disulfide.¹¹³ The crude acid (**139**) (0.5 g) was dissolved in absolute ethanol (1.7 mL) and treated with thionyl chloride (0.13 mL) at 0 °C under an Ar stream. The reaction mixture was stirred at 0 °C for 20 min, heated at 65 °C for 2 h, then cooled, and diluted with water and ethyl acetate. The organic layer was removed and washed with a saturated solution of sodium hydrogen carbonate and brine, dried and filtered. Removal of the solvent gave a crude product that was purified by silica gel column chromatography (ethyl acetate:*n*-hexane = 1:1) to give **63** as a yellow solid (0.33 g, overall yield 70%), mp 150–152 °C (from ethanol). ¹H NMR (CDCl₃): δ 1.37 (t, *J* = 7.1 Hz, 3H), 3.72 (s, 6H), 3.80 (s, 3H), 4.43 (q, *J* = 7.8 Hz, 2H), 6.48 (s, 2H), 7.33 (d, *J* = 8.7 Hz, 1H), 7.43–7.46 (m, 1H) 7.74–7.75 (m, 1H), 9.23 ppm (broad s, disappeared on treatment with D₂O, 1H). IR: ν 1672, 3299 cm⁻¹.

Anal calcd for $C_{20}H_{20}BrNO_5S$ (452.32) C, 51.61; H, 4.33; Br, 16.97; N, 3.01; S, 6.87; found: C, 51.61; H, 4.32; Br, 16.97; N, 3.00; S, 6.87.

General Procedure for the Synthesis of Compounds 79, 81, 84, 87, 90, 93, 96, 99, 101, 103, 105 and 108. Example: 2-(1*H*-Pyrrol-2-yl)-3-[(3',4',5'-trimethoxyphenyl)thio]-1*H*-indole (79). 2-(1*H*-Pyrrol-2-yl)-1*H*-indole¹³⁸ (**126**) (0.25 g, 0.0014 mol) was carefully added to a suspension of sodium hydride (60% in mineral oil, 0.13 g, 0.0031 mol) in anhydrous DMF (2 mL) while stirring. After 10 min, bis-(3,4,5-trimethoxyphenyl)disulfide¹¹³ (0.62 g, 0.0015 mol) was added, and the reaction mixture was placed into the MW cavity (closed vessel mode, Pmax = 250 PSI). MW irradiation of 150 W was used, the temperature being ramped from 25 °C to 110 °C while stirring. Once 110 °C was reached, taking about 1 min, the reaction mixture was held at this temperature for 2 min. The mixture was diluted with water and extracted with ethyl acetate. The organic layer was washed with brine and dried. Removal of the solvent gave a residue that was purified by column chromatography (alumina, chloroform as eluent) to furnish **79** (0.1 g, 19%), mp 215-218 °C (from ethanol). ¹H NMR (DMSO-*d*₆): δ 3.52 (s, 6H), 3.55 (s, 3H), 6.18 (t, *J* = 2.9 Hz, 1H), 6.34 (s, 2H), 6.81 (d, *J* = 2.4 Hz, 1H), 6.96 (broad s, 1H), 7.04-7.08 (m, 1H), 7.12-7.16 (m, 1H), 7.42 (d, *J* = 8.1 Hz, 2H), 11.11 (broad s, disappeared on treatment with D₂O, 1H), 11.64 ppm (broad s, disappeared on treatment with D₂O, 1H). IR: ν 3329, 3422 cm⁻¹. Anal calcd. for $C_{21}H_{20}N_2O_3S$ (380.46) C, 66.29; H, 5.30; N, 7.36; found: C, 66.03; H, 5.26; N, 7.15.

2-(1*H*-Pyrrol-3-yl)-3-[(3',4',5'-trimethoxyphenyl)thio]-1*H*-indole (81). Was synthesized as **79**, starting from **128**, yield 10% as a brown solid, mp 200-204 °C (from ethanol). ¹H NMR (DMSO-*d*₆): δ 3.52 (s, 6H), 3.56 (s, 3H), 6.33 (s, 2H), 6.75-6.77 (m, 1H), 6.84-6.86 (m, 1H), 7.00-7.04 (m, 1H), 7.08-7.12 (m, 1H), 7.39 (d, *J* = 8.6 Hz, 2H), 7.48-7.50 (m, 1H), 11.11 (broad s, disappeared on treatment with D₂O, 1H), 11.58 ppm (broad s, disappeared on treatment with D₂O, 1H). IR: ν

3358, 3390 cm^{-1} . Anal calcd. for $\text{C}_{21}\text{H}_{20}\text{N}_2\text{O}_3\text{S}$ (380.46) C, 66.29; H, 5.30; N, 7.36; found: C, 65.97; H, 5.12; N, 6.91.

2-(Furan-2-yl)-3-[(3',4',5'-trimethoxyphenyl)thio]-1*H*-indole (84). Was synthesized as **79**, starting from **118**, yield 38% as a white solid, mp 180-184 °C (from ethanol). ^1H NMR (CDCl_3): δ 3.65 (s, 6H), 3.77 (s, 3H), 6.38 (s, 2H), 6.54 (q, J = 1.8 Hz, 1H), 7.17-7.20 (m, 1H), 7.24-7.25 (m, 2H), 7.44 (d, J = 8 Hz, 1H), 7.50 (m, 1H), 7.67 (d, J = 8 Hz, 1H), 8.94 ppm (broad s, disappeared on treatment with D_2O , 1H). IR: ν 3333 cm^{-1} . Anal calcd. for $\text{C}_{21}\text{H}_{19}\text{NO}_4\text{S}$ (381.44) C, 66.12; H, 5.02; N, 3.67; found: C, 65.85; H, 4.98; N, 3.57.

2-(Furan-3-yl)-3-[(3',4',5'-trimethoxyphenyl)thio]-1*H*-indole (87). Was synthesized as **79**, starting from **130**, yield 42% as a brown solid, mp 185-190 °C (from ethanol). ^1H NMR ($\text{DMSO}-d_6$): δ 3.64 (s, 6H), 3.76 (s, 3H), 6.34 (s, 2H), 6.87 (m, 1H), 7.16 (t, J = 7.5 Hz, 1H), 7.22-7.26 (m, 1H), 7.41 (d, J = 8.0 Hz, 1H), 7.51 (t, J = 1.6 Hz, 1H), 7.65 (dd, J = 0.6 and 7.8 Hz, 1H), 8.08-8.09 (m, 1H), 8.50 ppm (broad s, disappeared on treatment with D_2O , 1H). IR: ν 3330 cm^{-1} . Anal calcd. for $\text{C}_{21}\text{H}_{19}\text{NO}_4\text{S}$ (381.44) C, 66.12; H, 5.02; N, 3.67; found: C, 65.90; H, 4.92; N, 3.41.

2-(Thiophen-2-yl)-3-[(3',4',5'-trimethoxyphenyl)thio]-1*H*-indole (90). Was synthesized as **79**, starting from **133** yield 60% as a yellow solid, mp 195-198 °C (from ethanol). ^1H NMR ($\text{DMSO}-d_6$): δ 3.53 (s, 6H), 3.56 (s, 3H), 6.35 (s, 2H), 7.09-7.13 (m, 1H), 7.19-7.24 (m, 2H), 7.47-7.49 (m, 2H), 7.65 (dd, J = 1.1 and 5.0 Hz, 1H), 7.77 (dd, J = 1.1 and 3.7 Hz, 1H), 12.11 ppm (broad s, disappeared on treatment with D_2O , 1H). IR: ν 3317 cm^{-1} . Anal calcd. for $\text{C}_{21}\text{H}_{19}\text{NO}_3\text{S}_2$ (397.51) C, 63.45; H, 4.82; N, 3.52; found: C, 63.28; H, 4.78; N, 3.23.

2-(Thiophen-3-yl)-3-[(3',4',5'-trimethoxyphenyl)thio]-1*H*-indole (93). Was synthesized as **79**, starting from **134**, yield 83% as a white solid, mp 220-225 °C (from ethanol). ^1H NMR (CDCl_3): δ 3.64 (s, 6H), 3.78 (s, 3H), 6.37 (s, 2H), 7.17-7.21 (m, 1H), 7.25-7.29 (m, 1H), 7.42-7.44 (m, 2H), 7.64 (dd, J = 1.3 and 5.0 Hz,

1H), 7.68 (d, $J = 7.8$ Hz, 1H), 7.85 (dd, $J = 1.3$ and 3.0 Hz, 1H), 8.62 ppm (broad s, disappeared on treatment with D₂O, 1H). IR: ν 3331 cm⁻¹. Anal calcd. for C₂₁H₁₉NO₃S₂ (397.51) C, 63.45; H, 4.82; N, 3.52; found: C, 63.28; H, 4.75; N, 3.41.

2-Phenyl-3-((3,4,5-trimethoxyphenyl)thio)-1*H*-indole (96). Was synthesized as **79**, starting from 2-phenyl-1*H*-indole, yield 3% as yellow solid, mp 158-160 °C (from ethanol). ¹H NMR (CDCl₃): δ 3.64 (s, 6H), 3.78 (s, 3H), 6.37 (s, 2H), 7.18-7.22 (m, 1H), 7.27-7.30 (m, 2H), 7.41-7.50 (m, 3H), 7.69 (d, $J = 7.9$ Hz, 1H), 7.80-7.82 (m, 2H), 8.56 ppm (broad s, disappeared on treatment with D₂O, 1H). IR: ν 3329 cm⁻¹. Anal calcd. for C₂₃H₂₁NO₃S (391.48) C, 70.56; H, 5.41; N, 3.58; S, 8.19; found: C, 70.50; H, 5.37; N, 3.54; S, 8.12.

2-(Pyridin-2-yl)-3-((3,4,5-trimethoxyphenyl)thio)-1*H*-indole (99). Was synthesized as **79**, starting from **119**, yield 25% as a yellow oil. ¹H NMR (CDCl₃): δ 3.63 (s, 6H), 3.76 (s, 3H), 6.39 (s, 2H), 7.18 (t, $J = 7.1$ Hz, 1H), 7.24-7.27 (m, 2H), 7.45 (d, $J = 8.1$ Hz, 1H), 7.70-7.77 (m, 2H), 8.63-8.64 (m, 1H), 8.73 (d, $J = 8.1$ Hz, 1H), 10.23 ppm (broad s, disappeared on treatment with D₂O, 1H). IR: ν 2828, 2933, 3003, 3056 cm⁻¹. Anal calcd. for C₂₂H₂₀N₂O₃S (392.47) C, 67.33; H, 5.14; N, 7.14; S, 8.17; found: C, 67.28; H, 5.09; N, 7.11; S, 8.13.

2-(Pyridin-3-yl)-3-((3,4,5-trimethoxyphenyl)thio)-1*H*-indole (101). Was synthesized as **79**, starting from **120**, yield 20% as a yellow solid, mp 188-193 °C (from ethanol). ¹H NMR (CDCl₃): δ 3.65 (s, 6H), 3.76 (s, 3H), 6.33 (s, 2H), 7.22 (m, 1H), 7.31 (m, 1H), 7.37-7.41 (m 1H), 7.48 (d, $J = 8.1$ Hz, 1H), 7.70 (d, $J = 7.6$ Hz, 1H), 8.17 (dt, $J = 1.7$ and 8.0 Hz, 1H), 8.62 (m, 1H), 9.02 (m, 1H), 9.26 ppm (broad s, disappeared on treatment with D₂O, 1H). IR: ν 2923, 3674 cm⁻¹. Anal calcd. for C₂₂H₂₀N₂O₃S (392.47) C, 67.33; H, 5.14; N, 7.14; S, 8.17; found: C, 67.26; H, 5.07; N, 7.10; S, 8.11.

2-(Pyridin-4-yl)-3-((3,4,5-trimethoxyphenyl)thio)-1*H*-indole (103). Was synthesized as **79**, starting from **121**, yield 60% as a yellow solid, mp 215-220 °C

(from ethanol). ^1H NMR ($\text{DMSO}-d_6$): δ 3.53 (s, 6H), 3.57 (s, 3H), 6.32 (s, 2H), 7.14-7.18 (m, 1H), 7.27-7.31 (m, 1H), 7.53-7.57 (m, 2H), 7.92 (dd, J = 1.7 and 4.5 Hz, 2H), 8.71 (dd, J = 1.6 and 4.5 Hz, 2H), 12.36 ppm (broad s, disappeared on treatment with D_2O , 1H). IR: ν 3320 cm^{-1} . Anal calcd. for $\text{C}_{22}\text{H}_{20}\text{N}_2\text{O}_3\text{S}$ (392.47) C, 67.33; H, 5.14; N, 7.14; S, 8.17; found: C, 67.24; H, 5.06; N, 7.08; S, 8.08.

2-(Naphthalen-1-yl)-3-((3,4,5-trimethoxyphenyl)thio)-1*H*-indole (105). Was synthesized as **79**, starting from **136**, yield 44% as a white solid, mp 227-230 °C (from ethanol). ^1H NMR (CDCl_3): δ 3.56 (s, 6H), 3.71 (s, 3H), 6.30 (s, 2H), 7.22-7.26 (m, 1H), 7.29-7.33 (m, 1H), 7.39-7.55 (m, 4H), 7.61 (dd, J = 7.1 and 1.2 Hz, 1H), 7.74-7.76 (m, 1H), 7.82-7.84 (m, 1H), 7.90-7.95 (m, 2H), 8.59 ppm (broad s, disappeared on treatment with D_2O , 1H). IR: ν 3229 cm^{-1} . Anal calcd. for $\text{C}_{27}\text{H}_{23}\text{NO}_3\text{S}$ (441.54) C, 73.44; H, 5.25; N, 3.17; S, 7.26; found C, 73.37; H, 5.19; N, 3.11; S, 7.21.

2-(Naphthalen-2-yl)-3-((3,4,5-trimethoxyphenyl)thio)-1*H*-indole (108). Was synthesized as **79**, starting from **122**, yield 44% as a white solid, mp 157-160 °C (from ethanol). ^1H NMR (CDCl_3): δ 3.65 (s, 6H), 3.79 (s, 3H), 6.42 (s, 2H), 7.22-7.34 (m, 2H), 7.50-7.56 (m, 3H), 7.74-7.75 (m, 1H), 7.88-7.90 (m, 2H), 7.93-8.00 (m, 2H), 8.25 (m, 1H), 8.71 ppm (broad s, disappeared on treatment with D_2O , 1H). IR: ν 3318 cm^{-1} . Anal calcd. for $\text{C}_{27}\text{H}_{23}\text{NO}_3\text{S}$ (441.54) C, 73.44; H, 5.25; N, 3.17; S, 7.26; found C, 73.39; H, 5.21; N, 3.13; S, 7.23.

Methyl 5-methoxy-3-(3,4,5-trimethoxyphenylsulfinyl)-1*H*-indole-2-carboxylate (70). To a cold solution of **69¹¹³** (0.05 g, 0.00012 mol) in chloroform (5 mL) was added 3-chloroperoxybenzoic acid (0.021 g, 0.00012 mol). The reaction mixture was stirred at 25 °C for 1.5 h, then diluted with water and extracted with chloroform. The organic layer was washed with brine, dried and filtered. Removal of the solvent gave a residue that was purified by silica gel column chromatography (ethyl acetate as eluent) to furnish **70** as a brown solid (0.05 g, yield 99%), mp 161-

163 °C (from ethanol). ^1H NMR (CDCl_3): δ 3.74 (s, 3H), 3.84 (s, 9H), 3.85 (s, 3H), 6.96 (d, J = 9.1 Hz, 1H), 7.10 (s, 2H), 7.31 (dd, J = 1.9 and 9.0 Hz, 1H), 7.42 (d, J = 2.2 Hz, 1H), 9.37 ppm (broad s, disappeared on treatment with D_2O , 1H). IR: ν 1708, 2831, 2933 cm^{-1} . Anal calcd for $\text{C}_{20}\text{H}_{21}\text{NO}_7\text{S}$ (419.45) C, 57.26; H, 5.05; N, 3.34; S, 7.63; found: C, 57.27; H, 5.06; N, 3.34; S, 7.63.

Methyl 5-methoxy-3-(3,4,5-trimethoxyphenylsulfonyl)-1*H*-indole-2-carboxylate (71). Was synthesized as **70**, treating **69¹¹³** with 3-chloroperoxybenzoic acid (2 eq.), 96%, yellow solid, mp 176–180 °C (from ethanol). ^1H NMR ($\text{DMSO}-d_6$): δ 3.33 (s, 3H), 3.82 (s, 6H), 3.83 (s, 3H), 3.93 (s, 3H), 7.04 (dd, J = 6.5 Hz, 1H), 7.40 (s, 2H), 7.45 (d, J = 9.0 Hz, 1H), 7.59 (d, J = 2.4 Hz, 1H), 12.99 ppm (broad s, disappeared on treatment with D_2O , 1H). IR: ν 1701, 3298 cm^{-1} . Anal calcd for $\text{C}_{20}\text{H}_{21}\text{NO}_8\text{S}$ (435.45) C, 55.15; H, 4.86; N, 3.22; S, 7.35; found: C, 55.14; H, 4.85; N, 3.22; S, 7.35.

General Procedure for the Synthesis of Compounds 111–116. Example: Ethyl 2-(2-(4-bromophenyl)hydrazone)propanoate (111). A mixture of 4-bromophenylhydrazine hydrochloride (5.7 g, 0.0255 mol), ethyl pyruvate (2 g, 1.91 mL, 0.017 mol) and sodium acetate (2.79 g, 0.034 mol) in ethanol (40 mL) was placed into the MW cavity (open vessel mode). MW irradiation at 250 W was used, the temperature being ramped from 25 °C to 100 °C. Once 100 °C was reached, taking about 2 min, the reaction mixture was held at this temperature for 5 min, while stirring. The reaction mixture was cooled at 0 °C, with stirring, and filtered to give **111**, yield 90%, mp 142–144 °C (from ethanol). ^1H NMR (CDCl_3): δ 1.39 (t, J = 7.2 Hz, 3H), 2.12 (s, 3H), 4.33 (q, J = 7.1 Hz, 2H), 7.10 (d, J = 6.7 Hz, 2H), 7.40 (d, J = 6.9 Hz, 2H), 7.64 ppm (broad s, disappeared on treatment with D_2O , 1H). IR: ν 1576, 1675, 3290 cm^{-1} .

1-(1-(Furan-2-yl)ethylidene)-2-phenylhydrazine (112). Synthesized as **111**, starting from phenylhydrazine hydrochloride and 2-acetyl furane, yield 96%, orange

solid, mp 79-84 °C (from ethanol). ^1H NMR (DMSO-*d*₆): δ 2.19 (s, 3H), 6.54-6.55 (m, 1H), 6.70-6.71 (m, 1H), 6.74-6.77 (m, 1H), 7.18-7.23 (m, 4H), 7.68-7.69 (m, 1H), 9.22 ppm (broad s, disappeared on treatment with D₂O, 1H). IR: ν 3342 cm⁻¹.

2-(1-(2-Phenylhydrazono)ethyl)pyridine (113). Synthesized as **111**, starting from phenylhydrazine hydrochloride and 2-acetylpyridine, yield 90%, yellow solid, mp 150-153 °C (from ethanol). ^1H NMR spectrum was identical to that reported in lit.¹³⁹

3-(1-(2-Phenylhydrazono)ethyl)pyridine (114). Synthesized as **111**, starting from phenylhydrazine hydrochloride and 3-acetylpyridine, yield 85%, yellow solid, mp 140-143 °C (from ethanol). ^1H NMR spectrum was identical to that reported in lit.¹⁴⁰

4-(1-(2-Phenylhydrazono)ethyl)pyridine (115). Synthesized as **111**, starting from phenylhydrazine hydrochloride and 4-acetylpyridine, yield 90%, yellow solid, mp 143-145 °C (from ethanol). ^1H NMR (CDCl₃): δ 2.22 (s, 3H), 6.92-6.96 (m, 1H), 7.20-7.22 (m, 2H), 7.30-7.34 (m, 2H), 7.58 (broad s, disappeared on treatment with D₂O, 1H), 7.66 (dd, *J* = 1.6 and 4.6 Hz, 2H), 8.59 ppm (dd, *J* = 1.6 and 4.6 Hz, 2H). IR: ν 3225 cm⁻¹.

1-(1-(Naphthalen-2-yl)ethylidene)-2-phenylhydrazine (116). Synthesized as **111**, starting from phenylhydrazine hydrochloride and 2-acetylnaphthalene, yield 90%, white solid, mp 175-178 °C (from ethanol). ^1H NMR (DMSO-d 6): δ 2.39 (s, 3H), 6.67-6.80 (m, 1H), 7.23-7.32 (m, 4H), 7.47-7.54 (m, 2H), 7.87-7.90 (m, 2H), 7.95-7.97 (m, 1H), 8.14 (m, 1H), 8.20 (dd, *J* = 1.8 and 8.7 Hz, 1H), 9.40 ppm (broad s, disappeared on treatment with D₂O, 1H). IR: ν 3348 cm⁻¹.

General Procedure for the Synthesis of Compounds 117-122. Example: Ethyl 5-bromo-1*H*-indole-2-carboxylate (117). **111** (35.15 g, 0.123 mol) was added in portions to PPA (350 g) preheated at 110 °C. The mixture was stirred at the same temperature for 30 min and then quenched with ice-water. The solid was filtered,

washed with water, dried and recrystallized from ethanol to give **117** as a brown solid (32.95 g, 60%), mp 160-161 °C. ^1H NMR (CDCl_3): δ 1.43 (t, J = 7.1 Hz, 3H), 4.43 (q, J = 7.1 Hz, 2H), 7.15-7.16 (m, 1H), 7.31 (d, J = 8.1 Hz, 1H), 7.41 (dd, J = 7.0 Hz, 1H), 7.84 (m, 1H), 9.98 ppm (broad s, disappeared on treatment with D_2O , 1H). IR: ν 1690, 3311 cm^{-1} .

2-(Furan-2-yl)-1*H*-indole (118). Synthesized as **117**, starting from **112**, yield 55%, yellow solid, mp 123-125 °C (from ethanol). lit.¹⁴¹ 120-123 °C.

2-(Pyridin-2-yl)-1*H*-indole (119). Synthesized as **117**, starting from **113**, yield 73%, white solid, mp 153-155 °C (from toluene). ^1H NMR spectrum was identical to that reported in lit.¹³⁹

2-(Pyridin-3-yl)-1*H*-indole (120). Synthesized as **117**, starting from **114**, yield 73%, yellow solid, mp 145-150 °C (from toluene). ^1H NMR spectrum was identical to that reported in lit.¹⁴⁰

2-(Pyridin-4-yl)-1*H*-indole (121). Synthesized as **117**, starting from **115**, yield 68%, brown solid, mp 210-215 °C (from toluene). ^1H NMR spectrum was identical to that reported in lit.¹⁴²

2-(Naphthalen-2-yl)-1*H*-indole (122). Synthesized as **117**, starting from **116**, yield 45%, white solid, mp 200-203 °C (from cycloesane/ethanol). ^1H NMR spectrum was identical to that reported in lit.¹⁴³

5-Bromo-1*H*-indole-2-carboxylic acid (123). A mixture of **117** (0.25 g, 0.001 mol) in 3 N sodium hydroxide (2 mL) was placed into the MW cavity (closed vessel mode, Pmax = 250 PSI). MW irradiation at 150 W was used, the temperature being ramped from 25 °C to 110 °C. Once 110 °C was reached, taking about 1 min, the reaction mixture was held at this temperature for 2 min, while stirring. After cooling, the reaction mixture was made acidic with 3 N hydrochloric acid (pH = 2) and extracted with ethyl acetate; the organic layer was washed with brine, dried, filtered and evaporated to give **123** as a brown solid (0.23 g, 95%), mp 188 °C (from ethanol). ^1H NMR ($\text{DMSO}-d_6$): δ 7.05 (s, 1H), 7.32 (dd, J = 8.9 Hz, 1H), 7.39 (d, J =

= 8.8 Hz, 1H), 7.85 (d, J = 2.1 Hz, 1H), 11.94 (broad s, disappeared on treatment with D₂O, 1H), 12.61 ppm (broad s, disappeared on treatment with D₂O, 1H). IR: ν 1652, 2850, 3422 cm⁻¹.

Methyl 5-bromo-1*H*-indole-2-carboxylate (124). To a cold suspension of **123** (3.4 g, 0.014 mol) in anhydrous methanol (13.4 mL) was added thionyl chloride (1.6 mL) dropwise. The reaction mixture was stirred at the same temperature for 20 min, then heated at 65 °C for 2 h under an Ar stream, then cooled and diluted with water and ethyl acetate. The layers were separated, and the organic phase was washed with a saturated solution of sodium hydrogen carbonate and brine, dried, filtered and evaporated to give **124** as a white solid (3.43 g, 96%), mp 217-220 °C (from ethanol/cyclohexane), lit.¹⁴⁴ 211.8-213.6 °C.

3-Bromo-1*H*-indole (125). A solution of bromine (2.77 g, 0.9 mL, 0.0173 mol) in DMF (15 mL) is dropped within a few minutes into a DMF solution (40 mL) of 1-*H*-indole (2 g, 0.0171 mol) at 25 °C under stirring. The reaction mixture was poured into NaHCO₃(ss) and extracted with CH₂Cl₂; organic layer was washed with brine, dried and filtered. The solution of **125** in CH₂Cl₂ was used for further reaction without evaporation of the solvent.

2-(1*H*-Pyrrol-2-yl)-1*H*-indole (126). To a solution of **125** (3.35 g, 0.0171 mol) in CH₂Cl₂ (150 mL) was added 1*H*-pyrrole (1.15 g, 1.19 mL, 0.0171 mol) and CF₃COOH (0.775 g, 0.52 mL, 0.007 mol). The reaction mixture was stirred at 25 °C for 20 minutes, made basic with aqueous ammonia and extracted with NaHCO₃(ss); organic layer was washed with brine, dried and filtered. Removal of the solvent gave a residue that was purified by aluminium oxide chromatography (ethyl acetate : n-hexane = 2 : 8 as eluent) to furnish **126** as a white solid (0.55 g, 18%), mp 240-245 °C (from ethanol). ¹H NMR spectrum was identical to that reported in lit.¹⁴⁵

2-(2-Nitrophenyl)-1-[1-(phenylsulfonyl)-1*H*-pyrrol-3-yl]ethan-1-one (127). Oxalyl chloride (2.46 g, 1.64 mL, 0.019 mol) and a catalytic amount of anhydrous DMF were added at 0 °C to 2-(2-nitrophenyl)acetic acid (3.52 g, 0.019 mol) in

anhydrous 1,2-dichloroethane (88 mL) under an Ar stream. After 30 min, 1-(phenylsulfonyl)-1*H*-pyrrole (4.04 g, 0.0019 mol) and anhydrous aluminum chloride (2.59 g, 0.0019 mol) were added. The reaction mixture was stirred at 0 °C for 25 min, quenched on 1 N HCl/crushed ice and extracted with chloroform. The organic layer was washed with brine and dried. Removal of the solvent gave a residue that was purified by column chromatography (silica gel, acetone:*n*-hexane 1:2 as eluent) to furnish **127** as a yellow solid (0.7 g, 10%), mp 135 °C (from ethanol). ¹H NMR (DMSO-*d*₆): δ 4.45 (s, 2H), 6.41-6.43 (m, 1H), 7.25-7.30 (m, 2H), 7.45-7.60 (m, 5H), 7.85-7.86 (m, 1H), 7.90-7.92 (m, 2H), 8.06 ppm (dd, *J* = 1.2 and 8.2 Hz, 1H). IR: ν 1680 cm⁻¹.

2-[1-(Phenylsulfonyl)-1*H*-pyrrol-3-yl]-1*H*-indole (128). A mixture of **127** (0.25 g, 0.0007 mol) and iron powder (0.27 g, 0.0049 ga) in glacial acetic acid (8 mL) was heated at 60 °C overnight. After cooling, the mixture was diluted with water while stirring and extracted with ethyl acetate. The organic layer was washed with brine and dried. Removal of the solvent gave a residue that was purified by column chromatography (silica gel, ethyl acetate:*n*-hexane 1:3 as eluent) to furnish **128** as a white solid (0.7 g, 10%), mp 180-185 °C (from ethanol). ¹H NMR (DMSO-*d*₆): δ 6.66 (d, *J* = 1.4 Hz, 1H), 6.83-6.85 (m, 1H); 6.93-6.97 (m, 1H), 7.02-7.07 (m, 1H), 7.31 (d, *J* = 8.0 Hz, 1H), 7.44-7.46 (m, 2H), 7.65-7.69 (m, 2H), 7.74-7.79 (m, 1H), 7.84 (t, *J* = 1.9 Hz, 1H), 7.98-8.00 (m, 2H), 11.30 ppm (br s, 1H, disappeared on treatment with D₂O). IR: ν 3407 cm⁻¹.

2-(Furan-3-yl)-1*H*-indole (130). A mixture of 2-iodo-1*H*-indole¹¹⁹ (**129**) (0.25 g, 0.001 mol), furan-3-boronic acid pinacol ester (0.26 g, 0.00134 mol), potassium carbonate (0.18 g, 0.00134 mol), Pd(II) acetate (0.03 g, 0.000134 mol, 10% mol) in 1-methyl-2-pyrrolidinone (2.3 mL) containing 0.18 mL of water was irradiated at 200 W in the MW cavity (closed vessel mode, Pmax = 250 PSI), the temperature being ramped from 25 °C to 110 °C while stirring. Once 110 °C was reached, taking

about 2 min, the reaction mixture was held there for 15 min. After cooling, the mixture was diluted with water and extracted with ethyl acetate. The organic layer was washed with brine and dried. Removal of the solvent gave a residue that was purified by column chromatography (silica gel, ethyl acetate:*n*-hexane 1:5 as eluent) to furnish **130** as a white solid (0.18 g, 95%), mp 145-148 °C (from ethanol). ¹H NMR (CDCl₃): δ 6.61-6.62 (m, 1H), 6.70-6.71 (m, 1H), 7.09-7.19 (m, 2H), 7.36 (dd, *J* = 0.9 and 8.0 Hz, 1H), 7.50-7.52 (m, 1H), 7.58-7.60 (m, 1H), 7.75 (m, 1H), 8.10 ppm (broad s, disappeared on treatment with D₂O, 1H). IR: ν 3417 cm⁻¹.

2-Bromo-1-(thiophen-2-yl)ethan-1-one (131). A solution of bromine (2.53 g, 0.82 mL, 0.0158 mol) in dichloromethane (8 mL) was added dropwise to 2-acethylthiophene (2.0 g, 1.71 mL, 0.0158 mol) in the same solvent (10 mL). The reaction mixture was stirred at 25 °C for 1 h and neutralized with a saturated solution of sodium hydrogen carbonate. The organic layer was washed with brine and dried. Removal of the solvent gave a residue that was purified by column chromatography (silica gel, ethyl acetate:*n*-hexane 5:95 as eluent) to furnish **131** as a yellow oil (2.60 g, 80%).¹⁴⁶

2-Bromo-1-(thiophen-3-yl)ethanone (132). Synthesized as **131**, starting from 3-acethylthiophene, yield 57%, brown solid, mp 60-65 °C (from ethanol). ¹H NMR (CDCl₃): δ 4.34 (s, 2H), 7.35-.737 (m, 1H), 7.57 (dd, *J* = 1.3 and 5.1 Hz, 1H), 8.17-8.18 ppm (m, 1H). IR: ν 1672 cm⁻¹.

2-(Thiophen-2-yl)-1*H*-indole (133). A mixture of **131** (0.5 g, 0.0024 mol) and aniline (0.4 g, 0.4 mL, 0.0041 mol) was kept at 25 °C for 3 h with occasional stirring, then a catalytic amount of anhydrous DMF was added, and the reaction mixture was placed into the MW cavity (closed vessel mode, Pmax = 250 PSI). MW irradiation of 150 W was used, the temperature being ramped from 25 °C to 100 °C while stirring, with 100 °C being reached in about 1 min, and the reaction mixture was held at this temperature for an additional min. The mixture was diluted with 1 N HCl

and extracted with ethyl acetate. The organic layer was washed with brine and dried. Removal of the solvent gave a residue that was purified by column chromatography (silica gel, ethyl acetate:*n*-hexane 3:7 as eluent) to furnish **133** as a yellow solid (0.19 g, 40%), mp 175-180 °C (from cyclohexane). lit.¹⁴⁷ 167-168 °C (from hexane).

2-(Thiophen-3-yl)-1*H*-indole (134). Synthesized as **133** starting from **132**. Yield 16% as a yellow solid, mp 210-215 °C (from cyclohexane). lit.¹⁴⁸ 212-214 °C.

2-Bromo-1-(naphthalen-1-yl)ethanone (135). A solution of bromine (5.27 g, 1.69 mL) in CH₂Cl₂ (17 mL) was added dropwise to a stirred solution of 1-acetonaphthone (5.59 g, 5 mL, 0.033 mol) in the same solvent (20 mL). the reaction mixture was stirred at 25 °C for 1 h, then basified with NaHCO₃ and extracted with CH₂Cl₂; organic layer was washed with brine, dried and filtered. Removal of the solvent gave a residue that was purified by silica gel column chromatography (ethyl acetate:*n*-hexane 1:10 as eluent) to furnish **135** as a yellow oil (0.74 g, 90%).

¹H NMR spectrum was identical to that reported in lit.¹⁴⁹

2-(Naphthalen-1-yl)-1*H*-indole (136). A solution of aniline (1.24 g, 1.22 mL, 0.0133 mol) in *N,N*-dimethylaniline (2.34 mL) was heated at 175 °C. **135** (1 g, 0.0040 mol) was added and the reaction mixture was stirred for 15 minutes. After cooling 6 N HCl was added and the mixture was extracted with AcOEt; organic layer was washed with 6 N HCl, brine, dried and filtered. Removal of the solvent gave a residue that was purified by silica gel column chromatography (ethyl acetate:*n*-hexane 1:10 as eluent) to furnish **136** as a yellow solid (0.27 g, 28%), mp 95-97 °C (from petroleum ether). ¹H NMR spectrum was identical to that reported in lit.¹⁴¹

2-(3,4,5-Trimethoxyphenyl)acetyl chloride. This compound was synthesized by treating a cold solution of 3,4,5-trimethoxyphenylacetic acid (0.25 g, 0.0011 mol) in anhydrous THF (5 mL) with oxalyl chloride (0.28 g, 0.19 mL, 0.0022 mol). Immediately afterwards, a catalytic amount (2 drops) of anhydrous DMF was added, and vigorous bubbling ensued. After 10 min, the reaction mixture was carefully

concentrated in vacuo to provide a viscous oil. Fresh anhydrous THF was added, and the solution was concentrated in vacuo again to furnish 2-(3,4,5-trimethoxyphenyl)acetyl chloride (0.27 g, yellow oil), which was used without further purification.

9.3 Molecular Modeling.

All molecular modeling studies were performed on a MacPro dual 2.66GHz Xeon running Ubuntu 9. The tubulin structure was downloaded from the PDB data bank (<http://www.rcsb.org/> - PDB ID: 1SA0,¹⁵⁰ 3KHC and 3KHE.¹⁵¹ Hydrogen atoms were added to the protein, using Molecular Operating Environment (MOE) 2007.09,¹⁵² and minimized keeping all the heavy atoms fixed until a RMSD gradient of 0.05 kcal mol⁻¹ Å⁻¹ was reached. Ligand structures were built with MOE and minimized using the MMFF94x forcefield until a RMSD gradient of 0.05 kcal mol⁻¹ Å⁻¹ was reached. The docking simulations were performed using FlexX,¹³¹ Plants1.1¹³² and GLIDE.¹³³ Molecular dynamics was performed with AMBER 9 package¹⁵³ on 1SA0 crystal structure. The minimized structure was solvated in a periodic octahedron simulation box using TIP3P water molecules, providing a minimum of 10 Å of water between the protein surface and any periodic box edge. The water molecules and sodium ions were energy minimized keeping the coordinates of the protein-ligand complex fixed (1000 cycle) then the whole system was minimized (5000 cycle). Following minimization, the entire system was heated to 298 K (10 ps). The production simulation was conducted at 298 K (time step 0.002 psec) The periodic boundary condition was settled. The used cutoff was 8 Å. Shake bond length condition was used (ntc = 2). The polyphorylated compounds (GTP and GDP) were parametrized using orbital molecular calculation at the RHF/6-31+G* level.¹⁵⁴ Compound was parametrized by Gamess^{155, 156} at the HF/6-31+G* level. Trajectories analysis and the H-bonds rate of formation were carried

our by ptraj program,¹⁵⁷ visual inspection were carried out by VMD.¹⁵⁸ The images in the manuscript were created with Pymol.¹⁵⁹

9.4 Biology.

Tubulin assembly. The reaction mixtures contained 0.8 M monosodium glutamate (pH 6.6 with hydrochloric acid in 2 M stock solution), 10 μ M tubulin, and varying concentrations of drug. Following a 15 min preincubation at 30 °C, samples were chilled on ice, GTP to 0.4 mM was added, and turbidity development was followed at 350 nm in a temperature controlled recording spectrophotometer for 20 min at 30 °C. Extent of reaction was measured.¹⁶⁰

[³H]Colchicine binding assay. The reaction mixtures contained 1.0 μ M tubulin, 5.0 μ M [³H]colchicine, and 5.0 μ M inhibitor and were incubated 10 min at 37 °C. Complete details were described previously.¹⁶¹

Cell lines. Methodology for the evaluation of the growth of human MCF-7 breast carcinoma cells was previously described.¹⁶¹ Human HeLa cells (from carcinoma of the uterine cervix) and HCT116/chr3 cells (from colon carcinoma) were grown at 37 °C in a humidified atmosphere containing 5% carbon dioxide in D-MEM (Gibco BRL, UK) supplemented with 10% fetal calf serum, 4 mM glutamine, 2 mM sodium pyruvate, 100 U/mL penicillin and 0.1 mg/mL streptomycin (all reagents were from Celbio, Italy). For the HCT116/chr3 cells, the medium also included 500 μ g/mL of the selection compound G418 (Gibco). Cells were trypsinized when subconfluent and seeded in T75 flasks at a concentration of 10⁵/mL. U937 (human monocytic leukemia cell line) and J774.1 cells (murine macrophage cell line) were cultured in RPMI 1640 medium containing 10% fetal calf serum, 50 μ g/mL each of penicillin and streptomycin, and 2 mM glutamine. Human melanoma M14 cells and human embryonic kidney (HEK) 293 cells were grow at 37 °C in Dulbecco's modified Eagle's medium containing 10 mM glucose (DMEM-HG) supplemented with 10%

fetal calf serum and 50 $\mu\text{g}/\text{mL}$ each of penicillin and streptomycin. The *P. tridactylis* PtK2 cells, the A10 rat embryonic aortic smooth muscle cells, the human umbilical vein endothelial cells, and the human aortic smooth muscle cells were obtained from the American Type Tissue Collection and grown as recommended by the supplier, except that a 5% CO₂ atmosphere was used with all cells.

Morphological analysis. Cells grown in T75 flasks and treated with 100 μM **57** for 24 h were observed with an Olympus IX71 microscope and photographed with a Cool SNAPES_{ES} Photometric digital camera.

Cell Viability Assay. *MCF-7 cells.* MCF-7 cell growth was quantitated by measuring cell protein with the dye sulforhodamine B after 48 h in the presence of various compound concentrations.¹⁶¹

HeLa and HCT116/chr3 cells. Cells were seeded in 96 well-plates at a density of 1x10³ cells/100 μL well. Twenty-four hours later, cells were treated with the test compound (stock solution: 10 mM in DMSO, kept at room temperature in the dark) used at increasing concentrations (0.1-100 μM) for 24 h. Cells were harvested at the end of the treatment or washed with phosphate-buffered saline and incubated in drug-free medium for an additional 24 h. To rule out a possible effect of the solvent, parallel samples were incubated in complete medium containing 1% DMSO. At the end of the treatments, 20 μL of CellTiter96 Aqueous One Solution Reagent (Promega) was added to each well. The plates were then incubated for 4 h at 37 °C and analyzed with a microplate reader (Gio. De Vita, Roma, Italy) at 492 nm. Experiments were performed in quadruplicate and repeated three times.

M14, HEK, U937 and J774.1 cells. Cell viability was determined using the 3-[4,5-demethylthiazol-2,5-diphenyl-2H-tetrazolium bromide (MTT) colorimetric assay. The test is based on the ability of mitochondrial dehydrogenase to convert, in viable cells, the yellow MTT reagent into a soluble blue formazan dye. Cells were seeded into 96-well plates to a density of 10⁵ cells/100 μL well. After 24 h of growth

to allow attachment to the wells, compounds were added at various concentrations (10, 30, 50, 100, 150 and 200 nM). After 24 or 48 h of growth and after removal of the culture medium, 100 μ L/well of medium containing 1 mg/mL of MTT was added. Cell cultures were further incubated at 37 °C for 2 h in the dark. The MTT solution was then removed, and 100 μ L DMSO was added to dissolve formazan crystals. Absorbance at 550 nm was measured using a plate reader. Experiments were performed in triplicate. As a control, 0.5% DMSO was added to untreated cells.

Time-lapse microscopy. Effect of drug treatment on HEK and M14 cell morphology was determined by TLM using a Leica CTR6500 microscope. Images were captured every hour for a 48 h period. Ninty-six well plates were incubated under standard culture conditions and kept at 37 °C in a 5% carbon dioxide atmosphere for the observation period (up to 48 h).

Yeast. *S. cerevisiae* yeast wild type strain BY4741 (*Mat a his3Δ1 leu2Δ0 met15Δ0 ura3Δ0*) was used. Cells were grown at 28 °C in minimal medium (0.67% yeast nitrogen base without amino acids) containing 2% glucose (synthetic dextrose, SD) supplemented with 20 μ g/ μ L of the appropriate nutritional supplements. 5x10⁶ cells/mL of a fresh exponential culture of the yeast were incubated for 18 h at 28 °C with the compound of interest at 20 μ M. The cells were then centrifuged for 5 min at 13,000 x g at 4 °C, washed twice with distilled water and resuspended in SD (1 mL). Cell suspensions (15 μ L) were transferred in 60 μ L of fresh SD medium, serially diluted ten-fold, incubated overnight at 28 °C and spotted onto YP plates (1% yeast extract, 2% peptone) supplemented with 2% glucose (YPD). The plates were incubated at 28 °C for three days before recording cell growth.

Cell cultures and treatment. Cell lines were obtained from the American Tissue Culture Collection (ATCC), unless specified otherwise. Cells were grown in Dulbecco's Modified Eagle medium (D-MEM) supplemented with 10% fetal bovine serum (FBS) at 37 °C with 5% CO₂. In all experiments 300.000 cells were plated in

9 cm² dishes and exposed to ATI compounds dissolved in DMSO (0.1% final concentration) at the indicated concentrations. Methodology for the evaluation of the growth of human MCF-7 breast carcinoma, OVCAR-8 and NCI/ADR-RES cells, obtained from the National Cancer Institute for drug screening, was previously described, except that cells were grown for 96 h for IC₅₀ determinations.¹⁶¹ HeLa, PC3, HT29 and A549 cell lines were grown at 37 °C in D-MEM containing 10 mM glucose supplemented with 10% FBS, 100 units/mL each of penicillin and streptomycin and 2 mM glutamine. At the onset of each experiment, cells were placed in fresh medium and cultured in the presence of ATI compounds from 0.01 to 25 µM. 231-MDA and A549 were cultured in DMEM supplemented with 10% FBS for 24, 48 and 72 h in a 96-well tissue culture plate at 37 °C and 5% CO₂ in the absence or presence of different drug concentrations. The *P. tridactylis* PtK2 cells, the A10 rat embryonic aortic smooth muscle cells, the human umbilical vein endothelial cells, and the human aortic smooth muscle cells were obtained from ATCC and grown as recommended, except that a 5% CO₂ atmosphere was used with all cells. Evaluation of growth inhibition of A2780wt, A2780-CIS and OVCAR-3 cell lines was performed as previously reported.¹⁶²

Cell Viability Assay. Cell viability was generally determined using the MTT colorimetric assay. Cells were seeded into 96-well plates to a density of 7x10³/100 µL well. After 24 h of growth to allow attachment to the wells, compounds were added at various concentrations (from 0.01 to 25 µM). After 48 h of growth and removal of the culture medium, 100 µL/well of medium containing 1 mg/mL of MTT was added. Cell cultures were further incubated at 37 °C for 2 h in the dark. The solution was then gently aspirated from each well and the formazan crystals within the cells were dissolved with 100 µL of DMSO. Optical densities were read at 550 nm using a Multiskan Spectrum Thermo Electron Corporation reader. Results were expressed as percentage relative to vehicle-treated control (0.5% DMSO was added to untreated cells), and IC₅₀ values were determined by linear and polynomial

regression. Experiments were performed in triplicate. 231-MDA and A549 cells were plated at different cellular densities in order to test the drugs on logarithmic phase. The drugs were added after cell adhesion. On the day of the assay, 10 µL MTT (5 mg/mL) was added to each well, and cells were incubated for 2 h (37 °C, 5% CO₂). When dark crystals appeared at the well bottom, culture medium was discarded, and ethanol (100 µL) was added to each well to solubilize the crystals, to yield a purple solution. Absorbance was read with an enzyme-linked immunosorbent assay (ELISA) reader at 570 nm.

Immunofluorescence Assay. Cells to be processed for immunofluorescence were grown on sterile poly-L-lysine (SIAL) coated coverslips. After treatment, cells were either simultaneously fixed and permeabilized in MeOH for 6 min at -20 °C or, alternatively, first fixed in 3.7% paraformaldehyde (PFA) for 10 min followed by permeabilization in 0.1% Triton-X 100. The following antibodies were used: anti-β-tubulin unconjugated (Sigma clone B5.1.2, 1:2000) or FITC-conjugated (Sigma, 1:150); anti-γ-tubulin (Sigma, 1:1000); anti-processed caspase-3 (Cell Signalling Technology, 9661 1:500). Antibodies attached to their antigens were detected using secondary antibodies: anti-mouse Texas Red (Vector, TI-2000, 1:800), anti-mouse FITC (Jackson Immunoresearch Laboratories, 115-095-068; 1:200), anti-mouse AMCA (1:50), anti-rabbit FITC (Santa Cruz, sc-2090, 1:100), anti-rabbit Cy3 (Jackson Immunoresearch Laboratories, 711-165-152, 1:1000). The DNA was stained with DAPI (Sigma, 0.05 µg/mL in H₂O). Slides were finally mounted in Vectashield (Vector).

Microscopy. Bright-field images of growing cells were taken under an inverted fluorescence microscope (Nikon TE 300) equipped with a DMX1200-type CCD (resolution 1280x1024 pixels) using ACT-1 software. Immunofluorescence images were obtained under an epifluorescence Olympus AX70 microscope equipped with a CCD camera (Diagnostic Instruments, Spot RT slider model 2.3.0) or a Nikon

Eclipse 90i microscope equipped with Qimaging camera and the NisElements AR 3.1 software (Nikon).

Flow Cytometry. Cell cycle distribution was analyzed after cell incubation with propidium iodide (Sigma). Apoptosis was analyzed after incubation of cells with annexin V-FITC (Immunofluorescence Science). Cell samples were analyzed in a Coulter Epics XL cytofluorimeter (Beckman Coulter) equipped with EXPO 32 ADC software. Data for at least 10000 cells per sample were acquired.

Western Blotting Analysis. Cells were plated in flasks (1×10^6 cells) and incubated with or without an ATI compound respectively. At the indicated times, cells were lysed using ice cold lysis buffer (50 mM Tris, 150 mM NaCl, 10 mM EDTA, 1% Triton) supplemented with protease inhibitor cocktail (antipain, bestatin, chymostatin, leupeptin, pepstatin, phosphoramidon, Pefabloc, EDTA and aprotinin, all from Boehringer,). Whole cell extracts were loaded on 8–12% sodium dodecyl sulfate polyacrylamide gels and electrophoresed, followed by blotting onto nitrocellulose membranes (BioRad). After membrane blocking with 5% (w/v) fat-free milk powder, 0.1% Tween 20 in Tris buffered saline (TBS), it was incubated overnight at 4°C with specific antibodies at the concentrations indicated by the manufacturer (Cell Signaling Technology and Santa Cruz Biotechnology) in Tris-buffered saline/Tween-20/5% milk . Following incubation with horseradish peroxidase-conjugated secondary antibody, bands were detected by enhanced chemiluminescence (ECL kit, Amersham). Each filter was reprobed with mouse monoclonal anti-tubulin antibody. The signal intensity of detected bands was quantified by NIH ImageJ 1.40 after normalization with actin.

Metabolic Stability. Test compounds in duplicate at the final concentration of 1 μM were dissolved in DMSO and pre-incubated for 10 min at 37 °C in potassium phosphate buffer pH 7.4, 3 mM MgCl₂, with rat liver microsomes (Xenotech) at a final concentration of 0.5 mg/mL. After the pre-incubation period, reactions were started by adding the cofactors mixture (NADP, glucose-6-phosphate, glucose-6-

phosphate dehydrogenase). Samples were taken at time 0, 5, 10, 15, 20 and 30 min and added to acetonitrile to stop the reaction and centrifuged. Supernatants were analyzed and quantified by LC-MS/MS. A control sample without cofactors was always added in order to check the stability of test compounds in the reaction mixtures. 7-Ethoxycoumarin was used as a reference standard. A fixed concentration of verapamil was added in every sample as an internal standard for LC-MS/MS. Samples were analyzed on a UPLC (Waters) interfaced with a Premiere XE Triple Quadrupole (Waters). Eluents were: phase A: 95% H₂O, 5% acetonitrile + 0.1% HCOOH; phase B: 5% H₂O, 95% acetonitrile + 0.1% HCOOH. Flow rate 0.6 mL/min; column, Acquity BEH C18, 50 x 2.1 mm, 1.7 µm at 50 °C; injection volume, 5 µL. Samples were analyzed under the following conditions: electron spray ionization positive, desolvation temperature 450 °C, capillary 3.5 kV, extractor 5V. The percent of test compound remaining after a 30 min incubation period was calculated from the peak area relative to the area of the compound at time zero.

Aqueous Solubility. The solubility of compound **81** was measured by means of the HTS. Samples are placed in a 96-well filter plate and incubated at room temperature for 90 min. The plate is then filtered, and solutions are analyzed by LC/MS-UV.

In Vivo Drug Pharmacokinetic Studies. Pharmacokinetic experiments were performed using 4 week old male nude CD-1 mice (Charles River Laboratories). Animals were quarantined for approximately 1 week prior to the study. They were housed under standard conditions and had free access to water and standard laboratory rodent diet. Compound **81** was dissolved in a mixture 3% DMSO + 30% PEG400 + NaCl 0.9% at the concentration for the iv (rapid bolus) administration or a mixture 5% DMSO + 20% PEG400 + water for the oral (gavage) dose (dose volume 5 ml/kg). Compound **81** were administered to mice either by iv or oral route, and blood samples were collected after different time points after dosing. Plasma

was separated immediately after blood sampling by centrifugation, plasma proteins were precipitated using Sirocco filtration plates or Oasis HLB elution plates according to the distributor instructions, and the plasma samples were kept frozen at –80 °C until submission to LC/MS/MS analysis. Sample analysis was performed on an Acquity UPLC using either a Acquity BEH C18 column (50 mm × 2.1 mm × 1.7 µm) or a Acquity HSS T3 column (50 mm × 2.1 mm × 1.8 µm), coupled with a sample organizer and interfaced to a triple quadrupole Premiere XE (Waters). The mass spectrometer was operated using electrospray interface (ESI) with a capillary voltage of 3–4 kV, cone voltage of 25–52 V, source temperature of 115–120 °C, desolvation gas flow of 800 L/h, and desolvation temperature of 450–480 °C. Collision energy was optimized for each compound. LC–MS/MS analyses were carried out using a positive electrospray ionization (ESI(+)) interface in MRM (multiple reaction monitoring) mode. Pharmacokinetic parameters were calculated by a noncompartmental method using WinNolin 5.1 software (Pharsight).

10. References

1. Lengauer, C.; Kinzler, K. W.; Vogelstein, B. Genetic instabilities in human cancers. *Nature* **1998**, *396*, 643-649.
2. Nasmyth, K. Segregating sister genomes: the molecular biology of chromosome separation. *Science* **2002**, *297*, 559-565.
3. Hartwell, L. H.; Kastan, M. B. Cell cycle control and cancer. *Science* **1994**, *266*, 1821-1828.
4. Hartwell, L. H.; Weinert, T. A. Checkpoints: controls that ensure the order of cell cycle events. *Science* **1989**, *246*, 629-634.
5. White, E. Life, death, and the pursuit of apoptosis. *Genes Dev.* **1996**, *10*, 1-15.
6. Sampath, D.; Plunkett, W. Design of new anticancer therapies targeting cell cycle checkpoint pathways. *Curr. Opin. Oncol.* **2001**, *13*, 484-490.
7. Jordan, M. A.; Wilson, L. Microtubules as a target for anticancer drugs. *Nature* **2004**, *4*, 253-265.
8. Dutcher, S. K. The tubulin fraternity: alpha to eta. *Curr. Opin. Cell Biol.* **2001**, *13*, 49-54.
9. Nogales, E.; Wolf, S. G.; Downing, K. H. Structure of the $\alpha\beta$ tubulin dimer by electron crystallography. *Nature* **1998**, *391*, 199-203.
10. Löwe, J.; Li, H.; Downing, K. H.; Nogales, E. Refined structure of $\alpha\beta$ -tubulin at 3.5 Å resolution. *J. Mol. Biol.* **2001**, *313*, 1045-1057.
11. Gigant, B.; Curmi, P. A.; Martin-Barbey, C.; Charbaut, E.; Lachkar, S.; Lebeau, L.; Siavoshian, S.; Sobel, A.; Knossow, M. The 4 Å X-ray structure of a tubulin:stathmin-like domain complex. *Cell* **2000**, *102*, 809-816.
12. Ravelli, R. B. G.; Gigant, B.; Curmi, P. A.; Jourdain, I.; Lachkar, S.; Sobel, A.; Knossow, M. Insight into tubulin regulation from a complex with colchicine and a stathmin-like domain. *Nature* **2004**, *428*, 198-202.

13. Walker, R. A.; O'Brien, E. T.; Pryer, N. K.; Soboeiro, M. F.; Voter, W. A.; Erickson, H. P.; Salmon, E. D. Dynamic instability of individual microtubules analyzed by video light microscopy: Rate constants and transition frequencies. *J. Cell. Biol.* **1988**, *107*, 1437-1448.
14. Bailly, E.; Bornens, M. Cell biology. Centrosome and cell division. *Nature* **1992**, *355*, 300-301.
15. Moudjou, M.; Bordes, N.; Paintrand, M.; Bornens, M. gamma-Tubulin in mammalian cells: The centrosomal and the cytosolic forms. *J. Cell. Sci.* **1996**, *109*, 875-887.
16. Moritz, M.; Braunfeld, M. B.; Guenepaut, V.; Heuser, J.; Agard, D. A. Structure of the gamma-tubulin ring complex: A template for microtubule nucleation. *Nat. Cell. Biol.* **2000**, *2*, 365-370.
17. Oakley, B. R. Cell biology. A nice ring to the centrosome. *Nature* **1995**, *378*, 555-556.
18. Schnackenberg, B. J.; Khodjakov, A.; Rieder, C. L.; Palazzo, R. E. The disassembly and reassembly of functional centrosomes in vitro. *Proc. Natl. Acad. Sci. USA* **1998**, *95*, 9295-9300.
19. Mitchison, T.; Kirschner, M. Microtubule assembly nucleated by isolated centrosomes. *Nature* **1984**, *312*, 232-237.
20. Mitchison, T.; Kirschner, M. Dynamic instability of microtubule growth. *Nature* **1984**, *312*, 237-242.
21. Leung, C. L.; Liem, R. K.; Parry, D. A.; Green, K. J. The plakin family. *J. Cell. Sci.* **2001**, *114*, 3409-3410.
22. Leung, C. L.; Green, K. J.; Liem, R. K. Plakins: A family of versatile cytolinker proteins. *Trends Cell Biol.* **2002**, *12*, 37-45.
23. Lewis, S. A.; Gilmartin, M. E.; Hall, J. L.; Cowan, N. J. Three expressed sequences within the human beta-tubulin multigene family each define a distinct isotype. *J. Mol. Biol.* **1985**, *182*, 11-20.

24. Villasante, A.; Wang, D.; Dobner, P.; Dolph, P.; Lewis, S. A.; Cowan, N. J. Six mouse α -tubulin mRNAs encode five distinct isotypes: Testis-specific expression of two sister genes. *Mol. Cell Biol.* **1986**, *6*, 2409-2419.
25. Laing, N.; Dahllof, B.; Hartley-Asp, B.; Ranganathan, S.; Tew, K. D. Interaction of estramustine with tubulin isotypes. *Biochemistry* **1997**, *36*, 871-878.
26. Pape, M.; Schnieder, T.; von Samson-Himmelstjerna, G. Investigation of diversity and isotypes of the β -tubulin cDNA in several small strongyle (Cyathostominae) species. *J. Parasitol.* **2002**, *88*, 673-677.
27. Woo, K.; Jensen-Smith, H. C.; Luduena, R. F.; Hallworth, R. Differential synthesis of β -tubulin isotypes in gerbil nasal epithelia. *Cell Tissue Res.* **2002**, *309*, 331-335.
28. Andersen, S. S. Spindle assembly and the art of regulating microtubule dynamics by MAPs and Stathmin/Op18. *Trends Cell Biol.* **2000**, *10*, 261-267.
29. Mandelkow, E.; Mandelkow, E. M. Microtubules and microtubule-associated proteins. *Curr. Opin. Cell Biol.* **1995**, *7*, 72-81.
30. Masson, D.; Kreis, T. E. Binding of E-MAP-115 to microtubules is regulated by cell cycle-dependent phosphorylation. *J. Cell. Biol.* **1995**, *131*, 1015-1024.
31. Ookata, K.; Hisanaga, S. I.; Sugita, M.; Okuyama, A.; Murofushi, H.; Kitazawa, H.; Chari, S.; Bulinski, J. C.; Kishimoto, T. MAP4 is the in vivo substrate for CDC2 kinase in HeLa cells: Identification of an M-phase specific and a cell cycle-independent phosphorylation site in MAP4. *Biochemistry* **1997**, *36*, 15873-15883.
32. Ookata, K.; Hisanaga, S.; Bulinski, J. C. Cyclin B interaction with microtubule-associated protein 4 (MAP4) targets p34cdc2 kinase to microtubules and is a potential regulator of M-phase microtubule dynamics. *J. Cell Biol.* **1995**, *128*, 849-862.

33. Belmont, L.; Mitchison, T.; Deacon, H. W. Catastrophic revelations about Op18/stathmin. *Trends Biochem. Sci.* **1996**, *21*, 197-198.
34. Belmont, L. D.; Mitchison, T. J. Identification of a protein that interacts with tubulin dimers and increases the catastrophe rate of microtubules. *Cell* **1996**, *84*, 623-631.
35. Marklund, U.; Osterman, O.; Melander, H.; Bergh, A.; Gullberg, M. The phenotype of a “Cdc2 kinase target site-deficient” mutant of oncoprotein 18 reveals a role of this protein in cell cycle control. *J. Biol. Chem.* **1994**, *269*, 30626-30635.
36. Marklund, U.; Larsson, N.; Brattsand, G.; Osterman, O.; Chatila, T. A.; Gullberg, M. Serine 16 of oncoprotein 18 is a major cytosolic target for the Ca²⁺/calmodulin-dependent kinase-Gr. *Eur. J. Biochem.* **1994**, *225*, 53-60.
37. Walczak, C. E.; Mitchison, T. J.; Desai, A. XKCM1: A Xenopus kinesin-related protein that regulates microtubule dynamics during mitotic spindle assembly. *Cell* **1996**, *84*, 37-47.
38. Mandelkow, E.; Hoenger, A. Structures of kinesin and kinesin-microtubule interactions. *Curr. Opin. Cell Biol.* **1999**, *11*, 34-44.
39. Jordan, M. A.; Wilson, L. Microtubules and actin filaments: Dynamic targets for cancer chemotherapy. *Curr. Opin. Cell Biol.* **1998**, *10*, 123-130.
40. Janmey, P. A. The cytoskeleton and cell signaling: Component localization and mechanical coupling. *Physiol. Rev.* **1998**, *78*, 763-781.
41. Liu, X. M.; Wang, L. G.; Kreis, W.; Budman, D. R.; Adams, L. M. Differential effect of vinorelbine versus paclitaxel on ERK2 kinase activity during apoptosis in MCF-7 cells. *Br. J. Cancer.* **2001**, *85*, 1403-1411.
42. Wendell, K. L.; Wilson, L.; Jordan, M. A. Mitotic block in HeLa cells by vinblastine: Ultrastructural changes in kinetochore microtubule attachment and in centrosomes. *J. Cell. Sci.* **1993**, *104*, 261-274.

43. Jordan, M. A.; Thrower, D.; Wilson, L. Effects of vinblastine, podophyllotoxin and nocodazole on mitotic spindles. Implications for the role of microtubule dynamics in mitosis. *J. Cell. Sci.* **1992**, *102*, 401-416.
44. Fukasawa, K.; Choi, T.; Kuriyama, R.; Rulong, S.; Vande Woude, G. F. Abnormal centrosome amplification in the absence of p53. *Science* **1996**, *271*, 1744-1747.
45. Wahl, A. F.; Donaldson, K. L.; Fairchild, C. Lee, F. Y. F.; Foster, S. A.; Demers, G. W.; Galloway, D. A. Loss of normal p53 function confers sensitization to Taxol by increasing G2/M arrest and apoptosis. *Nat. Med.* **1996**, *2*, 72-79.
46. Vikhanskaya, F.; Vignati, S.; Beccaglia, P.; Ottoboni, C.; Russo, P.; D'Incalci, M.; Broggini, M. Inactivation of p53 in a human ovarian cancer cell line increases the sensitivity to paclitaxel by inducing G2/M arrest and apoptosis. *Exp. Cell. Res.* **1998**, *241*, 96-101.
47. Kingston, D. G. I.; Newman, David J. Taxoids: cancer-fighting compounds from nature. *Curr. Opin. Drug Discovery Dev.* **2007**, *10*, 130-144.
48. Service, R. F. Biomedicine: Hazel trees offer new source of cancer drug. *Science* **2000**, *288*, 27-28.
49. He, L.; Jagtap, P. G.; Kingston, D. G. I.; Shen, H. J.; Orr, G. A.; Horwitz, S. B. A Common Pharmacophore for Taxol and the Epothilones Based on the Biological Activity of a Taxane Molecule Lacking a C-13 Side Chain. *Biochemistry* **2000**, *39*, 3972-3978.
50. Nicolaou, K. C.; Yang, Z.; Liu, J. J.; Ueno, H.; Nantermet, P. G.; Guy, R. K.; Claiborne, C. F.; Renaud, J.; Couladouros, E. A.; Paulvannan, K.; Sorensin, E. J. Total synthesis of taxol. *Nature* **1994**, *367*, 630-634.
51. Ojima, I.; Wang, T.; Miller, M. L.; Lin, S.; Borella, C. P.; Geng, X.; Pera, P.; Bernacki, R. J. Synthesis and structure-activity relationships of new second-generation taxoids. *Bioorg. Med. Chem. Lett.* **1999**, *9*, 3423-3428.

52. Kingston, D. G. I. Recent Advances in the Chemistry of Taxol. *J. Nat. Prod.* **2000**, *63*, 726-734.
53. Appendino, G.; Dannieli, B.; Jackupovic, J.; Belloro, E.; Scambia, G.; Bomberdelli, E. Synthesis and evaluation of C-seco paclitaxel analogs. *Tetrahedron Lett.* **1997**, *38*, 4273-4276.
54. Parness, J.; Kingston, D. G. I.; Powel, R. C.; Harracksing, C.; Horwitz, S. B. Structure-activity study of cytotoxicity and microtubule assembly in vitro by taxol and related taxanes. *Biochem. Biophys. Res. Commun.* **1982**, *105*, 1082-1089.
55. Gueritte-Voegelein, F.; Guenard, D.; Lavelle, F.; Le Goff, M. T.; Mangatal, L.; Potier, P. Relationships between the structure of taxol analogs and their antimitotic activity. *J. Med. Chem.* **1991**, *34*, 992-998.
56. Saicic, R. N.; Matovic, R. An efficient semisynthesis of 7-deoxypaclitaxel from taxine. *J. Chem. Soc. Perkin Trans.* **2000**, *1*, 59-65.
57. Appendino, G. The phytochemistry of the yew tree. *Nat. Prod. Rep.* **1995**, *12*, 349-360.
58. Ringel, I.; Horwitz, S. B. Studies with RP 56976 (taxotere): a semisynthetic analog of taxol. *J. Natl. Cancer Inst.* **1991**, *83*, 288-291.
59. Moon, C.; Verschraegen, C. F.; Bevers, M.; Freedman, R.; Kudelka, A. P.; Kavanagh, J. J. Use of docetaxel (taxotere) in patients with paclitaxel (taxol) hypersensitivity. *Anti-Cancer Drugs* **2000**, *11*, 565-568.
60. Appendino, G.; Gariboldi, P.; Gabetta, B.; Pace, R.; Bombardelli, E.; Viterbo, D. 14 β -Hydroxy-10-deacetylbaaccatin III, a new taxane from Himalayan yew (*Taxus wallichiana* Zucc.). *J. Chem. Soc. Perk. Trans.* **1992**, *21*, 2925-2929.
61. Ojima, I.; Slater, J. C.; Michaud, E.; Kuduk, S. D.; Bounaud, P. Y.; Vrignaud, P.; Bissery, M. C.; Veith, J. M.; Pera, P.; Bernacki, R. J. Syntheses and Structure-Activity Relationships of the Second-Generation Antitumor Taxoids:

- Exceptional Activity against Drug-Resistant Cancer Cells. *J. Med. Chem.* **1996**, *39*, 3889-3896.
- 62. Ojima, I.; Kuduk, S. D.; Pera, P.; Veith, J. M.; Bernacki, R. J. Synthesis and Structure-Activity Relationships of Non-aromatic Taxoids: Effects of Alkyl and Alkenyl Ester Groups on Cytotoxicity. *J. Med. Chem.* **1997**, *40*, 279-285.
 - 63. Ojima, I.; Slater, J. C.; Kuduk, S. D.; Takeuchi, C. S.; Gimi, R. H.; Sun, C. M.; Park, Y. H.; Pera, P.; Veith, J. M.; Bernacki, R. J. Syntheses and Structure-Activity Relationships of Taxoids Derived from 14 β -hydroxy-10-deacetylbaccatin III. *J. Med. Chem.* **1997**, *40*, 267-278.
 - 64. Ojima, I.; Lin, S.; Wang, T. Recent advances in the medicinal chemistry of taxoids with novel β -amino acid side chains. *Curr. Med. Chem.* **1999**, *6*, 927-954.
 - 65. Cheng, Q.; Oritani, T.; Horiguchi, T.; Yamada, T.; Mong, Y. Synthesis and biological evaluation of novel 9-functional heterocyclic coupled 7-deoxy-9-dihydropaclitaxel analogue. *Bioorg. Med. Chem. Lett.* **2000**, *10*, 517-521.
 - 66. Klar, U.; Graf, H.; Schenk, O.; Rohr, B.; Schulz, H. New synthetic inhibitors of microtubule depolymerisation. *Bioorg. Med. Chem. Lett.* **1998**, *8*, 1397-1402.
 - 67. Damen, E. W. P.; Wiegerinck, P. H. G.; Braamer, L.; Sperling, D.; de Vos, D.; Scheeren, H. W. Paclitaxel esters of malic acid as prodrugs with improved water solubility. *Bioorg. Med. Chem.* **2000**, *8*, 427-432.
 - 68. Huang, C. M.; Wu, Y. T.; Chen, S. T. Targeting delivery of paclitaxel into tumor cells via somatostatin receptor endocytosis. *Chem. Biol.* **2000**, *7*, 453-461.
 - 69. Capraro, H. G.; Brossi, A. The Alkaloids. Brossi, A. ed., Academic Press, New York, **1984**.

70. Niel, E.; Scherrmann, J. M. Colchicine today. *Joint Bone Spine* **2006**, *73*, 672-678.
71. Bai, R.; Covell, D. G.; Pei, X. F.; Ewell, J. B.; Nguyen, N. Y.; Brossi, A.; Hamel, E. Mapping the binding site of colchicinoids on β -tubulin: 2-chloroacetyl-2-demethylthiocolchicine covalently reacts predominantly with cysteine 239 and secondarily with cysteine 354. *J. Biol. Chem.* **2000**, *275*, 40443-40452.
72. Hamel, E. Microtubule Proteins. Avila, J. ed., CRC Press: Boca Raton, Fl, **1990**.
73. Uppuluri, S.; Knipling, L.; Sackett, D. L.; Wolff, J. Localization of the colchicine-binding site of tubulin. *Proc. Natl. Acad. Sci. USA* **1993**, *90*, 11598-602.
74. Bai, R.; Pei, X. F.; Boye, O.; Getahun, Z.; Grover, S.; Bekisz, J.; Nguyen, N. Y.; Brossi, A.; Hamel, E. Identification of cysteine 354 of β -tubulin as part of the binding site for the A ring of colchicine. *J. Biol. Chem.* **1996**, *271*, 12639-12645.
75. Dumortier, C.; Gorbunoff, M. J.; Andreu, J. M.; Engelborghs, Y. Different Kinetic Pathways of the Binding of Two Biphenyl Analogs of Colchicine to Tubulin. *Biochemistry* **1996**, *35*, 4387-4395.
76. Andreu, J. M.; Perez-Ramirez, B.; Gorbunoff, M. J.; Ayala, D.; Timasheff, S. N. Role of the Colchicine Ring A and Its Methoxy Groups in the Binding to Tubulin and Microtubule Inhibition. *Biochemistry* **1998**, *37*, 8356-8368.
77. Andreu, J. M.; Timasheff, S. N. Conformational states of tubulin liganded to colchicine, tropolone methyl ether, and podophyllotoxin. *Biochemistry* **1982**, *21*, 6465-6476.

78. Luduena, R. F.; Roach, M. C. Tubulin sulfhydryl groups as probes and targets for antimitotic and antimicrotubule agents. *Pharmacol. Ther.* **1991**, *49*, 133-152.
79. Shi, Q.; Chen, K.; Morris-Natschke, S. L.; Lee, K. H. Recent progress in the development of tubulin inhibitors as antimitotic antitumor agents. *Curr. Pharm. Des.* **1998**, *4*, 219-248.
80. Al-Tel, T. H.; Abu Zarga, M. H.; Sabri, S. S.; Freyer, A. J.; Shamma, M. New natural colchicinoids: indications of two possible catabolic routes for the colchicine alkaloids. *J. Nat. Prod.* **1990**, *53*, 623-629.
81. Banwell, M. G.; Peters, S. C.; Greenwood, R. J.; Mackay, M. F.; Hamel, E.; Lin, C. M. Semisyntheses, x-ray crystal structures, and tubulin-binding properties of 7-oxodeacetamidocolchicine and 7-oxodeacetamidoisocolchicine. *Aust. J. Chem.* **1992**, *45*, 1577-1588.
82. Hamel, E. Antimitotic natural products and their interactions with tubulin. *Med. Res. Rev.* **1996**, *16*, 207-231.
83. Boy, E. O.; Brossi, A. The Alkaloids. Brossi, A. Ed.; Academic Press, Inc., **1992**.
84. Itoh, Y.; Brossi, A.; Hamel, E.; Lin, C. M. Colchicine models: synthesis and binding to tubulin of tetramethoxybiphenyls. *Helv. Chim. Acta* **1988**, *71*, 1199-1209.
85. ter Haar, E.; Rosenkranz, H. S.; Hamel, E.; Day, B. W. Computational and molecular modeling evaluation of the structural basis for tubulin polymerization inhibition by colchicine site agents. *Bioorg. Med. Chem.* **1996**, *4*, 1659-1671.
86. Lee, K. H.; Xiao, Z. Antitumor agents 240. Podophyllotoxins and analogs. *Anticancer Agents Nat. Prod.* **2005**, *1*, 71-87.
87. Ji, Z.; Wang, H. K.; Bastow, K. F.; Zhu, X. K.; Cho, S. J.; Cheng, Y. C.; Lee, K. H. Antitumor agents. 177. Design, syntheses, and biological evaluation of

- novel etoposide analogs bearing pyrrolecarboxamidino group as DNA topoisomerase II inhibitors. *Bioorg. Med. Chem. Lett.* **1997**, *7*, 607-612.
88. Ohnuma, T.; Obata, R.; Nishiyama, Y.; Yamasaki, T.; Kamei, H.; Naito, T.; Oki, T. Preparation and antitumor activity of 2"-O-, 3"-O- and 2",3"-di-O-substituted derivatives of etoposide. *Chem. Pharm. Bull.* **1992**, *40*, 1783-1788.
89. Lee, K. H. Anticancer drug design based on plant-derived natural products. *J. Biomed. Sci.* **1999**, *6*, 236-250.
90. Solary, E.; Leteurtre, F.; Paull, K. D.; Scudiero, D.; Hamel, E.; Pommier, Y. Dual inhibition of topoisomerase II and tubulin polymerization by azatoxin, a novel cytotoxic agent. *Biochem. Pharmacol.* **1993**, *45*, 2449-2456.
91. Pettit, G. R.; Singh, S. B.; Boyd, M. R.; Hamel, E.; Pettit, R. K.; Schmidt, J. M.; Hogan, F. Antineoplastic Agents. 291. Isolation and Synthesis of Combretastatins A-4, A-5, and A-6. *J. Med. Chem.* **1995**, *38*, 1666-1672.
92. Pettit, G. R.; Singh, S. B.; Hamel, E.; Lin, C. M.; Alberts, D. S.; Garcia-Kendall, D. Isolation and structure of the strong cell growth and tubulin inhibitor combretastatin A-4. *Experientia* **1989**, *45*, 209-211.
93. Jordan, A.; Hadfield, J. A.; Lawrence, N. J.; McGown, A. T. Tubulin as a target for anticancer drugs: agents which interact with the mitotic spindle. *Med. Res. Rev.* **1998**, *18*, 259-296.
94. Tron, G. C.; Pirali, T.; Sorba, G.; Pagliai, F.; Busacca, S.; Genazzani, A. A. Medicinal chemistry of combretastatin A4: Present and future directions. *J. Med. Chem.* **2006**, *49*, 3033-3044.
95. Pettit, G. R.; Grealish, M. P.; Herald, D. L.; Boyd, M. R.; Hamel, E.; Pettit, R. K. Antineoplastic Agents. 443. Synthesis of the Cancer Cell Growth Inhibitor Hydroxyphenstatin and Its Sodium Diphosphate Prodrug. *J. Med. Chem.* **2000**, *43*, 2731-2737.

96. Brown, R. T.; Fox, B. W.; Hadfield, J. A.; McGown, A. T.; Mayalarp, S. P.; Pettit, G. R.; Woods, J. A. Synthesis of water-soluble sugar derivatives of combretastatin A-4. *J. Chem. Soc. Perkin Trans.* **1995**, *5*, 577-5781.
97. Bedford, S. B.; Quarterman, C. P.; Rathbone, D. L.; Slack, J. A.; Griffin, R. J.; Stevens, M. F. G. Synthesis of water-soluble prodrugs of the cytotoxic agent combretastatin A4. *Bioorg. Med. Chem. Lett.* **1996**, *6*, 157-160.
98. Pettit, G. R.; Rhodes, M. R. Antineoplastic agents. 389. New syntheses of the combretastatin A-4 prodrug. *Anti-Cancer Drug Des.* **1998**, *13*, 183-191.
99. Pettit, G. R.; Temple, C.; Narayanan, V. L.; Varma, R.; Simpson, M. J.; Boyd, M. R.; Rener, G. A.; Bansal, N. Antineoplastic agents. 322. Synthesis of combretastatin A-4 prodrugs. *Anti-Cancer Drug Des.* **1995**, *10*, 299-309.
100. Mukherjee, A. K.; Basu, S.; Sarkar, N.; Ghosh, A. C. Advances in cancer therapy with plant based natural products. *Curr. Med. Chem.* **2001**, *8*, 1467-1486.
101. Svoboda, G. H. Alkaloids of Vinca rosea. IX. Extraction and characterization of leurosidine and leurocristine. *Lloydia* **1961**, *24*, 173-178.
102. Neuss, N.; Gorman, M.; Svoboda, G. H.; Maciak, G.; Beer, C. T. Vinca alkaloids. III. Characterization of leurosine and vincaleukoblastine, new alkaloids from Vinca rosea. *J. Am. Chem. Soc.* **1959**, *81*, 4754-4755.
103. Iwasaka, S. Antimitotic agents: Chemistry and recognition of tubulin molecule. *Med. Res. Rev.* **1993**, *13*, 183-198.
104. Gigant, B.; Wang, C.; Ravelli, R.B.G.; Roussi, F.; Steinmetz, M.O.; Curmi, P.A.; Sobel, A.; Knossow, M. Structural Basis for the Regulation of Tubulin by Vinblastine. *Nature* **2005**, *435*, 519-522.
105. Pettit, G. R. Progress in the Discovery of Biosynthetic Anticancer Drugs. *J. Nat. Prod.* **1996**, *59*, 812-821.
106. Barnett, C. J.; Cullinan, G. J.; Gerzon, K.; Hoying, R. C.; Jones, W. E.; Newlon, W. M.; Poore, G. A.; Robison, R. L.; Sweeney, M. J. Structure-

- activity relationships of dimeric Catharanthus alkaloids. 1. Deacetyl vinblastine amide (vindesine) sulfate. *J. Med. Chem.* **1978**, *21*, 88-96.
107. Budman, D. R. New vinca alkaloids and related compounds. *Sem. Oncol.* **1992**, *19*, 639-645.
108. Canobbio, L.; Boccardo, F.; Pastorino, G.; Brema, F.; Martini, C.; Resasco, M.; Santi, L. Phase-II study of Navelbine in advanced breast cancer. *Sem. Oncol.* **1989**, *16*, 33-36.
109. Martins, R. G.; Dienstmann, R.; de Biasi, P.; Dantas, K.; Santos, V.; Toscano, E.; Roriz, W.; Zamboni, M.; Sousa, A.; Small, I. A.; Moreira, D.; Ferreira, C. G.; Zukin, M. Phase II trial of neoadjuvant chemotherapy using alternating doublets in non-small-cell lung cancer. *Clin. Lung Cancer* **2007**, *8*, 257-263.
110. Kruczynski, A.; Etievant, C.; Perrin, D.; Chansard, N.; Duflos, A.; Hill, B. T. Characterization of cell death induced by vinflunine, the most recent Vinca alkaloid in clinical development. *Br. J. Cancer* **2002**, *86*, 143-150.
111. Rowinsky, E. K. The development and clinical utility of the taxane class of antimicrotubule chemotherapy agents. *Annu. Rev. Med.* **1997**, *48*, 353-374.
112. Verrills, N. M.; Kavallaris, M. Improving the targeting of tubulin-binding agents: Lessons from drug resistance studies. *Curr. Pharm. Des.* **2005**, *11*, 1719-1733.
113. De Martino, G.; La Regina, G.; Coluccia, A.; Edler, M. C.; Barbera, M. C.; Brancale, A.; Wilcox, E.; Hamel, E.; Artico, M.; Silvestri, R. Arylthioindoles, potent inhibitors of tubulin polymerization. *J. Med. Chem.* **2004**, *47*, 6120-6123.
114. De Martino, G.; Edler, M. C.; La Regina, G.; Coluccia, A.; Barbera, M. C.; Barrow, D.; Nicholson, R. I.; Chiosis, G.; Brancale, A.; Hamel, E.; Artico, M.; Silvestri, R. Arylthioindoles, potent inhibitors of tubulin polymerization. 2. Structure activity relationships and molecular modeling studies. *J. Med. Chem.* **2006**, *49*, 947-954.

115. La Regina, G.; Edler, M. C.; Brancale, A.; Kandil, S.; Coluccia, A.; Piscitelli, F.; Hamel, E.; De Martino, G.; Matesanz, R.; Díaz, J. F.; Scovassi, A. I.; Prosperi, E.; Lavecchia, A.; Novellino, E.; Artico, M.; Silvestri, R. New arythioindoles inhibitors of tubulin polymerization. 3. Biological evaluation, SAR and molecular modeling studies. *J. Med. Chem.* **2007**, *50*, 2865-2874.
116. Tron, G. C.; Pirali, T.; Sorba, G.; Pagliai, F.; Busacca, S.; Genazzani, A. A. Medicinal chemistry of combretastatin A4: present and future directions. *J. Med. Chem.* **2006**, *49*, 1-12.
117. Liou, J.-P.; Chang, Y.-L.; Kuo, F.-M.; Chang, C.-W.; Tseng, H.-Y.; Wang, C.-C.; Yang, Y.-N.; Chang, J.-Y.; Lee, S.-J.; Hsieh, H.-P. Concise synthesis and structure-activity relationships of combretastatin A-4 analogues, 1-aryloylindoles and 3-aryloylindoles, as novel classes of potent antitubulin agents. *J. Med. Chem.* **2004**, *47*, 4247-4257.
118. Ciapetti, P.; Giethlen, B. Molecular variations based on isosteric replacement. Carboxylic esters bioisosteres in the practice of medicinal chemistry, 3rd Ed. Wermuth C. G. Elsevier Ltd: Oxford, UK, **2008**, 310-313.
119. Bergman, J.; Venemalm, L. Efficient synthesis of 2-chloro-, 2-bromo-, and 2-iodoindole. *J. Org. Chem.* **1992**, *57*, 2495-2497.
120. Botstein, D.; Chervitz, S. A.; Cherry, J. M. Yeast as a model organism. *Science* **1997**, *277*, 1259-1260.
121. Almeida, B.; Silva, A.; Mesquita, A.; Sampaio-Marques, B.; Rodrigues, F.; Ludovico, P. Drug-induced apoptosis in yeast. *Biochim Biophys Acta* **2008**, *1783*, 1436-1448.
122. Zabrocki, P.; Bastiaens, I.; Delay, C.; Bammens, T.; Ghillebert, R.; Pellens, K.; De Virgilio, C.; Van Leuven, F.; Winderick, J. Phosphorylation, lipid raft interaction and traffic of alpha-synuclein in a yeast model for Parkinson's disease. *Biochim. Biophys. Acta* **2008**, *1783*, 1767-1780.

123. Cassidy-Stone, A.; Chipuk, J. E.; Ingberman, E.; Song, C.; Yoo, C.; Kuwana, T.; Kurth, M. J.; Shaw, J. T.; Hinshaw, J. E.; Green, D. R.; Nunnari, J. Chemical inhibition of the mitochondrial division dynamin reveals its role in Bax/Bak-dependent mitochondrial outer membrane permeabilization. *Dev. Cell.* **2008**, *14*, 193-204.
124. Shi, J.; Orth, J. D.; Mitchison, T. Cell type variation in responses to antimitotic drugs that target microtubules and kinesin-5. *Cancer Res.* **2008**, *68*, 3269-3276.
125. Gascoigne, K. E.; Taylor, S. S. Cancer cells display profound intra- and interline variation following prolonged exposure to antimitotic drugs. *Cancer Cell* **2008**, *14*, 111-122.
126. Sudakin, V.; Yen, T. G. Targeting mitosis for anti-cancer therapy. *BioDrugs* **2007**, *21*, 225-233.
127. Gascoigne, K. E.; Taylor, S. S. How do anti-mitotic drugs kill cancer cells? *J. Cell Sci.* **2009**, *122*, 2579-2585.
128. La Regina, G.; Sarkar, T.; Bai, R.; Edler, M. C.; Saletti, R.; Coluccia, A.; Piscitelli, F.; Minelli, L.; Gatti, V.; Mazzoccoli, C.; Palermo, V.; Mazzoni, C.; Falcone, C.; Scovassi, A. I.; Giansanti, V.; Campiglia, P.; Porta, A.; Maresca, B.; Hamel, E.; Brancale, A.; Novellino, E.; Silvestri, R. New arylthioindoles and related bioisosteres at the sulfur bridging group. 4. Synthesis, tubulin polymerization, cell growth inhibition, and molecular modeling studies. *J. Med. Chem.* **2009**, *52*, 7512-7527.
129. (a) Bhalla, K. N. Microtubule-targeted anticancer agents and apoptosis. *Oncogene* **2003**, *22*, 9075-9086; (b) Impens, F.; Van Damme, P.; Demol, H.; Van Damme, J.; Vandekerckhove, J.; Gevaert, K. Mechanistic insight into taxol-induced cell death. *Oncogene* **2008**, *27*, 4580-4591; (c) McGrogan, B.T.; Gilmartin, B.; Carney, D. N.; McCann, A. Taxanes, microtubules and chemoresistant breast cancer. *Biochim. Biophys. Acta* **2008**, *2*, 96-132; (d) Mollinedo, F.; Gajate, C. Microtubules, microtubule-interfering agents and

- apoptosis. *Apoptosis* **2003**, *8*, 413-450.
130. Kerns, E. H.; Di, L. Plasma stability methods. In *Drug-like properties: concepts, structure design and methods*. Academic Press: Burlington, MA, **2008**; 329-347.
131. FlexX 3.0. BioSolveIT GmbH, Sankt Augustin, Germany. <http://www.biosolveit.de>.
132. Korb, O.; Stützle, T.; Exner, T. E.. PLANTS: Application of ant colony optimization to structure-based drug design. In Dorigo, M.; Gambardella, L. M.; Birattari, M.; Martinoli, A.; Poli, R.; Stützle T. (Eds.). *Ant Colony Optimization and Swarm Intelligence, 5th Int. Workshop, ANTS 2006, LNCS 4150*, 247-258.
133. Friesner, R. A.; Banks, J. L.; Murphy, R. B.; Halgren, T. A.; Klicic, J. J.; Mainz, D. T.; Repasky, M. P.; Knoll, E. H.; Shelley, M.; Perry, J. K.; Shaw, D. E.; Francis, P.; Shenkin, P. S. GLIDE: a new approach for rapid, accurate docking and scoring. 1. Method and assessment of docking accuracy. *J. Med. Chem.* **2004**, *47*, 1739-1749.
134. Coluccia, A.; Sabbadin, D.; Brancale, A. Molecular modelling studies on Arylthioindoles as potent inhibitors of tubulin polymerization. *Eur. J. Med. Chem.* **2011**, *46*, 3519-3525.
135. Dupeyre, G.; Chabot, G. G.; Thoret, S.; Cachet, X.; Seguin, J.; Guenard, D.; Tillequin, F.; Scherman, D.; Koch, M.; Michel, S. Synthesis and biological evaluation of (3,4,5-trimethoxyphenyl)indol-3-yl-methane derivatives as potential antivascular agents. *Bioorg. Med. Chem.* **2006**, *14*, 4410-4426.
136. Liou, J.-P.; Wu, C.-Y.; Hsieh, H.-P.; Chang, C.-Y.; Chen, C.-M.; Kuo, C.-C.; Chang, J.-Y. 4- and 5-Aroylindoles as novel classes of potent antitubulin agents. *J. Med. Chem.* **2007**, *50*, 4548-4552.

137. Jia, Y.; Zhu, J. Palladium-catalyzed, modular synthesis of highly functionalized indoles and tryptophans by direct annulation of substituted *o*-haloanilines and aldehydes. *J. Org. Chem.* **2006**, *71*, 7826-7834.
138. Hugon, B.; Pfeiffer, B.; Renard, P.; Prudhomme, M. Synthesis of isogranulatimide analogues possessing a pyrrole moiety instead of an imidazole heterocycle. *Tetrahedron Lett.* **2003**, *44*, 3927-3930.
139. Thummel, R. P.; Hegde, V. Polyaza-cavity shaped molecules. 14. Annelated 2-(2'-pyridyl)indoles, 2,2'-biindoles, and related systems. *J. Org. Chem.* **1989**, *54*, 1720-1725.
140. Jennings, L. D.; Foreman, K. W.; Rush, T. S.; Tsao, D. H. H.; Mosyak, L.; Kincaid, S. L.; Sukhdeo, M. N.; Sutherland, A. G.; Ding, W.; Kenny, C. H.; Sabus, C. L.; Liu, H.; Dushin, E. G.; Moghazeh, S. L.; Labthavikul, P.; Petersen, P. J.; Tuckman, M.; Ruzin, A. V. Combinatorial synthesis of substituted 3-(2-indolyl)piperidines and 2-phenyl indoles as inhibitors of ZipA-FtsZ interaction. *Bioorg. Med. Chem.* **2004**, *12*, 5115-5131.
141. Kraus, G. A.; Guo, H. One-Pot Synthesis of 2-substituted indoles from 2-aminobenzyl phosphonium salts. A formal total synthesis of arcyriacyanin A. *Org. Lett.* **2008**, *10*, 3061-3063.
142. Barolo, S. M.; Lukach, A. E.; Rossi, R. A. Syntheses of 2-Substituted Indoles and Fused Indoles by Photostimulated Reactions of *o*-Iodoanilines with Carbanions by the SRN1 Mechanism. *J. Org. Chem.* **2003**, *68*, 2807-2811.
143. Nador, F.; Moglie, Y.; Vitale, C.; Yus, M.; Alonso, F.; Radivoy G. NMR Reduction of polycyclic aromatic hydrocarbons promoted by cobalt or manganese nanoparticles. *Tetrahedron* **2010**, *66*, 4318-4325.
144. Tullberg, E.; Schacher, F.; Peters, D.; Frejd, T. Solvent-free Heck-Jeffery reactions under ball-milling conditions applied to the synthesis of unnatural amino acids precursors and indoles. *Synthesis* **2006**, *7*, 1183-1189.
145. Bocchi, V.; Palla, G. Synthesis and spectroscopic characteristics of 2,3'-

- biindolyls and 2,2'-indolylpyrroles. *Ist. Chim. Org., Univ. Parma, Parma, Italy. Tetrahedron* **1984**, *40*, 3251-3256.
146. Ostrowski, T.; Golankiewicz, B.; De Clercq, E.; Andrei, G.; Snoeck, R. Synthesis and anti-VZV activity of 6-heteroaryl derivatives of tricyclic acyclovir and 9-{[cis-1',2'-bis(hydroxymethyl)cycloprop-1'-yl]methyl}guanine analogues. *Eur. J. Med. Chem.* **2009**, *44*, 3313-3317.
147. Hudkins, R. L.; Diebold, J. L.; Marsh, F. D. Synthesis of 2-aryl- and 2-vinyl-1*H*-indoles via palladium-catalyzed cross-coupling of aryl and vinyl halides with 1-carboxy-2-(tributylstanny)indole. *J. Org. Chem.* **1995**, *60*, 6218-6220.
148. Fang, Y.-Q.; Lautens, M. A highly selective tandem cross-coupling of gem-dihaloolefins for a modular, efficient synthesis of highly functionalized indoles. *J. Org. Chem.* **2008**, *73*, 538-549.
149. Imran, M.; Dudhe, R.; Sharma, P. K.; Khan, S. A. Synthesis and anticonvulsant activity of 3-chloro-4-substituted phenyl-1-[{4-(1-naphthyl)-1,3-thiazol-2-yl}amino]azetidin-2-ones. K.I.E.T. School of Pharmacy, Krishna Institute of Engineering and Technology, Ghaziabad, India. *International Journal of Chemical Sciences* **2007**, *5*, 189-200.
150. Ravelli, R. B. G.; Gigant, B.; Curmi, P. A.; Jourdain, I.; Lachkar, S.; Sobel, A.; Knossow, M. Insight into tubulin regulation from a complex with colchicine and a stathmin-like domain. *Nature* **2004**, *428*, 198-202.
151. Dorleans, A.; Gigant, B.; Ravelli, R. B. G.; Mailliet, P.; Mikol, V.; Knossow, M. Variations in the colchicine-binding domain provide insight into the structural switch of tubulin. *PNAS* **2009**, *106*, 13775-13779.
152. Molecular Operating Environment (MOE 2007.09), Chemical Computing Group, Inc., Montreal, Quebec, Canada, <http://www.chemcomp.com>.
153. Case, D. A.; Cheatham, T. E., III; Darden, T.; Gohlke, H.; Luo, R.; Merz, K. M., Jr.; Onufriev, A.; Simmerling, C.; Wang, B.; Woods, R. J. The amber biomolecular simulation programs. *J. Comput. Chem.* **2005**, *26*, 1668-1688.

154. Meagher, K. L.; Redman, L. T.; Carlson, H. A. Development of polyphosphate parameters for use with the AMBER force field. *J. Comput. Chem.* **2003**, *24*, 1016-1025.
155. Schmidt, M. W.; Baldridge, K. K.; Boatz, J. A.; Elbert, S. T.; Gordon, M. S.; Jensen, J. H.; Koseki, S.; Matsunaga, N.; Nguyen, K. A.; *et al.* General atomic and molecular electronic structure system. *J. Comput. Chem.* **1993**, *14*, 1347-63.
156. Gordon, M. S.; Schmidt, M. W. Advances in electronic structure theory: GAMESS a decade later. *Theory and Applications of Computational Chemistry: The First Forty Years* **2005**, 1167-1189.
157. <http://ambermd.org/#AmberTools>.
158. de Groot, B. L.; van Aalten, D. M. F.; Scheek, R. M.; Amadei, A.; Vriend, G.; Berendsen, H. J. C. Prediction of protein conformational freedom from distance constraints. *Proteins* **1997**, *29*, 240-251.
159. PyMOL, DeLano Scientific LLC, San Carlos, California, U.S.A. www.pymol.org.
160. Hamel, E. Evaluation of antimitotic agents by quantitative comparisons of their effects on the polymerization of purified tubulin. *Cell Biochem. Biophys.* **2003**, *38*, 1-21.
161. Verdier-Pinard, P.; Lai, J.-Y.; Yoo, H.-D.; Yu, J.; Marquez, B.; Nagle, D. G.; Nambu, M.; White, J. D.; Falck, J. R.; Gerwick, W. H.; Day, B. W.; Hamel, E. Structure-activity analysis of the interaction of curacin A, the potent colchicine site antimitotic agent, with tubulin and effects of analogs on the growth of MCF-7 breast cancer cells. *Mol. Pharmacol.* **1998**, *53*, 62-76.
162. Ferlini, C.; Raspaglio, G.; Mozzetti, S.; Cicchillitti, L.; Filippetti, F.; Gallo, D.; Fattorusso, C.; Campiani, G.; Scambia, G. The seco-taxane IDN5390 is able to target class III β -tubulin and to overcome paclitaxel resistance. *Cancer Research* **2005**, *65*, 2397-2405.

11. Acknowledgments

Prof. R. Silvestri, Dott. G. La Regina, Dott. A. Coluccia, Dott. F. Piscitelli,
Dipartimento di Chimica e Tecnologia del Farmaco, Sapienza Università di Roma.

Prof. A. Brancale, Welsh School of Pharmacy, Cardiff University.

Prof. A. Lavecchia, Prof. E. Novellino, Dipartimento di Chimica Farmaceutica e
Tossicologica, Università degli Studi di Napoli.

B. Maresca, P. Campiglia, A. Porta, Dipartimento di Scienze Farmaceutiche,
Sezione Biomedica, Università degli Studi di Salerno.

E. Hamel, T. Sarkar, R. Bai, M. C. Edler, National Cancer Institute, Frederick.

P. Lavia, A. Bolognesi, CNR, National Research Council, Institute of Molecular
Biology and Pathology, Sapienza Università di Roma.

A. I. Scovassi, V. Giansanti, IGM-CNR, Pavia.

M. Varasi, European Institute of Oncology, Milano.

F. Ferlini, Danbury Hospital Research Institute, Tumor Reproductive Biology
Research Laboratory, Danbury.

Istituto Pasteur, Fondazione Cenci Bolognetti.